The use of RFID technology to measure dielectric coefficient of diethyl ether-oil-brine mixtures for enhanced imbibition experiments

By
A.M. Hassan
November 20, 2015

The use of RFID technology to measure dielectric coefficient of diethyl ether-oil-brine mixtures for enhanced imbibition experiments

By

A.M. Hassan

in partial fulfilment of the requirements for the degree of

Master of Science
in Applied Earth Sciences

at Delft University of Technology,
to be defended publicly on Friday November 20, 2015 at 10:00 AM.

Supervisor:	Prof. dr. W. R. (William) Rossen,	TU Delft
Thesis committee:	Prof. dr. J. (Hans) Bruining,	TU Delft
	Prof. dr. ir. E. C. (Evert) Slob,	TU Delft
	Prof. dr. P. L. J. (Pacelli) Zitha,	TU Delft
	Dr. R. (Ranajit) Ghose,	TU Delft
	Dr. S. (Shohei) Minato,	TU Delft
	Prof. C. P. J. (Cor) van Kruijsdijk,	TU Delft/ Shell Global Solutions

TU Delft

Challenge the future

Preface

Characterization of fluid properties is significant in the petroleum engineering practice, especially in solvent-based enhanced oil recovery SEOR where the use of injected chemicals should ideally be reduced to the bare minimum in order to minimize the costs and environmental impact of SEOR. However, current techniques for measurement inside cores, pipes and other enclosed spaces are inconvenient as the measurement devices must be connected from the inside to the outside, inevitably causing leakage problems. A possible solution to this problem is the usage of a Radio Frequency Identification RFID communication system. RFID is the use of wireless electromagnetic fields to transfer data. This research examines the feasibility of using RFID technology for wireless laboratory measurement of the dielectric coefficients of diethyl ether-oil-brine mixtures in enhanced imbibition experiments.

The implementation of RFID technology for fluid characterization in the oil and gas industry is a cutting-edge field of research. This research hopefully contributes to uncovering the full potential of the use of RFID in oil recovery processes.

This thesis would not have been possible without the contribution of many people. I regret it is not possible to name them all. Prof. dr. Pacelli Zitha and Dr. Christiaan Schoemaker suggested the use of RFID technology as a promising field. Prof. ir. Cor van Kruijsdijk (TU Delft/ Shell Global Solutions) has been active in finding ways to provide financial support, without which the project would not have been as successful as it was. I thank Prof. dr. W. R. (William) Rossen and Prof. dr. J. (Hans) Bruining for supervising this thesis.
Sincere thanks must also go to the staff of Geoscience & Engineering Laboratory, with special mention of Ing. Karel Heller. Ing. Wim Verwaal gave support to indicate the safety aspects and solutions. Last but not least, I would like to thank CISC Semiconductor GmbH for the co-operation and support in providing the RFID CISC Xplorer-2000 setup. Particularly, I would like to thank Josef Preishuber-Pflüegl and Bernhard Santer.

Anas Hassan Author
Delft, November 2015

The use of RFID technology to measure dielectric coefficients of diethyl ether-oil-brine mixtures for enhanced imbibition experiments

Anas Hassan *

November 24, 2015

Contents

*TU Delft, Civil Engineering and Geosciences, Stevinweg 1, 2628 CE Delft, The Netherlands. E-mail: A.M.Hassan@student.tudelft.nl

List of Figures

List of Tables

1 Abstract

Recent developments in ultra-high frequency (800MHz-1000MHz) Radio Frequency Identification RFID devices suggest that it is possible to use RFID for wireless laboratory measurements of the dielectric coefficients of fluid mixtures with possible spin-off for use in the petroleum engineering practice. One of the major advantages of using RFID devices is the system's wireless communication protocol; wireless communication omits the use of connecting cables, which often lead to leakage problems. Another important advantage of RFID communication devices is the possibility of using tags that are small in size. In this experiment we use a tag with the dimensions $0.095 \times 0.008 \times 0.001$ m^3. The complex dielectric coefficients can be used to characterize the composition of aqueous and oleic phase mixtures. Our interest in this research is in diethyl ether-oil and diethyl ether-brine mixtures, as they are important in solvent enhanced oil recovery SEOR. As a precursor to the RFID measurements, we determined the concentration dependent partition coefficient, i.e., the ratio of the of diethyl ether concentrations in the oleic and aqueous phases, using an Anton Paar density meter. The experiments were duplicated to determine the reproducibility. In addition we measured the real part of the dielectric coefficient ε of the pure liquids (water, brine, diethyl ether and hexadecane) at $\pm 23^o$C and at a frequency range up to 15kHz. We applied the Böttcher mixing rule to determine the range of values and the sensitivity required to obtain useful information on the composition of the mixture, i.e., the effective dielectric coefficient. The phase behavior measurements are followed by simulations of the RFID setup in COMSOL^{TM} to provide an understanding of the response dependence on the presence of the tag's encasement and the thicknesses of the blocks (media) surrounding the tag. Subsequently, we continue with the experiment of using a state of the art RFID device (RFID CISC Xplorer-2000) to examine the relation between RFID response and diethyl ether volume fractions in the oleic and aqueous phase. This section begins with a detailed description of the RFID CISC Xplorer-2000 setup, theoretical background information and a specification of the measurement procedures. The output data of the measurements indicate a strong dependence between the RFID response in terms of the response parameters, i.e., the S-parameter S_{21}, the minimum power to

activate the tag, P_{min}, the backscattered radiation $P_{backscattered}$ and the tag radar cross-section ΔRCS, as a function of the dielectric coefficients surrounding the tag and at various frequencies. From the graphs where we plotted the RFID response versus the dielectric coefficient we can conclude that some frequencies show a larger dependence on the dielectric coefficient in the domain of interest than other frequencies. When plotting the RFID response versus the volume fraction of diethyl ether in the oleic and the aqueous phase, we observe that in some cases the dependence of the optimal frequency of the response versus volume fraction resulted in a curve containg one or several maxima. In this scenario more frequencies must be used to obtain a unique response result. By combining the response function at various frequencies we are able to achieve both accuracy and uniqueness. From the response functions versus the diethyl ether volume fraction in the oleic and aqueous phase plots, we could furthermore conclude that the advisable response parameter for measurements in an oil-solvent-water system is the 'minimum power at the tag position' or P_{min}. Due to the strong dependency of the RFID response on the dielectric coefficient, the system can therefore be used for identification of dielectric coefficients. Nonetheless, we need more measurements of media with dielectric coefficients ranging from 4.43 to 79.08 for the aqueous phase compositions and dielectric coefficients ranging from 2.05 to 4.43 for the oleic phase compositions to further investigate the full potential of the RFID CISC Xplorer-2000. The measurements until now, however, show feasibility of using RFID technology to determine the diethyl ether-water and diethyl ether-oil compositions.

2 Introduction

Naturally fractured reservoirs contain around 20% of the world oil reserves [27][79][77]. Oil recovery from these fractured reservoirs is generally low due to the fact that injected fluids prefer to flow into high permeable layers (fractures) rather than into the matrix layers, which leads to poor sweep efficiency and therefore a low oil recovery factor RF [35][40][51][92]. The oil recovery factor RF in the conventional recovery methods (primary and secondary) ranges between 20 and 40% [86][87]. However, the advanced methods (ternary) or enhanced oil recovery EOR can raise the RF up to 70% [33][86][43][46]. One of the most attractive applications of EOR is Chemical-EOR, which we abbrviate here as CEOR [96]. There are various methods of CEOR, such as foam and polymer surfactants injection [39][6][5][80]; however in this paper we will focus on oil recovery by solvents that are mutually soluble in water, salt solutions and oil [37][38]. Solvent-based oil recovery, which we abbrviate as SEOR, is a process whereby a solvent is injected into an oil reservoir in order to increase the macroscopic and microscopic displacement efficiency, due to a number of mechanisms such as oil swelling, oil density and viscosity reduction and wettablity alteration [99][85][55]. However, due to the high costs of solvents, SEOR only becomes economically viable for larger reservoirs and when the oil price is high. A key factor to minimize the costs in SEOR is to reduce the amount

of solvent to the minimum required amount necessary to realize optimal oil recovery. Using minimal amounts of solvent is not only economically attractive but also enhances the effectiveness of the production process. Namely, a surplus of solvent may lead to retention of the flow in the reservoir [32][33][30]. Moreover, minimizing the quantity of injected solvent would reduce the environmental impact of SEOR. For these reasons it would be very useful to be able to accurately monitor solvent concentrations in real-time from within the reservoir. This is where R(adio) F(requency) ID(entification) could potentially play an interesting role [8][42][91][98] . Some of the main benefits of RFID in this context are: wireless communication between reader and the tag and that the tag can be very small in size [67][15][98] so it could fit inside a pipeline to measure for example the solvent concentrations in the oleic phase when the oil reaches the surface. The aim of the RFID experiment is to verify the feasibility of using ultra-high frequency (800MHz-1000MHz) RFID technology to identify fluid media by providing information on the dielectric properties of the media. In a later stage of this study the feasibility is explored of using the RFID system to monitor solvent concentrations in fluid media. If this feasibility study indicates its potential to succeed, RFID technology might in the future be used in a pipeline or even in the flow of a real reservoir.

First, however, the possibility of using RFID technology must be thoroughly examined in the laboratory. A typical setup consists of an oil saturated core immersed in brine containing a solvent (diethyl ether). It is expected that RFID technology can be used to determine the concentration history of the solvent and the produced oil. Therefore, for this research it is important to determine the phase behaviour of the diethyl ether-oil-brine system, i.e., the partition coefficient of diethyl ether between the oleic and aqueous phases. Section (3) describes the use of the Anton Paar density meter DMA-4100M to determine the phase behaviour of the diethyl ether-brine-oil system and the partition coefficient at room temperature $\pm 23^o$C and 1 atmospheric pressure (103150 ± 5000 Pa). In addition we describe the measurement of the complex impedance of the pure liquids water, brine, diethyl ether, oil and various alcohols including methanol, as a function of frequencies (and temperature $\pm 23^oC$) using the insulation diagnostic system (IDAX-300) and the impedance network analyzer (Wayne Kerr precision-6640A). In section (3.2.1 and appendix A; section 7.1) we measured with the insulation diagnostic system (IDAX-300) the pure components diethyl ether, hexadecane, squalene, olive oil and several type of alcohol such as propanol, butanol, ethanol and methanol. In section (3.2.2 and appendix A; section7.2), the complex impedance is used to derive the complex dielectric coefficient of the pure components constituting the mixture (water, salt solutions with different salinity 1mM, 2mM, 5mM and 0.5M). The data obtained with the impedance network analyzer is compared with a theoretical model [13][14] (section 3.2.2 and appendix A; section 7.2.4) that derives the complex dielectric coefficient for electrolytes while correcting the electrode polarization in the low frequency regime. Section (3) ends with the Böttcher [10][82] mixing rule (section 3.3.1) (Eq.5). The Böttcher mixing rule is used to estimate the effective dielectric coefficient of mixtures of the diethyl ether-brine-oil system

as a function of composition (Eq.5). The dielectric coefficient in absence of salt in the diethyl ether-brine-oil mixture ranges between 4.43 and 79.08, while the dielectric coefficient between diethyl ether and hexadecane varies between 4.73 and 2.05 at $\pm 23^{o}C$.

Section (4) presents three models of RFID setups simulated in COMSOL^{TM} and derives the relevant model equations (details of the derivation are presented in appendix B; section (8.6). Model-1 consists of a receiving Rx antenna (port-2) and a transmitting Tx antenna (port-1) mounted on a square sheet with a constant dielectric coefficient and zero conductivity. The transmitting antenna Tx consist of a conducting part and lumped port (50Ω) and an inductor ($66nH$). The receiving antenna Rx is a copy of the transmitting antenna Tx except the lumped port does not have power source. Model-2 consists of a RFID tag, which replaces the receiving antenna Rx. The RFID tag is a meandering "micro" dipole antenna and element of constant impedance $Z = 11 + j143\ \Omega$ at 951MHz. Model-3 keeps the receiving antenna Rx as port-3 and places the RFID tag (port-2) between the antennae. With this setup we measured S_{21} and S_{11} in the first and second models as function of the frequency and the dielectric coefficients of the material surrounding the tag, and additionally S_{31} in the third model. The scattering parameters are the ratio of the voltage on the Rx antenna or tag and the input voltage to the Tx antenna. Section (4)also describes the numerical models and presents numerical results for the three RFID models as function of frequency and dielectric coefficients. The model equations are solved with the help of COMSOL^{TM}, a commercial finite element software package.

Section (5) describes the experimental setup. The CISC RFID Xplorer-2000 setup consists of a reader, a Tx antenna, a Rx antenna and a tag. The reader sends a high frequency voltage to the Tx antenna via a coaxial cable and measures the voltage at the Rx antenna. The tag is mounted at a distance of 0.5 meter from the reader antennae, which represents the far field. In addition, we describe the measurement process and measurement results of Xplorer-2000. In section (5.6) we discuss the experimental results in view of the computed results with COMSOL^{TM}, and determine the level of sensitivity of the RFID CISC Xplorer-2000 setup to enable identification of the dielectric coefficients of the solutions (media) surrounding the tag. In section (10.3.3) we end with some conclusions.

3 Phase behavior

This section describes the behavior of phases in a system of diethyl ether-brine-oil in terms of the diethyl ether concentration distribution in the aqueous and oleic phase and the dielectric coefficient for both phases of both pure components and the mixture of these components (effective dielectric coefficient).

3.1 Partition coefficient

Phase behavior can be characterized by the partition coefficient, also known as the distribution coefficient; one of the most important physical properties of compounds [90][53][83][44][16][93]. The partition coefficient is the ratio between the amounts of diethyl ether in the oleic phase and the aqueous phase [49][53][84][76]. This ratio can be expressed as the concentrations ratio ($\frac{mole}{liter}/\frac{mole}{liter}$) or as a mole fraction ratio. The ratio is influenced by the intermolecular forces between the solvent in the oleic phase and in the aqueous phase at equilibrium conditions [44][85][89][3]. The thermodynamic condition for the partition coefficient $K_{oleic,aqueous}$ of diethyl ether between the oleic phase and the aqueous phase at a constant temperature can be defined by

$$K_{oleic,aqueous} = \frac{C_{oleic}}{C_{aqueous}} \; [\frac{mole}{liter}/\frac{mole}{liter} \text{ or } \frac{mole}{kg}/\frac{mole}{kg}], \tag{1}$$

where, C_{oleic} and $C_{aqueous}$ are the concentrations of the diethyl ether in the oleic phase and the concentration of the diethyl ether in the aqueous phase respectively.

The partition coefficient has an important impact on the recovery factor for solvent-based enhanced oil recovery SEOR processes [25][44]. Various parameters affect the partition coefficient, such as temperature and salinity. For example, with an increase in temperature the partition coefficient will increase as well [47][76][78]. In case of salt solutions NaCl, increasing the salt concentration decreases the concentration in the aqueous phase and consequently increases the partition coefficient due to the salting out effect [4][3][72]. The salting out effect is an effect based on the electrolyte-nonelectrolyte interaction, in which the non-electrolyte could be less soluble at high salt concentrations (ionic strength I) [4][19][93].

The partion coefficient must be determined experimentally. We used a DMA-4100M Anton Paar density meter to accomplish this. First we created a curve for the oleic phase where we measure the density of diethyl ether-hexadecane mixtures of known compositions versus the weight fraction of diethyl ether in that mixture. Likewise, we created three curves for the aqueous phase, where we measure the density of diethyl ether-brine mixtures at zero salinity (demineralized water), low salinity brine 0.05M NaCl and brine 0.5M NaCl versus the diethyl ether concentration. From these four curves, the density of the mixtures was converted to partial molar volume and the diethyl ether weight fraction is converted to the mole fraction of diethyl ether in the oleic and aqueous phases. These resulting values formed the calibration curve for the subsequent density measurements. For the subsequent measurements we mixed brine (0.05M and 0.5M), hexadecane and diethyl ether. The mixture was left for 24 hours in order for the system to attain equilibrium. From the system, samples were extracted from both the oleic and aqueous phase, which densities were measured with the density meter. We used the reference curves to calculate the respective diethyl ether mole fractions. The ratio of the mole fractions of diethyl ether in oleic and

Component	NaCl	NaCl	NaCl	Solub.ether	Temp
[name]	[g/l]	[M]	[ppm]	[g in 100g]	[^{o}C]
Demi-water	0	0	0	6.5	22.96
Low salinity	2.92	0.05	2922	6.1	22.94
Brine	29.2	0.5	29221	5.6	22.98

Table 1: Solubility diethyl ether in water and salt solutions

aqueous phase determines the partition coefficient. The experimental procedure was repeated in the same manner for all aqueous phases (demineralized water, low salinity water 0.05M, and brine 0.5M). By adding solutions with varying levels of salt concentrations to the experiment, the effect of salinity on the patrition coefficient measurement can be examined. In the following parts of this section, the procedure of determining the partition coefficient is described in more detail.

3.1.1 Determining the maximum full solubility of diethyl ether

In order to be able to determine the partition coefficient, diethyl ether must be partly miscible both in the oleic and aqueous phase. Therefore it is essential to first determine the maximum full solubility of diethyl ether in different aqueous solutions. In this experiment the maximum solubility was obtained by performing a solubility test in which increasing levels of diethyl ether (0.5%,1%,1.5%, etc.) were added to the separate solutions, up to the point when a meniscus became visible, indicating the existence of two phases. The solubility test was set up as follows. The main solution was placed in a container and was subsequently weighed. By establishing the initial volume of the solution, evaporation of diethyl ether could be quantified and an appropriate correction could be made. To the weighed container filled with solution increasing amounts of diethyl ether were added. The container was then placed in a shaking-machine and was shaken for a period of 24 hours, after which it is assumed that a homogeneous equilibrium mixture has been established. After the shaking process the mixture was weighed again to review the volume, after which the density was determined. The measurements of each container were repeated three times, at three different locations in the container to verify reproducibility. From the solubility test the following weight percentages of diethyl ether were measured as the level of maximum full solubility at room temperature ($\pm 23^o$C): 6.5% in water, 6.1% in water with low salinity and 5.6% in brine. Note that when diethyl ether is cooled down the solubility increases. Diethyl ether is always fully soluble in oil. (Tab.1) shows the measured solubility of diethyl ether in water and salt solutions. (Fig.1)plots literature data on solubility [88] $S = S_{296.15}$ obtained from

$$\ln S/S_{288.15} = -\frac{\Delta H}{R}\left(\frac{1}{T} - \frac{1}{288.15}\right), \tag{2}$$

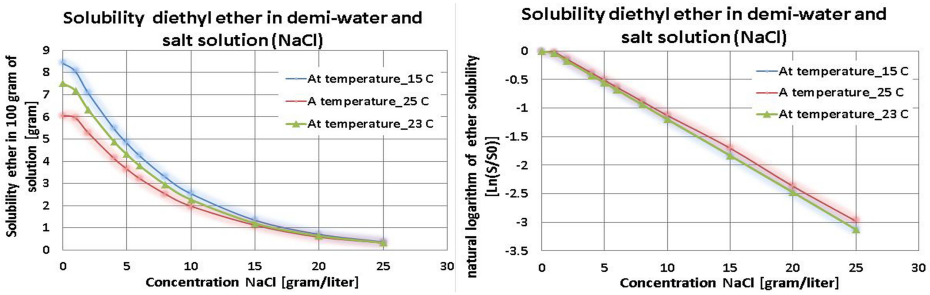

A. Diethyl ether solubility in salt water NaCl

B. Solubility semilogarithmic plot

Figure 1: Literature data of the solubility at 15, 23 and 25^{o}C

where $\Delta H/R$ is obtained by using the solubility $S_{288.15}$ at 288.15°k (or 15^{o}C). Here the calculated enthalpy ΔH= 10290.67 at T= 296.15°k and the gas constant R= 8.314 [88][83][54].

3.1.2 Establishing calibration curves

With the maximum full solubility of the diethyl ether in the main solutions known, the next step in the experiment is to measure the density of the binary mixtures (diethyl ether-hexadecane, diethyl ether brine (0M, 0.05M and 0.5M) with increasing levels of diethyl ether fractions at $\pm$23^{o}C. For the aqueous phase, the concentrations were kept equal or below the solubility limit of diethyl ether. As a result we established four curves, i.e., three for the aqueous phase for each level of salinity and one for the oleic phase (hexadecane-diethyl ether). As diethyl ether is volatile and can evaporate easily (boiling point at 34^{o}C) the measurements were performed in a closed system (Fig.2). The closed system was formed by a combination of a sealed glass tube and a metal syringe. In the sealed glass tube a known amount of the aqueous or oleic phase was placed. These known amounts of aqueous or oleic phase, were mixed with known amounts of diethyl ether to obtain the binary mixtures. The purpose of the metal syringe is to reduce the loss of ether in the system; a plastic syringe cannot be used as diethyl ether reacts with plastic.

This reaction would lead to changes in the composition of the binary mixture. The evaporation of diethyl ether can be slowed down by refrigeration, therefore in this stage the diethyl ether was cooled down to 0^{o}C in an ice container. The oleic and aqueous phases were used at $\pm$23^{o}C, at 1 atm. As in the solubility test, first the pure solution was placed in a chemically-resistant sample tube and weighed to determine the initial volume of the solution. To the weighed sample tube filled with solution, increased amounts of diethyl ether were added. In the case of the aqueous phase, the levels of diethyl ether were increased each time by weight percentages of 1% in brine (0.5% in the case of pure water), from 0% till the maximum solubility of diethyl ether in the pure components (water 6.5%, low salinity water 6.1% and brine 5.6%). Since diethyl ether is soluble

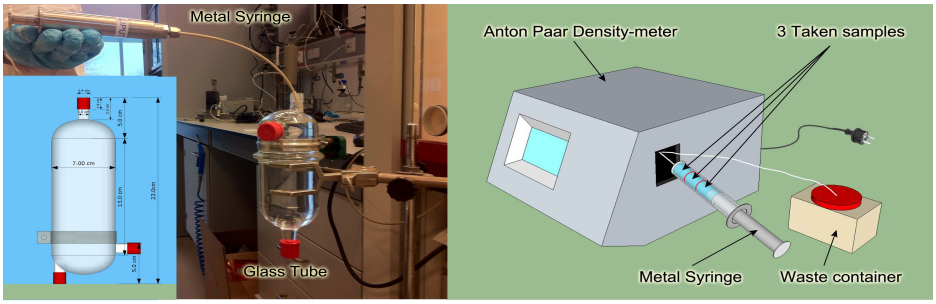

Figure 2: Closed system and establishing calibration curves (density-meter)

in oil at all proportions, in the oleic phase weighed percentages of diethyl ether were added from 0% up to 25%. After the preparation of each binary mixture, the sample tube was weighed and placed in a shaking-machine to be shaken for a period of 24 hours in order to achieve the most homogeneous solution possible. Subsequent to the shaking process, the mixture was weighed again to check the volume and detect possible errors in the volume of the mixture due to loss of ether. Now, the density of the mixture could be measured. The metal syringe is used again to take a sample of the binary mixture from the sample tube. The syringe was then attached to the density meter. The volume in the syringe is sufficient for three measurement samples. These samples were taken from three different locations within the syringe to test reproducibility (Fig.2). The measurements for each binary mixture were processed in four separate curves, where the density of the binary mixture was plotted against the concentration of diethyl ether in the solution. These curves however did not demonstrate a clear linear relation. Therefore, the density in grams per cubic meter [g/m^3] was converted to molar density in mole per cubic meter [mole/m^3]. The molar density was subsequently converted to partial molar volume, which is the inverse of the molar density. The converted values form linear curves representing the partial molar volume versus the diethyl ether mole fraction in the oleic and aqueous phases; these were used as our calibration curves. Note that the experimental measurement results of the calibration curves were compared with Aspen plus simulation results.

3.1.3 Experiment: determining the partition coefficient

After the calibration curves of diethyl ether concentrations in all aqueous phases (demineralized water, low salinity water 0.05M and brine 0.5M) and oleic phase (hexadecane) were established, the next step in the experiment was to determine the partition coefficient of diethyl ether between the aqueous and oleic phase. The setup in this stage of the experiment was similar to that of the previous stage. The conditions of the experiment were $\pm 23^o$C and 1.0 ± 0.05

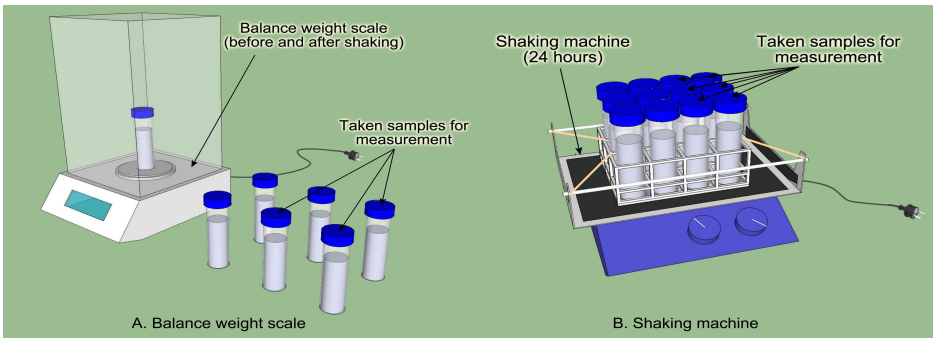

Figure 3: Balance weight scale and shaking machine (24hrs)

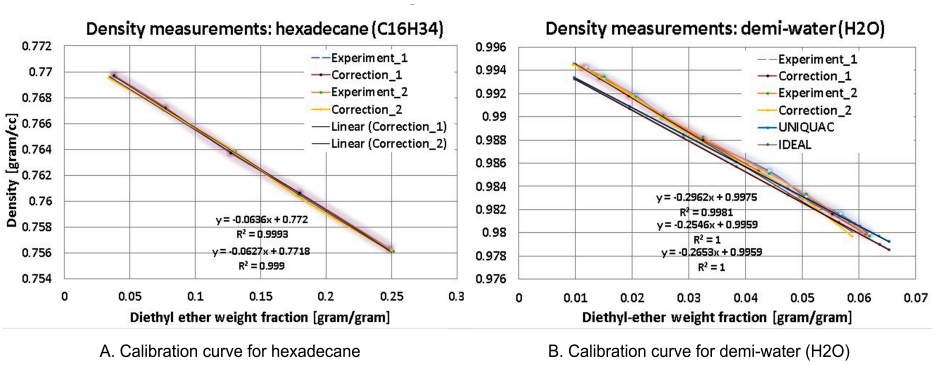

A. Calibration curve for hexadecane

B. Calibration curve for demi-water (H2O)

Figure 4: Density measurements for hexadecane and demi-water

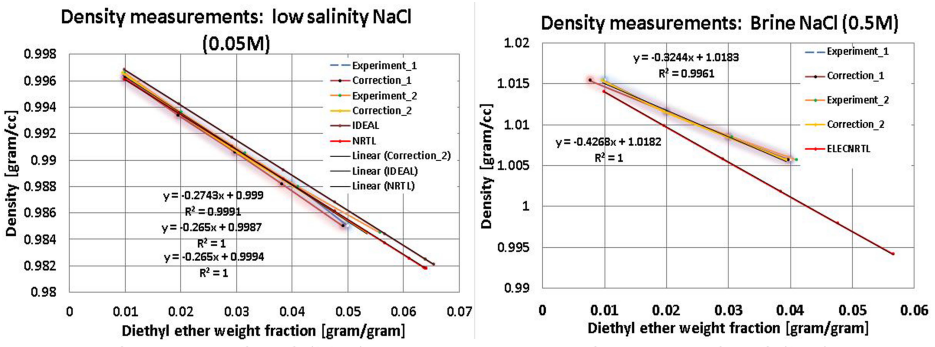

A. Calibration curve for NaCl (0.05M)

B. Calibration curve for NaCl (0.5M)

Figure 5: Density measurements for low salinity brine 0.05M and brine 0.5M

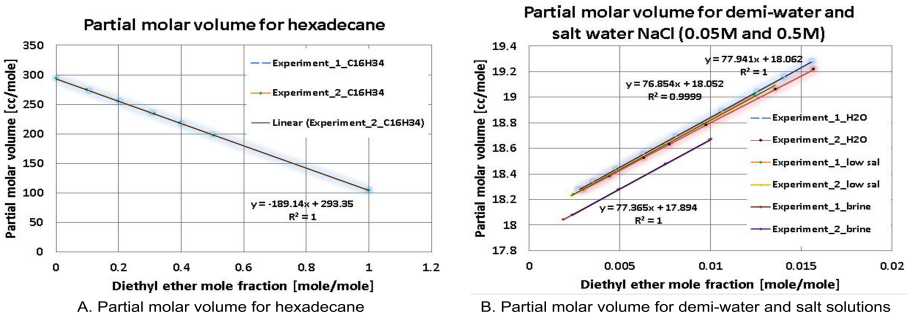

Figure 6: Partial molar volume calibration curves (oleic and aqueous phase)

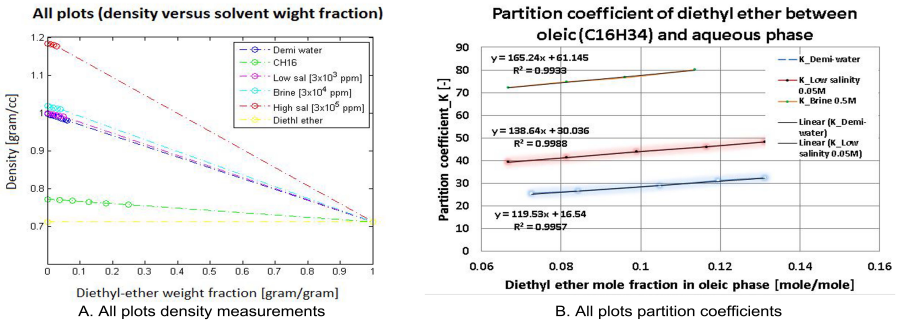

Figure 7: Partition coefficients between oleic and aqueous phase

atm, except for the diethyl ether, which was cooled down to 0^oC to minimize ether loss due to evaporation. The density meter was equipped with a temperature reader set at 23^oC. Again, the measurements were performed in a closed system to reduce the loss of diethyl ether and to hopefully improve the accuracy of the measurements; however this time the binary mixtures were prepared two times in order to ensure reproducibility of the measurements. In addition, the oleic phase was added to the binary aqueous mixture in equal proportions (50% aqueous mixture volume and 50% oleic phase volume). This research operates under the assumption that oil and water do not mix. As a result we have a mixture that consists of two phases (oleic and aqueous phase) and three components (e.g. brine, oil and solvent). This new mixture was shaken for 24 hours to generate a homogeneous equilibrium solution (Fig.3). Like before, the mixture was weighed to see the error due to the loss of diethyl ether. The metal syringe was used again as in the previous stage (calibration curve), however at this stage samples were taken from the top part of the new mixture (oleic phase) and from the bottom part (aqueous phase). A long needle was used to avoid contamination of the aqueous sample drawn from the bottom part. The

C16H34-exp1				
Diethyl ether	ρ	Mav	ρ-mole	V-mole
mole fraction	[g/cc]	[g/mole]	[mole/cc]	[cc/mole]
0	0.7717	226.446	0.003407	293.4378
0.107526333	0.7697	210.067	0.003664	272.9209
0.203938951	0.7672	195.381	0.003926	254.6681
0.308516322	0.7637	179.451	0.004255	234.9768
0.401293317	0.7606	165.319	0.004601	217.3543
0.502812999	0.7563	149.855	0.005046	198.1434
1	0.7108	74.1228	0.009589	104.2808

Table 2: Partial molar volume (Hexadecane)

H2O-exp1				
Diethyl ether	ρ	Mav	ρ-mole	V-mole
mole fraction	[g/cc]	[g/mole]	[mole/cc]	[cc/mole]
0	0.9974	18.0152	0.055364	18.0622
0.002727674	0.9942	18.1683	0.054721	18.2743
0.003535811	0.9933	18.2136	0.054535	18.3365
0.004795950	0.9918	18.2843	0.054243	18.4355
0.006324653	0.9901	18.3701	0.053891	18.5556
0.008112758	0.9880	18.4704	0.053490	18.6948
0.010630815	0.9853	18.6117	0.052939	18.8894
0.012562696	0.9831	18.7201	0.052515	19.0419
0.014064003	0.9816	18.8043	0.052201	19.1568
0.015608624	0.9799	18.8910	0.051871	19.2785
1	0.7108	74.1228	0.009589	104.2808

Table 3: Partial molar volume (demi-water)

densities of these samples were measured by the density meter (Fig.4 and Fig.5). The measured mass density was first converted to a molar density, and then to a molar volume in order to use the calibration curves (Fig.6). We extracted the solvent concentration in the aqueous and oleic phase from the previously established calibration curves. The ratio of the diethyl ether concentration in oleic phase divided by the concentration of diethyl ether in the aqueous phase is the partition coefficient (Fig.7). Tables (Tab.2,3,4 and 5) show the values of partial molar volume of hexadecane, demi-water, low salinity brine (0.05M) and brine (0.5M) respectively.

NaCl(0.05M)-exp1				
Diethyl ether	ρ	Mav	ρ-mole	V-mole
mole fraction	[g/cc]	[g/mole]	[mole/cc]	[cc/mole]
0	0.9991	18.0357	0.055395	18.0519
0.002466575	0.9962	18.1704	0.054814	18.2433
0.004816951	0.9934	18.3058	0.054266	18.4274
0.007398473	0.9906	18.4506	0.053689	18.6257
0.009555187	0.982	18.5716	0.053210	18.7933
0.01241423	0.9850	18.7319	0.052583	19.0172
1	0.7108	74.1228	0.009589	104.2808

Table 4: Partial molar volume (Low salinity brine 0.05M)

NaCl(0.5M)-exp1				
Diethyl ether	ρ	Mav	ρ-mole	V-mole
mole fraction	[g/cc]	[g/mole]	[mole/cc]	[cc/mole]
0	1.0178	18.216	0.05587	17.8974
0.00190047	1.0154	18.3222	0.05541	18.0443
0.00498346	1.0116	18.4946	0.05469	18.2825
0.00753824	1.0085	18.6374	0.05411	18.4803
0.00155834	1.0057	18.7781	0.05355	18.6717
1	0.7108	74.1228	0.00958	104.280

Table 5: Partial molar volume (Brine 0.5M)

Component	Coefficient (a)	Coefficient (b)
C16H34-exp1	-189.08	293.29
C16H34-exp2	-189.14	293.35
H2O-exp1	77.914	18.062
H2O-exp2	72.064	18.057
NaCl(0.05M)-exp1	77.687	18.052
NaCl(0.05M)-exp2	76.854	18.052
NaCl(0.5M)-exp1	76.988	17.899
NaCl(0.5M)-exp2	77.365	17.594

Table 6: The coefficients of the polynomial

3.1.4 Experimental results

The results were plotted in terms of the molar volume versus the mole fraction of diethyl ether in demi-water, low salinity water 0.05M NaCl, brine 0.5M NaCl and hexadecane. As mentioned previously, the advantage of using the molar volume is that the plots are more or less straight lines. To obtain the molar volume we need to convert the mass density to molar density. To achieve this, we divide the measured mass density by the mole fraction averaged molecular weight [83], i.e. $M_{av} = \sum_i x_i M_i$, where x_i is the mole fraction and M_i is the molecular weight of species i. The inverse of the molar density is the molar volume. (Fig.6) shows the plot of the molar volume for mixtures of diethyl ether with demi-water, low salinity brine 0.05M, brine 0.5M and hexadecane. We observe that the curves are more or less straight lines and can be accurately represented by a second order polynomial. (Fig.6) summarizes all calibration curves. The coefficients of the polynomials obtained that plot the mole fraction versus the molar volume are summarized in (Tab.6). To obtain the partition coefficient K, we use the measured mass densities of diethyl ether in the aqueous phase in equilibrium with diethyl ether in the oleic phase. The measured mass density must be converted to a molar density, and then to a molar volume to use the calibration curves. The procedure is as follows: (1) we use a first estimate of the mole fraction, (2) we use this estimate to obtain the molar density as the mass density divided by the mole fraction averaged molecular weight, (3) we use the coefficients in (Tab.6) to obtain the improved mole fraction value, (4) we repeat steps (2-3) iteratively until the estimated mole fraction and the improved mole fraction value are the same. We divide the mole fraction in the oleic phase by the mole fraction in the aqueous phase, which is the partition coefficient. (Fig.7) plots the partition coefficients between oil and demi-water, low salinity water, brine and high salinity water respectively, versus the mole fraction of diethyl ether in the oleic phase.

The relative error The error of the partition coefficient depends both on the measurement error in the aqueous phase mass density and the measurement er-

ror in the oleic phase mass density obtained by the density meter measurements and the corresponding calibration curves, i.e.,

$$\frac{\Delta K}{K} = \sqrt{\left(\frac{\Delta C}{C}\right)^2_{aqueous} + \left(\frac{\Delta C}{C}\right)^2_{oleic}} \tag{3}$$

where, ΔK/K is the error in the measurement of the partition coeffcient. We assume that no error stems from vaporization. Also the composition in terms of mole fraction can be obtained accurately. Therefore, the only place where a measurement error may occur is in the mass density, which we assume to be the least significant digit in the measured density values. The density measurement error $\Delta\rho = 0.0001\ \left[\mathrm{g/cm}^3\right]$. We can use a Monte Carlo method (Barreto, Evensen, Niederreiter) to determine the errors $(\Delta C/C)_{aqueous}$ and $(\Delta C/C)_{oleic}$. We add an error to the measured density values, which is drawn from a normal distribution. In EXCEL this can be accomplished by adding NORMINV $(rand(), 0, sd)$, where $rand()$ represents a uniformly distributed random number, 0 represents the average error, and sd= 0.0001 is the standard deviation. We generate in this way more calibration curves in addition to the previously established calibration curves. Also, we randomly perturb the measured data. We use the calibration curves to obtain the concentrations in the solutions, which have diethyl ether dissolved in the aqueous and oleic phase. The square root of the variance of the diethyl ether concentrations determines the standard deviations ΔC; the average of the diethyl-ether concentration determines C. From ΔC and C we can determine the relative error of the partition coefficient. In case of a demi-water, diethyl ether and hexadecane mixture, the relative error of the partition coefficient is the following:

$$\begin{aligned}\frac{\Delta K}{K} &= \sqrt{\left(\frac{0.00105061}{0.08175452}\right)^2_{Demi-water} + \left(\frac{0.00303992}{0.08175452}\right)^2_{Hexadecane}} \\ &= 0.023985372 \approx 2.4\%\end{aligned} \tag{4}$$

3.2 Dielectric coefficient

In this subsection we measure the real part of the dielectric coefficient of the pure components of the system (oil, diethyl-ether, alcohol, water and salt solution) as function of frequencies (and temperature $\pm 23^{\circ}$C). For the components oil, diethyl ether and alcohol we used the insulation diagnostic system (IDAX-300); the water and salt solutions were measured with the impedance network analyzer (Wayne Kerr precision-6640A). Subsequently, we used the Böttcher mixing rule to calculate the effective dielectric coefficients in specific mixtures with a known composition.

3.2.1 Insulation diagnostic system (IDAX-300)

Dielectric materials (insulators) were measured and analyzed with an insulation diagnostic system (Megger IDAX-300). The IDAX system measures the

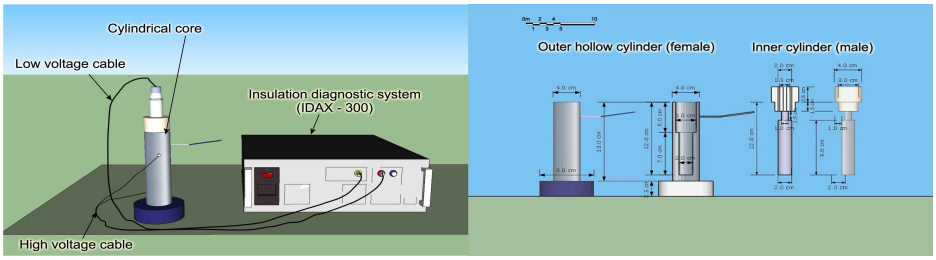

A. Insulation diagnostic system (IDAX=300) 3D view

B. Insulation diagnostic system (IDAX=300) section

Figure 8: Insulation diagnostic system (IDAX300)

Component	Formula	ε	temp
[name]	[-]	[-]	[°C]
hexadecane	C16H34	2.05	22.74
Squalene	C30H50	3	22.74
Diethyl ether	C4H10O	4.43	22.74
Propanol-2	C2H6-CHOH	17	22.74
Butanol	C4H5-OH	18	22.74
Ethanol	C2H5-OH	25	22.74
Methanol	CH3-OH	30	22.74

Table 7: Measured dielectric coefficients obtained from IDAX-300

impedance at different frequencies. The system applies a sinusoidal voltage (200V) with desired frequency range (up to 15kHz) over the sample (medium). This voltage will generate a current in the medium. By measuring the voltage and current, the sample impedance can be calculated; Z=(V/I) where Z, V and I represent the complex impedance, voltage and current respectively. Depending on the sample, several parameters can be calculated such as $\tan(\delta)$ (dissipation factor), capacitance, resistance etc. Through an external amplifier that is connected to the system, it is possible to repeat the measurements with different power (voltage) levels at specific frequencies [D*]. From the measured insulation impedance, the dielectric coefficients can be calculated at (± 23°C). We measured with this technique the pure components diethyl ether, hexadecane, squalene and several type of alcohol such as propanol, butanol, ethanol and methanol. The insulation diagnostic system (IDAX-300) is depicted in (Fig.8). The results of the measured dielectric coefficients in the media air, hexadecan, squalene, olive oil, diethyl ether and several type of alcohol are summarized in (Tab.7). More information regarding the setup and the measurement process are given in section (7.1).

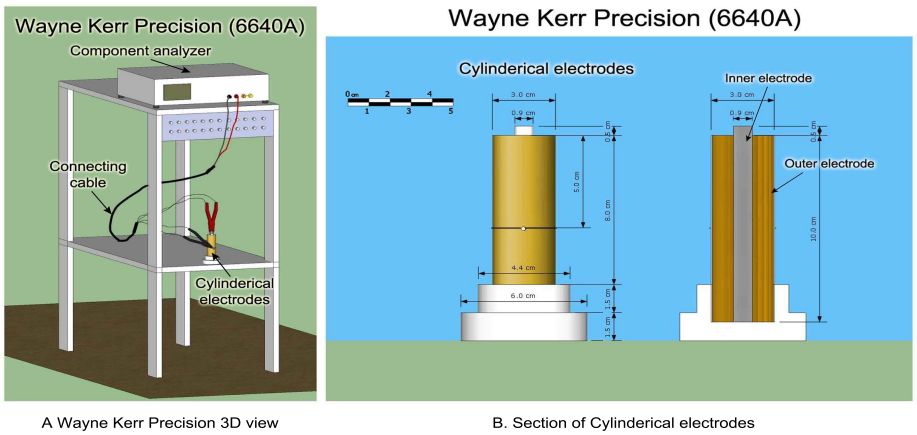

Figure 9: Wayne Kerr Precision (6640A)

3.2.2 Impedance analyzer (Wayne Kerr precision-6640A)

An impedance network analyzer is a device which measures the complex impedance Z^* of a medium. The impedance network analyzer used in this experiment is the Wayne Kerr precision-6640A; a one-path two port measuring network analyzer that covers a frequency range of 200Hz to 1000MHz at $\pm 23°C$. The data obtained with Wayne Kerr precision-6640A (the amplitude and phase as a function of the frequency sweep) is used to calculate the electric permittivity and the conductivity. Later on, the values of the calculated electric permittivity and the conductivity are compared with the analytical model ([13] and [14]) (section 7.2.4) for validation. In this part the permittivity and conductivity of the freshwater and saltwater with varying levels of salinity (1mM, 2mM, 5mM, and 0.5M) are determined. The impedance network analyzer (Wayne Kerr precision-6640A) is depicted in (Fig.9) and the results of the calculated dielectric coefficients are shown in (Fig.10,11 and 12). More information regarding measurement processes, model equations and model correction for electrode polarization can be found in section (7.2).

3.3 Mixing rules

Mixing rules are used to obtain the dielectric coefficients of mixtures. The assumption here is that a mixture responds to electromagnetic energy as if it were a homogeneous substance [82][10]. In this research we try to determine both the dielectric coefficient ε of simple media (linear, isotropic and homogeneous) and the effective dielectric coefficient ε_m of heterogeneous media (two-phase solution). The range of dielectric constants ε that can be expected will be estimated using the Böttcher equation, which will be given in the next section.

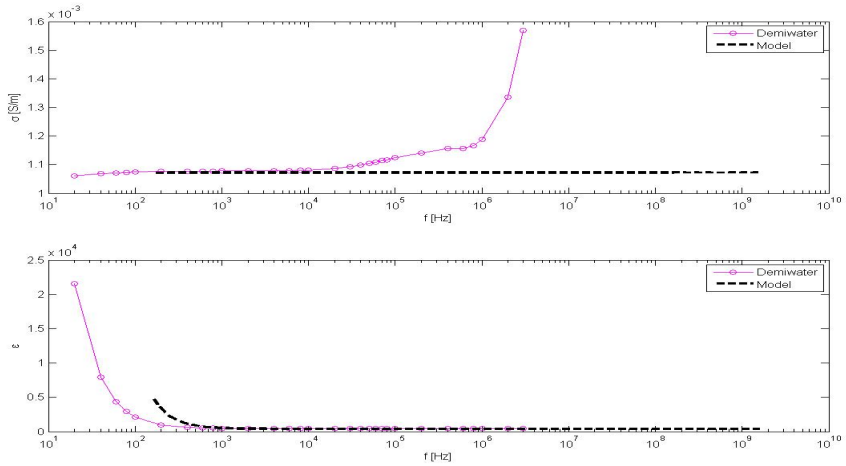

Figure 10: Measured dielectric coefficient of pure water

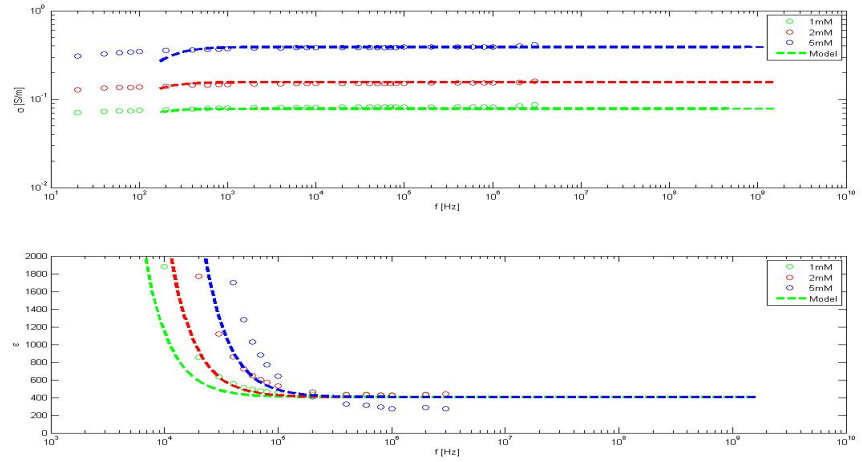

Figure 11: Measured dielectric coefficient of low salinity water 1,2,5mM

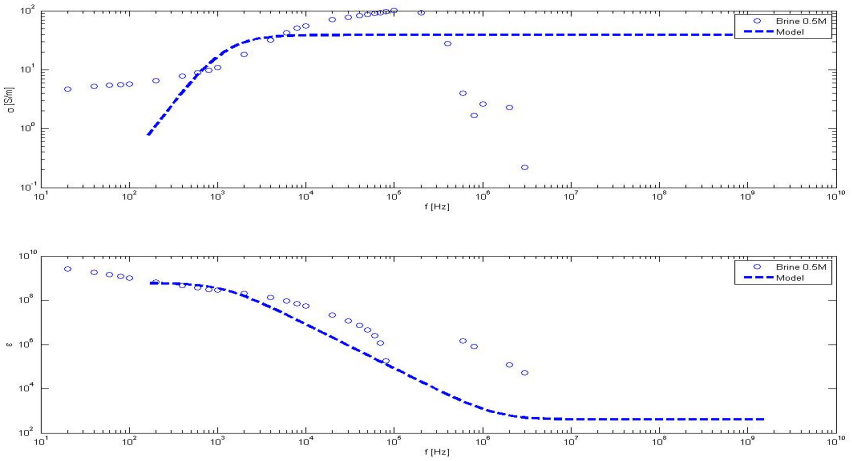

Figure 12: Measured dielectric coefficient of brine 0.5M

3.3.1 Böttcher equation

The following equation is the Böttcher equation:

$$\frac{\varepsilon_1 - \varepsilon_m}{\varepsilon_1 + 2\varepsilon_m} \upsilon_1 + \frac{\varepsilon_2 - \varepsilon_m}{\varepsilon_2 + 2\varepsilon_m} \upsilon_2 = 0, \tag{5}$$

where υ_1, υ_2 [-] are the volume fractions, ε_1 is the dielectric coefficient of water, ε_2 is the dielectric coefficient of diethyl ether and ε_m is the effective dielectric coefficient of the mixture. The volume fractions $\upsilon_{1,}$ $\upsilon_{2,}$ can be calculated as the molar density of the component in the mixture divided by the molar density of the pure component.

The dielectric coefficient of demineralized water is calculated to be 79.08414768, as derived from the following equation:

$$\varepsilon = EPS(T, 10) + \frac{a_0 \ln(a_1 + P)}{(a_1 + 10)}. \tag{6}$$

In the above equation $EPS(T, 10) = \varepsilon(T, P)$ is the dielectric constant (epsilon EPS) of water at a temperature T in Kelvin (°k) and a pressure of 10MPa and P is the pressure in units of MPa. Note that, at T= 298.15°k (25°C) the corresponding a_0 and a_1 are 14.1113 and 341.5902 respectively [28].

The dielectric coefficient of diethyl ether is given by [95]

$$\varepsilon = 4.235 - 0.0198\,(T - 25) + 5 \times 10^{-5}\,(T - 25)^2\,. \tag{7}$$

From the above equation we calculate that the dielectric coefficient of diethyl ether is 4.739 (at 23°C). The dielectric coefficient of hexadecane is given in [94][68]

$$\varepsilon = -1.24364 \times 10^{-3} T + 2.4176. \quad (8)$$

From the above equation we calculate that the dielectric coefficient of hexadecane is 2.049356014 (at 23°C).

As mentioned previously, the partition coefficient gives the ratio of concentrations in the oleic phase and the aqueous phase. As the partition coefficient is larger than one, it can be expected that the concentration of diethyl ether in the oleic phase is larger than in the aqueous phase. Therefore, we expect a larger effect of the dielectric constant in the oleic phase than in the aqueous phase. The maximum weight fraction of diethyl ether in the aqueous phase is 0.06 (minimal weight fraction of water 0.94). We obtain:

$$\upsilon_E = \frac{w_E \rho_{mix}}{\rho_E},\ \upsilon_W = \frac{w_W \rho_{mix}}{\rho_W}, \quad (9)$$

where ρ_{mix} is the mass density of the mixture, w_E (w_W)is the weight fraction of diethyl ether (water), and ρ_E (ρ_W) is the pure mass density of diethyl ether (water). Substitution of (Eq.5) shows that the dielectric coefficient of the mixture (with 0.6 diethyl ether weight fraction) is 70.2145, with respect to ε = 79.08414768 for demi-water at T= 296.15K. The partition coefficient for diethyl ether in the water-hexadecane mixture ranges between 32-25 [-]. Note that diethyl ether and hexadecane can mix in all proportions.

4 Numerical computation (COMSOL simulation)

In this simulation three RFID models were developed using COMSOL^{TM} Multiphysics, which enables analyses of a general RFID tag including substrate, antenna, chip geometry and media properties surrounding the tag. The aim of the COMSOL^{TM} simulation is to measure the scattering parameters (S-parameters) as a function of dielectric coefficient (1-80) and frequency (500-2000MHz); and to provide an understanding of the S-parameter (S_{21}) response dependence on the presence of the tag's encasement and the thickness of the blocks (media) surrounding the tag. In COMSOL^{TM} the encasement was simulated by means of a substrate on which the tag was mounted. The effect of different media surrounding the tag on the S-parameters was simulated by placing the tag in various blocks with different dielecric properties (1-80). In later simulations the thicknesses (volumes) of the blocks surrounding the tag was increased (0.01-0.1m) to examine the possible effect of medium volume on the S-parameters. In the simulation three models were simulated, which are described later in this section, followed by the theory and model equations and finally the results of the simulation. Firstly however, the concept S-parameters will be defined in more detail.

4.1 Scattering parameters (S-parameters)

The scattering parameters or S-parameters, in the most basic sense describe the input-output voltage ratio between ports in an electrical system. A port is any place to which voltage and current can be delivered. In a two-port system, the ports are simply labelled port-1 and port-2; in a multi-port network, ports are usually labeled with letters (S_{ij}; port-i and port-j). For the S-parameter subscripts 'ij', 'j' is the port that is excited (the input port), and 'i' is the output port. Thus, the S-parameter S_{11} represents the ratio of signal (voltage) that reflects from port-1 for a signal incident on port-1; S_{21}refers to the ratio of the input-voltage of port-2 to the output-voltage of port-1. S-parameter response is expressed in terms of decibel, i.e., $10 \times log_{10}(S_{11})$ dB. Note that, S-parameter response varies with frequency [81][41][24][11].

We proceed to describe the RFID Xplorer-2000 system. This system has a two-port system with separate transmitting antenna Tx and receiving antenna Rx (bistatic configuration). The reader is a device connected with two 50Ω coaxial cables to the transmitting Tx and receiving antenna Rx. The reader contains the electric circuit with a power source (battery) which is connected to the emitting antenna and an impedance circuit, which is connected to the receiving antenna Rx and allows an input and output voltage measurement. Therefore, in this system port-1 (the Tx antenna) is the terminal where the power that is transferred from the reader to the Tx antenna is measured. The tag acts as a re-emitting (unmodulated or modulated received signal) antenna and is not connected to the reader. Port-2 is connected to the Rx antenna and is the terminal where the voltage is measured that is received by the Rx antenna. Since the system is calibrated, we assume that the voltage transferred from the reader is equal to the voltage transmitted by the Tx antenna and the voltage received by the Rx antenna is equal to the voltage received by the reader. With the RFID Xplorer-2000 setup we measure S_{21}, the voltage ratio between the output voltage from port-1 (Tx antenna) and the input voltage from port-2 (Rx antenna; receives signals from both the emitting antenna and from the tag). However, in the COMSOL^{TM} simulation we simulate a three ports system. We measure S_{11}, which is the voltage ratio of emitted and received output in port-1, S_{21}, which is the voltage ratio of received antenna output from the tag (port-2) and the emitted voltage from port-1, and S_{31}; the voltage ratio between receiving antenna output in port-3 and emitting antted voltage from port-1. For instance, if $S_{31} = 0$dB implies that all the voltage delivered to port-1 ends up at the terminals of port 3. If $S_{31} = -10$dB, then 1 Watt (or 0dB) is delivered to port-1, then -10dB (0.1 Watts) of voltage is received at antenna 3. Note that in COMSOL^{TM}, when we measure the voltage scattered back from the tag, we measure the voltage of an unmodulated signal, unlike the backscattered signal in the RFID Xplorer-2000 setup.

4.2 RFID Model descriptions

This section describes the COMSOL^{TM} models for the operation of the radio frequency identifier. The first model (Fig.13) consists of a transmitting Tx antenna and a receiving Rx antenna. The Tx antenna is constructed from a ring with an inner radius of 0.033m and an outer radius of 0.036m. The ring is intersected with a strip with width 0.002m and a height of 0.08m, creating a gap of 0.002m at the top and the bottom of the ring. The resulting object consist of two half rings with a gap of 0.002m. On the lower end point of the left half ring we attached a plate with a height of 0.006m and width of 0.002m where the top right corner coincides with the edge of the ring. Symmetrically, we do the same for the right half ring. In the middle of the upper gap we place a strip with a height of 0.00125m and width of 0.002m. At the lower gap we place a strip between the end points of the attached plates with dimensions of 0.00125m height and 0.002m width. In both antennae, the lower strip has an impedance of $Z_1 = V_1/I_1 = Z_2 = V_2/I_2 (Z_l = 50\Omega)$ and the upper strip has an inductance of $L_1 = L_2 = 66$nH. In the Tx antenna we apply a voltage $V_e(1V)$ at UHF, for instance 915MHz, via a coaxial cable with an impedance of 50Ω. The Rx antenna can read the voltage V_r at the lower strip. The antennae are mounted on a Teflon plate with a dielectric coefficient ($\varepsilon = 2.1$), a magnetic relative permeability $\mu_r = 1$ and zero electrical conductivity. The Teflon plate has a thickness of 0.002m and a depth and height of 0.1m (dimensions $=0.1 \times 0.102$m) with its centre at (x,y,z)$=(-8.2, 0, 0)$ and $(x, y, z) = (8.2, 0, 0)$ respectively. Note that the Rx antenna is a copy of the Tx antenna except the lumped port at Rx does not have wave excitation (no power source). In the second model (Fig.13) the Tx antenna construction, properties and location remain exactly the same as in the first model, however the Rx antenna is replaced by an RFID tag. The RFID tag has a meandering "micro" dipole antenna and element of constant impedance 11+j143Ω at 915MHz. Detailed information regarding the tag geometry were not provided by the Xplorer-2000 manual of the physical setup. The manual did provide an image of the antenna design and the external dimensions. Therefore the dimension and design of this image were scaled and implemented as such in the equivalent model. (Fig.13) shows the image of the tag antenna and geometry that were used as a prototype for the COMSOL^{TM} models. In the third model (Fig.14), the construction, properties and location of the Tx antenna again remain unchanged to that of the first and second model. The same Rx antenna from the first model enters this model again, at a position parallel and at 0.2m from the Tx antenna. The tag is placed parallel at 0.5m distance from both antennae. The Rx antenna is oriented at 45° towards the tag (Fig.14).

The purpose of the COMSOL^{TM} simulation is to determine the S-parameters as a function of the frequency and the dielectric coefficients surrounding the tag. Therefore, in the first and second model S-parameters $S_{11}$and S_{21} are measured. S_{11} measures the voltage ratio between the Tx output power and the Rx input power (reflection coefficient). The reflection coefficient can be converted from volts and watts to decibel dB according to the logarithmic expression

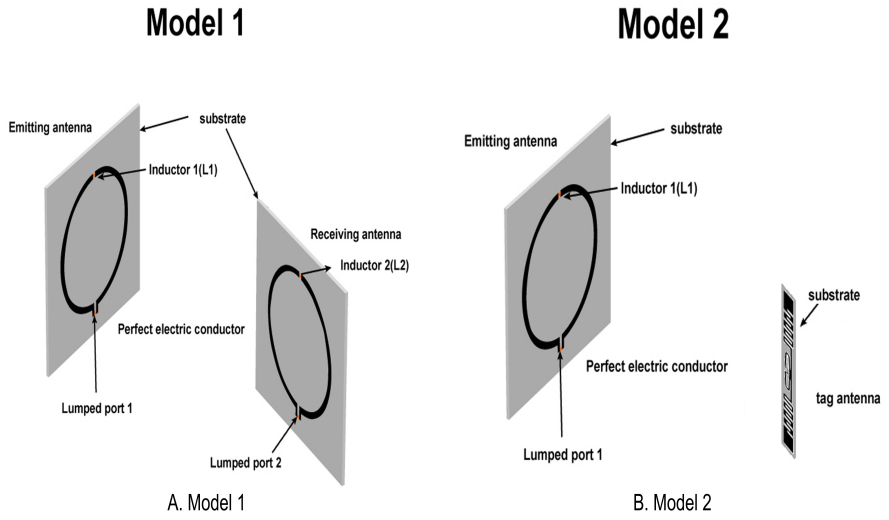

Figure 13: Comsol simulation: model-1 and 2

$10 \times log10(S_{11})dB$ and $20 \times log10(S_{11})dB$ respectively. The S-parameter S_{21} measures the power ratio between the Tx output power and the Rx input power (transmission coefficient or gain). The gain G can be converted from Watts to decibel with the same logarithmic expression as mentioned above. In the third model both the tag and the Rx antenna were included whereby the tag is referred to as port-2 and the Rx antenna is port-3, thus enabling measurement of the S-parameters S_{11}, S_{21} and S_{31}. As a final remark it should be mentioned that the whole setup is placed in a sphere, which acts as a perfectly matched layer PML, absorbing layer in which all electric fields attenuate: $(\nabla \times \mathbf{E})_{surface}$ is zero.

4.3 Theory and model equations

In this section, we used Maxwell's Equations (8) to describe how electric and magnetic fields propagate, interact, and how they are influenced by objects or media. The Maxwell equations (the known laws of electricity and magnetism) are a result of many years of research of the factors associated with electricity and magnetism. Controversially, the equations have not derived from a completely analytical methodology. Nevertheless, they produce reasonable results and so far no experiments have proved them to be wrong. Therefore, they are accepted by the scientific community as valid laws to characterize electromagnetic phenomena. RFID models can be built in COMSOL^{TM} using the electromagnetic waves and frequency domain formulation in the RF module, or the wave optics module. These modules provide similar interfaces for solving the frequency domain form of Maxwell's equations via the finite element method [97][66]. We consider a domain (sphere) filled with air. This sphere of air is limited by a PML that acts as an absorber of outgoing radiation. In the domain we

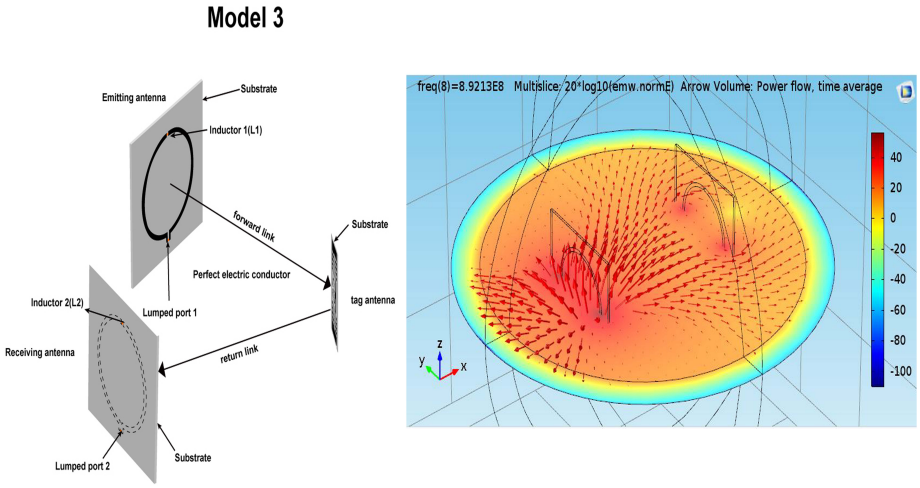

A. Model 3 B. Power flow at frequency=8.9213E8

Figure 14: Comsol simulation: model-3 and power flow distribution

have a Tx antenna and a Rx reader antenna, which are identical and mounted on a Teflon plate of dielectric coefficient ($\varepsilon = 2.1$), a magnetic relative permeability ($\mu_r = 1$) and zero electrical conductivity. The entire system is mounted inside a conducting sphere with zero voltage to eliminate all disturbances from the surroundings. The Maxwell equation that describes the electric field in the entire domain is

$$\nabla \times (\frac{1}{\mu_r} \nabla \times \mathbf{E}) - {k_0}^2 \varepsilon_r - \frac{j\sigma}{\omega \varepsilon_0} \mathbf{E} = 0 \tag{10}$$

Where μ_r is the relative magnetic permeability, which is 1 throughout the space considered by us, ε_r is the relative permittivity, ε_0 is the permittivity in free space, j indicates a complex number, σ is the conductivity, ω is the angular frequency, and $\mathbf{E}$ is the electric field vector. Moreover, $k_0 = 2\pi/\lambda_0$ is the wave number of the propagation in free space, i.e., $k_0 = \omega/c$ with $c = 2.99792458 \times 10^8$ $[m/s]$ (the velocity of light) and $\omega = 2\pi V$ (V = voltage) is the angular frequency. Except for the metallic rings constituting the antenna, the lumped port with impedance $Z = 50\Omega$ and lumped element with inductance L= $66nH$ and the teflon plates with dielectric coefficients ($\varepsilon_r = 2.1$), the rest of the domain has the electric properties of air ($\varepsilon_r = 1$) and zero conductance σ. The boundary condition of the conducting ring of the antenna is $(\nabla \times \mathbf{E})_{surface} = 0$), i.e., the electricfield $\mathbf{E}$ is constant tangential to the plane. For the magnetic element on the top plate of the ring the potential V= Ldi/dt, where i is the current through the circuit. The potential $\mathrm{V}(z,t) = -\int_{C_v} E_T \cdot dl$, i.e., integral of the transverse electric field E_T along a contour C_v, where z is the direction and t is time [65]. This can be used to write the boundary condition for the lumped port. The far-field pattern is computed on the boundary between the air and the PML domains. The derivation of equation (10) can be found in section (8.6).

4.4 Results & Discussion

In this section we provide an description of the output data results for models-1, 2 and 3. It is our intention that the figures show the behavior of the S-parameters for model-1, 2 and 3 in terms of the frequency dependence and its dependence on the dielectric coefficient. To test the dielectric coefficient dependence in the three models, we inserted the Rx antenna (or the tag) between blocks with varying dielectric coefficients, i.e., between $\varepsilon = 2.05$ (hexadecane) to $\varepsilon = 80$ (water). The figures (Fig.15, 16, 18, 19 and 20) describe the S-parameters as a function of frequency and the dielectric coefficient of the blocks. Note that only set-ups that measured backscattered signals are able to respond to the dielectric constant around the tag. To examine the effect of the tag's cover on the s-parameter measurements, we wrapped the Rx antenna (or the tag) in 0.002m Teflon ($\varepsilon = 2.1$) covers. Regarding the effect of the volume of the media blocks on the s-parameters, we varied the thickness of the blocks surrouding the tag, ranging from 0.01m to 0.10m. In model-2 and 3, the distance between the emitting antenna and the receiving antenna (tag) was increased from 0.15m to 0.5m. Starting with an analysis of the results of model-1, we see that in model-1 the S_{11}(reflection coefficient) parameter is neither affected by the dielectric coefficient of the teflon wrap nor by the blocks on both sides of the receiving antenna with various dielectric coefficients between 2.05 and 80 (Fig.15). The same behavior was displayed in the case of the absence of teflon wrap (no cover) (Fig.16). In other words, the response of S_{11}indicates an independence of the dielectric coefficients. (Fig.16). However, the results indicate that the teflon wrap does influence S_{21} and changes the resonance frequency (Fig.15). For example, with the teflon cover the optimal resonance frequency in the frequency range 500-1000MHz is observed at 868MHz for air and at 749MHz for demi-water. The simulation was repeated, however this time without the presence on the wrapped teflon covers. The response without the teflon cover shows that although the resonance frequency for air remains unchanged (868MHz), the resonance frequency in water changed to 630MHz. Note that in this research we ignore the effect of the conductivity. Moreover, we observe a distinguishably decrease of the resonance frequency with increasing dielectric coefficients (Fig.15 and 16). Finally, the tests regarding the effect of volume of the surrounding media show that S_{21} is affected by the thickness and dielectric coefficients of the surrounding blocks up to a thickness of 0.03m. Above 0.03m no significant effects can be discerned (Fig. 17).

In model-2, we observe that S_{11} is again not influenced by the teflon wrap ($\varepsilon = 2.1$) nor by the volume of the blocks surrounding the tag (Fig.18). However, in this model we do see a change in the S_{21} response (Fig.18); the response is different from the response observed in model-1. Indeed the resonance frequency starts to shift from 868MHz for $\varepsilon = 1$ towards lower frequencies 750MHz for ε = 1-2.05(hexadecane) but subsequently reverses its trend between squalene and butanol and shifts to higher frequencies (from 865MHz to 1100MHz) for dielectric coefficients changing from 3 (squalene) to 30 (methanol). However, for for methanol and water the resonance frequency is again lowered to 800MHz

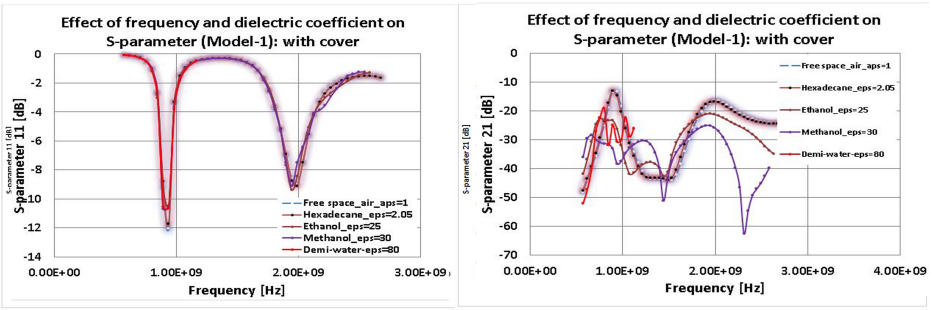

A. Model-1: S11 with Cover

B. Model-1: S21 with Cover

Figure 15: Model-1 with cover: S11 and S21 versus frequency

and 750MHz respectively. This change in trend in model-2 with repect to model-1 is possibly due to the changes in geometry of port-2 or a result of the increased distance between port-1 and 2 or a combination of both. An additional factor which was tested in model-2 was the influence of the thickness of the emitting antenna on the S- parameter response. When comparing results from simulation with a Tx antenna of 0.004m with that of one with a thickness of 0.04m, we notice a distinguishable change in S_{11} as expected (Fig.21).

In model-3, the response of S_{11} indicates the independence of the dielectric coefficients of the wrap and blocks surrounding the receiving antenna or tag, as was the case in model-1 and model-2 (Fig.19). The same behavior as was displayed in model-1 and 2 is also observed in model-3 for the S-parameter S_{31}(Fig.20). Also in model-3, the S- parameter S_{21} again demonstrates no clear trend regarding the influence of the increased dielectric coefficients (Fig. 19). Like we did in model-2, an additional factor which was tested in model-3 was the influence of the thickness of the emitting antenna on the S-parameter response. When comparing results from simulation with a Tx antenna of 0.004m with that of one with a thickness of 0.04m, again we notice a distinguishable change in S_{11} as expected (Fig.21).

5 RFID CISC Xplorer-2000

This section describes the features, measurements and data output of the CISC RFID Xplorer-2000 system. The section is structured as follows. First the experimental setup is described, followed by a detailed description of the hardware (physical set-up) and software (functional setup) incorporated in the Xplorer-2000. The section continues with determination of turn on power (P_{min}), backscattering power ($P_{backscattered}$) and the tag radar cross-section (ΔRCS). The section ends with results of the measured output parameters (S-parameters S_{21}, minimum power to activate the tag P_{min} and the scalar difference between radar cross-sections of the tag ΔRCS and backscattered power $P_{backscattered}$) of the Xplorer-2000. The Xplorer-2000 measurements are chosen based on insights

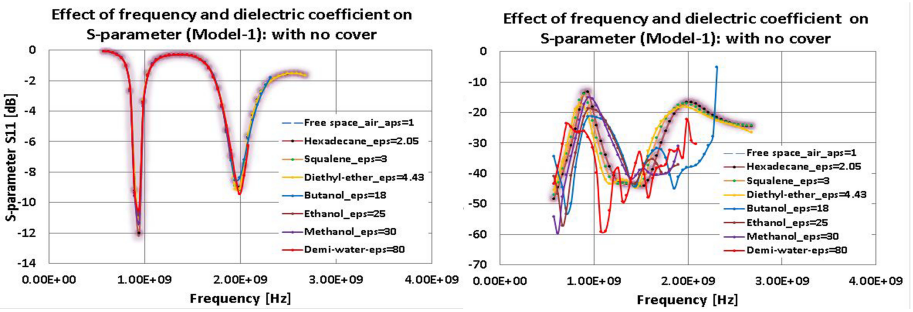

A. Model-1: S11 without Cover

B. Model-1: S21 without Cover

Figure 16: Model-1 without cover: S11 and S21 versus frequency

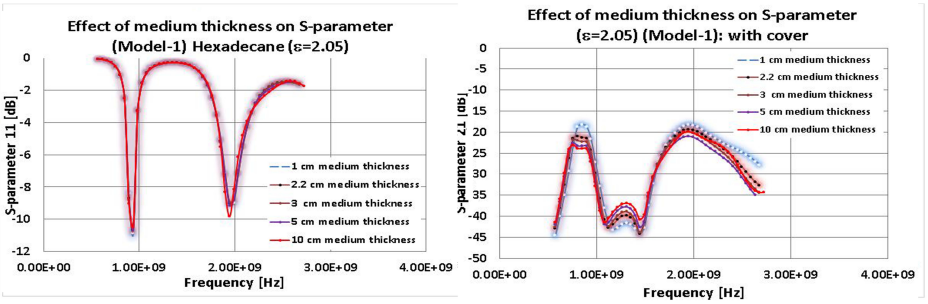

A. Model-1: S11 with Volume Cover

B. Model-1: S21 with Volume Cover

Figure 17: Model-1 with cover: Effect of medium thickness on S-parameters

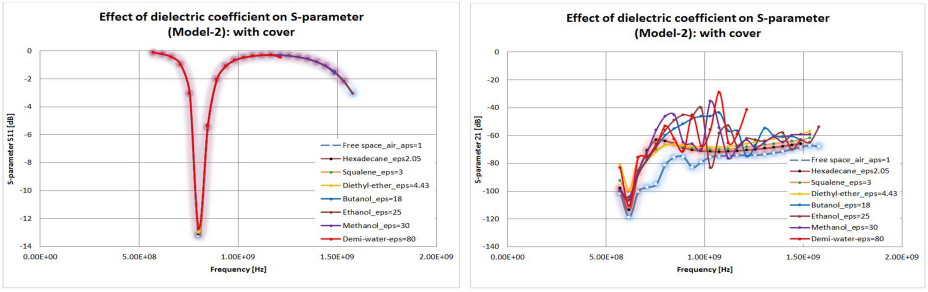

A. Model-2: S11 with Cover

B. Model-2: S21 with Cover

Figure 18: Model-2 with cover: S11 and S21 versus frequency

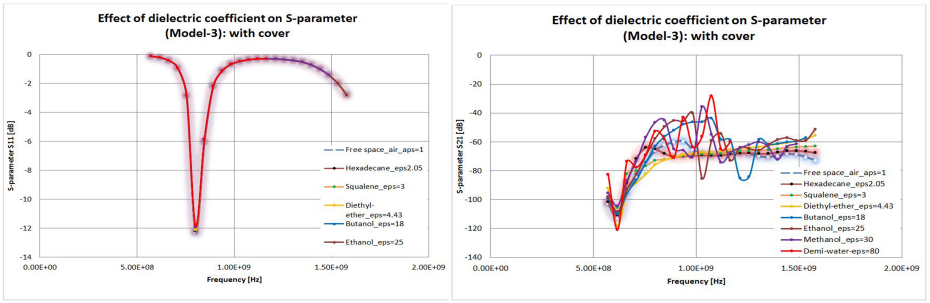

A. Model-3: S11 with Cover B. Model-3: S21 with Cover

Figure 19: Model-3 with cover: S11 and S21 versus frequency

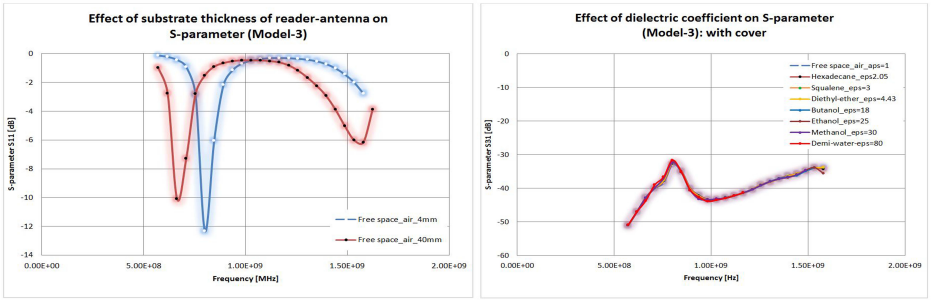

A. Model-3: S11 with Substrate Cover B. Model-3: S31 with Cover

Figure 20: Model-3 with cover: S13 and effect of substrate of emitting antenna

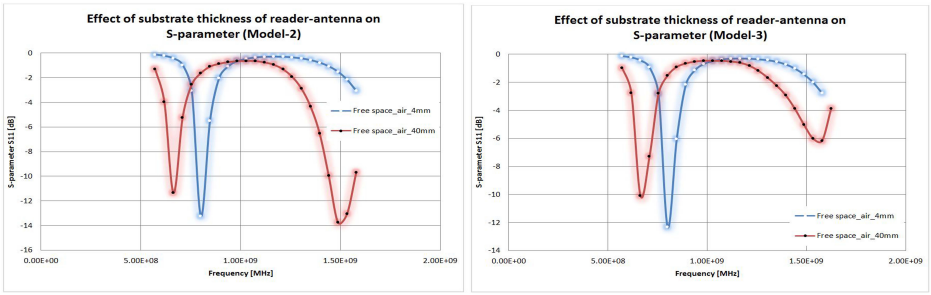

A. Model-2: S11 with Substrate Cover B. Model-3: S11 with Substrate Cover

Figure 21: Model-2 and 3 with cover: effect of substrate of emitting antenna

obtained with the COMSOL^{TM} simulation (4). The final results are plotted in a graphs that show the output parameters (S-parameter $S_{21}$and P_{min}) as a function of the composition of the relevant diethyl ether-water and diethyl ether-hexadecane mixtures.

5.1 Experimental setup

The CISC RFID Xplorer-2000 is a state of the art UHF RFID system that consists of a reader (interrogator), which is connected to two circular patch antennae, a laptop with the tag performance test software or Graphical User Interface GUI and the tag (transponder) [26][91][22][23]. As the system has separate transmit Tx and receive Rx antennae it is possible to transmit and receive signals simultaneously (full-duplex radio). The Xplorer-2000 allows to determine the S-parameters (voltage ratio's in dB), backscattered power (dBm), the minimum power (dBm) to activate the tag and the scalar difference between radar cross-sections of the tag ΔRCS, which is a function of the impedances of the tag antenna and the chip. The chip is able to modulate the backscattered signal, which can then be separately amplified. The dimensions of the reader of the CISC RFID Xplorer-2000 are $0.160 \times 0.250 \times 0.050$m, making it one of the smallest professional measurement tools nowadays. The communication protocol of the Xplorer-2000 works according to ISO/IEC 18000-63 (Type-C) / Gen-2 standard; CISC Semiconductor GmbH is one of the patent holder of the ISO/IEC 18000-63 protocol in Europe. More details on RFID systems in general, system protocol and operation can be found in section (10).

In the RFID Xplorer experiment we use the understanding obtained with the COMSOL^{TM} simulations (4), to measure the dependence of the output of the Xplorer-2000 as a function of the dielectric coefficient. However, we note that the Xplorer-2000 operates within the frequency range of this setup (800-1000MHz). For the execution of the measurements we place the tag in a tube, with a diameter of 0.05m and a height 0.35m, filled with fluids (till 0.02m height and volume of 0.00039m^3) of various known dielectric coefficients. We use the media air ($\varepsilon = 1$), hexadecane ($\varepsilon = 2.05$), squalane ($\varepsilon = 3.0$), olive oil ($\varepsilon = 4.1$), propanol-2 ($\varepsilon = 17.0$), iso-butanol ($\varepsilon = 18.0$), ethanol ($\varepsilon = 25.0$), methanol ($\varepsilon = 30.0$) and water ($\varepsilon = 79.08$). Firstly, we identify the resonance frequencies, being the maximum values of the output paramters of the Xplorer-2000. The resonance frequency shows a the dependence of the dielectric coefficient. Secondly, we plot the RFID response versus the dielectric coefficient. Lastly, we determine the RFID response at a specific frequency as a function of the volume fractions of diethyl ether in the oleic phase and aqueous phase, with the aim to identify a unique RFID response for each solvent concentration in the mixture.

5.1.1 Physical setup

This part briefly describes the geometric locations of the transmitting Tx and receiving Rx antennae and the tag (Fig.22). As mentioned above, the setup

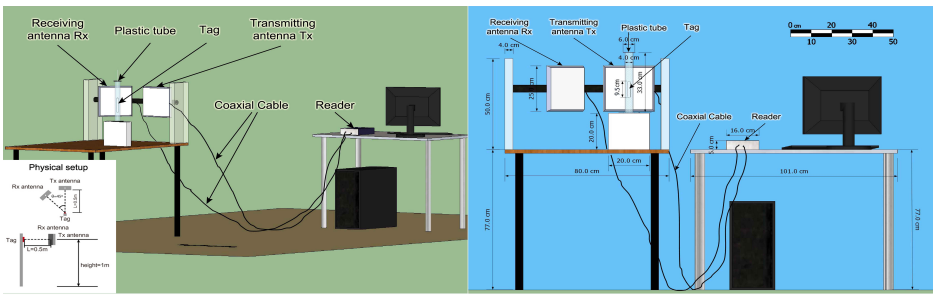

A. Setup 3D view B. Setup front view

Figure 22: RFID Xplorer-2000 setup

is characterized by its bistatic configuration, i.e., the transmitting and the receiving antenna are separate entities. Separate transmitting and receiving antennae allow to optimally align polarizations for accurate backscattered power measurements. In this setup, the Tx antenna is Left-Hand Circularly Polarized LHCP and the Rx antenna is Right-Hand Circularly Polarized RHCP. [18][20][7][61][74].

As (Fig. 22) shows, the Tx and Rx antennae are mounted on a square plastic cover with a constant dielectric ($\varepsilon = 2.1$) coefficient and a minimal conductivity ($\sigma \approx 0$). The antennae are placed parallel to each other with the center points of the devices at the same height as the center point of the tag. The tag has been placed in the intersection point of the perpedicular lines emerging from the center of the antennae (focusing point). This point is located at a distance (r) of $0,5$m (focusing distance) from the antennae, which represents the far field domain (Fig.22). The distance between the midpoints of the two antennae is 0.5m, and the Rx antenna is rotated at a 45-degree angle towards the tag (θ). Presently our setup is, suboptimally, not placed in a chamber with walls of zero reflection coefficient. For the room in which we placed the Xplorer-2000 has a minimum reflection isolation of the floor and ceiling at 1000MHz are 30 and 10 decibel dB respectively.

5.1.2 Functional setup

This part describes the functional setup, which controls the communication between reader antennae and the tag via a Graphic User Interface GUI. Figure (Fig.24) shows a block diagram of the RFID system. The user interface enables the creation, editing and selection of test cases and is linked to the Central Processing Unit CPU. In the CPU the source information is created, which is later sent to the transmitter. The transmitter, which is part of the reader, subsequently encodes the information into an RFID signal (Fig.23). The data is encoded according to pulse-interval encoding PIE. The encoded data is then modulated with the phase-reversal amplitude shift keying (PR-ASK) modulation scheme. A directional coupler directs part of the signal to

the power meter, which as a result is able to read the transmitted power without disturbing the actual signal. The RF signal is forwarded from the reader to the Tx antenna from where the modulated EM waves are transmitted towards the tag (forward link communication). Through commands sent and received between both devices (inventory round), a RFID reader can identify the electronic product code EPC of the tag. As in this experiment we use passive tags [1][31][50][63], the tag-reader communication process is always initiated by the reader [22][29][21][58][23]. That is to say, the reader starts an interrogation round with a query command to wake up the tag (turn on power) and the tag responds with the appropriate information. The turn on power is the minimum power that the tag requires in order to be activated. Looking at the RF signal in the first part of the interrogation round (forward link), we can see that the EM signal contains both continuous wave CW and a modulated wave command as shown in (Fig.23). As the forward link EM wave reaches the tag, it induces a voltage in the tag antenna, which is converted to a direct current DC by a voltage rectifier inside the tag's chip. The direct current powers the integrated circuit of the tag, starting with the state machine (Control Logic). The state machine demodulates the signal and determines the appropriate next command which is to be send to the reader. The transistor in the chip then re-modulates the signal, after which it is converted back into EM waveform and scattered back to the Rx antenna (reverse link) [75][57][60][22]. A functional block diagram of the tag can be found in (Fig.24). Because of the re-modulation of the EM wave, an encoded message can be transferred from the tag to the reader. This modulation is related to the complex (capacitive) impedance of both the chip and the tag antenna. The complex impedance of the tag also plays an important role in the determination of the radar cross section difference ΔRCS and the backscattering of the EM signal [17][31][34][52][9][71][73]. The principle of backscattering, modulation, RCS and impedance mismatching are explained in more detail later on in this part. The encoded message is scattered back to the reader during one of the CW periods when the tag impedance modulates the EM signal [57][59]. The reverse link signal is collected by the Rx antenna and passed to the reader's Quadrature Demodulator Receiver. Here the signal is RF filtered, down-converted, baseband filtered and converted into digital I and Q samples. These data samples are then passed to the CPU where they can be processed further. From the processed data selections can be made through the user interface and reports can be created using a specific software program.

5.2 Determination of turn on power ($\mathbf{P}_{min}$)

The turn on power is the power, which would be received by an isotropic receiving antenna (with gain equal to zero) at the position of the tag [Xplorer-2000 User Manual]. It is the minimum power that the tag requires in order to be activated and it is determined as follows [50]. The reader sends out a power sweep during the interrogation round, starting at a the maximum level of power (36dBm) and then gradually decreasing up to the point where the tag no longer responds to the interrogation signal. The level of power just above this point is

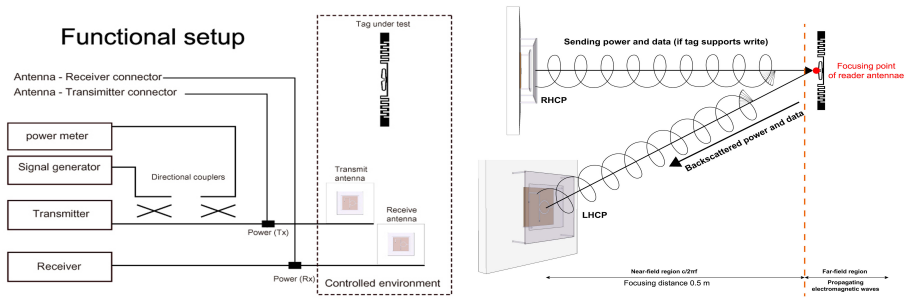

A. Functional setup RFID Xplorer-2000 B. RFID communication system

Figure 23: Funtional setup and RFID communication system

registered as the tags turn on power value or P_{min}. In case the reader reaches its minimum power (−6dBm) and the tag still responds, this value is considered to be P_{min}. Note that, the determination of the P_{min} value is also dependent on the reader sensitivity. Namely, if the receiver sensitivity is set too low (e.g. 5dB), noise could be misinterpreted as tag signal. On the other hand, if the receiver sensitivity is set too high (e.g. 20dB), the tag's response could be missed. This could lead to an inaccurate P_{min} value determination. Therefore, we chose to set the reader sensitivity at 15dB (default value) to achieve the optimum P_{min} value.

The relationship between the electric field strength (volt per meter) and the tag turn on power (dBm) is

$$\mathbf{E}_{tag}=\frac{4\pi}{\lambda}\sqrt{30P_{tag}} \tag{11}$$

where, λ is the wavelength in meters, $\mathbf{E}_{tag}$ is the electric field strenght at the tag position and P_{tag} is the backscatter power at P_{min}. Note that, P_{min} is the tag turn on power at the threshold [Xplorer-2000 User Manual].

5.3 Backscattering theory ($\mathbf{P}_{backscattered}$)

The technique that allows a tag to respond to the reader commands without the help of an external power source is based on the principal of backscattering; one of the most interesting aspects in the field of RFID. The backscattering process can be briefly summarized as follows.

A passive RFID tag consists of an antenna and a chip with an integrated circuit, both with complex impedance Z^*; Z^* =R+X (resistive R and capacitive or reactive X). Due to the resistive (real) and capacitive (imaginary) characteristic impedance, the tag is able to modulate and reradiate the incoming electromagnetic wave (from the transmitting reader-anenna Tx) back to the receiving reader-antenna Rx. The modulation of this EM wave occurs as the transistor on the chip rapidly switches between two discrete impedance states. [advanced RFID Measurements]. Note that the tag performs both phase and amplitude

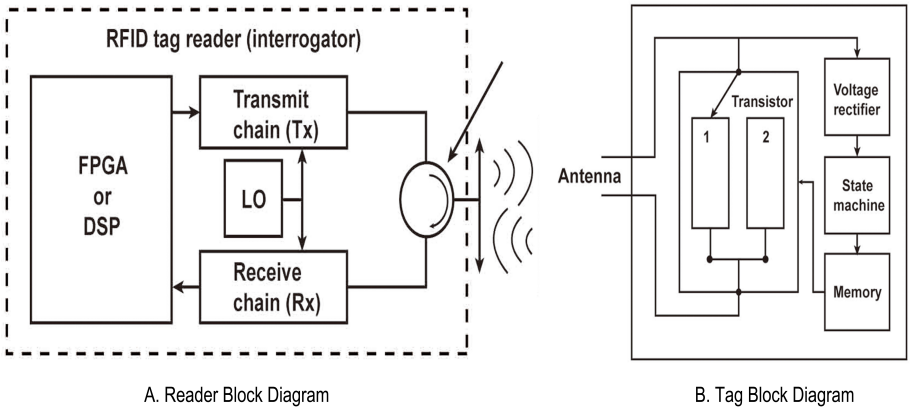

Figure 24: RFID reader and tag block-diagrams

modulation of the backscattered signal. According to a principle of EM theory (reciprocity), any structure that receives a wave can also transmit a wave. When we apply this theory to the RFID system we can see the following. When the tag antenna receives a EM signal from the Tx antenna (forward link), it induces a voltage in the tag antenna. As the tag antenna is attached to a chip (load) which presents complex impedance to the voltage, a current is induced. The induced current on the tag antenna consequently induces a voltage on the Rx antenna (reverse link). The power of the reflected EM wave from the RFID tag is called backscatter power ($P_{backscattered}$). The backscattered field of a tag antenna can be decomposed into two components: one is independent on the loading impedance (chip), called the structural mode scattering, and the other is dependent on the loading impedance, called the antenna mode scattering [36]. When an electromagnetic signal falls on an antenna surface, some part of the electromagnetic energy is scattered back to the space (structural mode scattering). The remaining part of the energy is absorbed due to the antenna effect. Some part of the absorbed energy is again scattered back into the space due to impedance mismatches (antenna mode scattering). [57][59][60][57][70][69][73].

We use the two-way radar equation to obtain the backscatterd power as following

$$P_{Rx} = \frac{P_{Tx} G_{Tx} G_{Rx} \lambda^2 \sigma}{(4\pi)^3 R^4} \tag{12}$$

Where:

P_{Rx} = Power at output of receiving reader-antenna [W]
P_{Rx} = Power into transmitting reader-antenna [W]
G_{Tx} = Transmitting antenna gain
G_{Rx} = Receiveing antenna gain
λ = Carrier wave lenght [m]

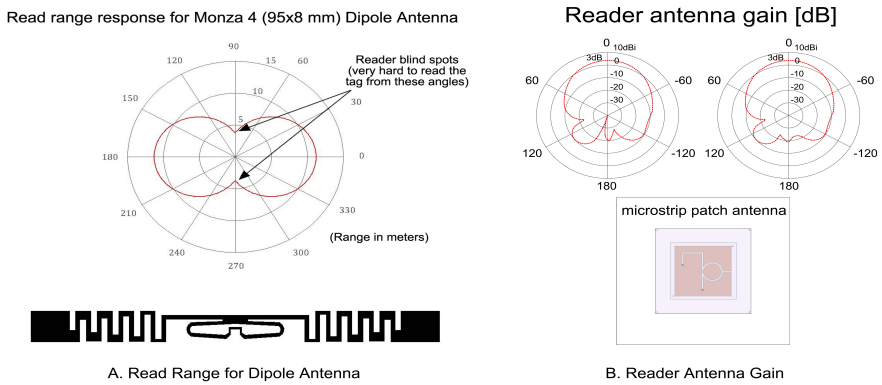

Figure 25: Tag read range and reader antenna gain (G)

σ = Tag's radar cross-section (RCS) [in m^2]
R= Distance from reader to tag [m]

5.4 Determining Tag Radar Cross-section (RCS)

In order to calculate the tag radar cross-section, we must first determine the power density received by the tag antenna. The power density S of an EM wave incident on the tag antenna (in free space) can be calculated as follows [62][57]

$$S = \frac{P_t G_t}{4\pi r^2}, \tag{13}$$

where P_t is the transmitted power, G_t is the gain of the transmitting antenna, and r is the distance to the tag [57][60]. The power P_a receiveded by the tag antenna is always the maximum power that can be delivered to the complex conjugate matched load:

$$P_a = SA_c = S\frac{\lambda^2}{4\pi}G, \tag{14}$$

where G is the tag antenna gain, SA_c is the power density at the tag antenna and λ is the wavelength of the radiation. The signal re-emitted by the tag antenna is divided by the signal emitted by the incident EM wave on the RFID tag, the radar cross-section σ_{RCS} is given by

$$\sigma_{RCS} = \frac{P_{re-radiated}}{S} = \frac{KP_aG}{S} = \frac{KS\frac{\lambda^2}{4\pi}G^2}{S} = \frac{\lambda^2 R_a^2 G^2}{\pi\left|Z_a + Z_c\right|^2}, \tag{15}$$

In this equation factor K indicates the influence of the load impedance mismatch on the amount of re-radiated power, and is given by

$$K = \frac{4R_a^2}{\left|Z_a + Z_c\right|^2}$$

where the impedance of the antenna is given by $Z_a = R_a + jX_a$ and the impedance of the chip is given by $Z_c = R_c + jX_c$. Typical values for the impedance

of the tag antenna are $Z_a = 70+j400\Omega$. A typical value for the chip impedance $12-j400\Omega$. A common value for the antenna gain is 1.8dBi, where dBi is the $10^{10} Log\,(P_2/P_1) = 20^{10} Log\,(V_2/V_1)$, with P meaning the power, and V the voltage and the i in dBi means isotropic. We need to subtract 2.84 to convert to dBd for a dipole antenna, or dBd=dBi−2.84 [57][59]. As the aim of this experiment is to examine the effect of the dielectric coefficient ε of different media on RFID tag response, complex impedance of the tag is a highly important factor. Namely, the tag's reactance (jX) is influenced by the dielectric coefficients of the surrounding media. As reactance forms a part of the complex impedance, the RFID tag's impedance will shift, which therefore presumably results in RFID response shift (e.g. resonance frequency shifts).

5.5 Experimental measurements

In this part of the experiment, the aim is to measure the RFID tag's response on various media (with dielectric coefficients between 2.05 and 80) in terms of the S-parameter (S_{21}), minimum power at tag position ($P_{\min}$), scalar difference between rader cross-sections of the tag ΔRCS and backscatter power ($P_{backscattered}$). The measurements are performed at a frequency range from 800MHz to 1000MHz. We started our measuring process with initial calibration measurements. As the system operates most optimally in air, the calibration took place in this medium ($\varepsilon = 1$). After we calibrated the system, we conducted S_{21} and sweep frequency measurements (P_{min}, RCS and $P_{backscattered}$). In the following parts we describe the calibration, S-parameter and sweep frequency measurements in more detail.

5.5.1 Calibration

In order to achieve reliable results, we start our measurements with calibration of the system setup. The calibration is performed in free air using a reference tag . The reference tag is placed at the position of the device under test (DUT), at a distance of 0.5m from both the Tx and Rx antenea (fig.22). Each time measurements are calibrated in the system, the results (calibration data) must be compared to the data from the reference data set. In case there is no match, a 'correction factor analysis' must be performed. Mismatches between the calibration data and the reference data might occur due to disturbance or noise in the environment. In case of too much noise in the system, we perform multiple measurements to test the consistency and and eliminate the outliers by taking the main average values of the multiple measurements. The calibration of the system has to be performed at every modification of the system setup (Xplorer-2000 User Manual). We performed multiple calibration measurements in order to test the reproducibility of the calibration data.

5.5.2 Frequency sweep & S-parameter measurements

After a successful calibration, the calibration tag is placed in a cylindrical plastic tube with diameter of 0.05m and height of 0.35m. The cylindrical plastic tube is filled with different liquids such as water, oil and alcohol (propanol, butanol, ethanol and methanol) with varying dielectric coefficients (between 1-80). The tube is filled till height of 0.2m, corresponding with a volume of 0.00039m^3. We first perform the frequency sweep measurements, by selecting a frequency setting with start frequency of 800MHz, a stop frequency of 1000MHz, with frequency steps of 5MHz. As result, the main window of the Xplorer-2000 shows the frequency sweep outputs (graphs) such as power at the tag position (P_{min}), the scalar difference between tag radar cross-sections ΔRCS and backscattered power ($\text{P}_{backscatter}$) versus frequency. After the frequency sweep outputs have been measured, the S-parameter measurement was performed. The measurement results are graphically shown in the S-parameter sweep window. The S-parameter graph shows the voltage ratio between received and the transmitted signal (Rx/Tx) in decibel per square meter (dBmsq) as a function of frequency. Depending on the hardware setup, the ratio either relates to the S_{11} or to the S_{21} parameter.

5.6 Experimental Results & Discussion

The aim of this experiment is to examine the effect of the dielectric coefficient ε on the response of the Xplorer-2000 communication system. We looked at the response in terms of four different parameters: the S-parameters (voltage ratio's in dB), back scattered power dBm, the minimum power dBm to activate the tag and the scalar difference between radar cross-section difference ΔRCS, which is a function of the impedances of the tag antenna and the chip.

Firstly, the data output was used to obtain four plots, in which the response parameters were represented as a function of frequency (800-1000MHz) (Fig.27, 28, 29 and 30). (Fig.27) plots S_{21} versus frequency. The plots for various dielectric coefficients (ε = 1-80) show a strong dependence on the frequency and a typical oscillating behavior. The scattering parameter S_{21} also depends strongly on the dielectric coefficient. We see this dielectric coefficient dependency for example if we look at (Fig.27). Here we see that the medium air ($\varepsilon = 1$) has a resonance frequency of 868MHz (lowest minimum ≈ -65dB). Methanol ($\varepsilon = 30$) has resonance frequency of 860MHz (lowest minimum ≈ -57dB). This shift in resonance frequency could possibly indicate a tendency where the resonance frequency decreases when the dielectric coefficient increases. However, in the case of the medium demi-water ($\varepsilon = 80$) we observe that the resonance frequency increases to 862MHz in comparison with methanol (860MHz). As demi-water has a higher dielectric coefficient than methanol, this result deviates from the hypothesis that a medium with a higher dielectric coefficient generates a lower resonance frequency. Based on observations from the COMSOL^{TM} simulation (4), this deviation could possibly be a consequence of the tag or setup geometry, or due to the influence of the tag encasement. Note that in this research we

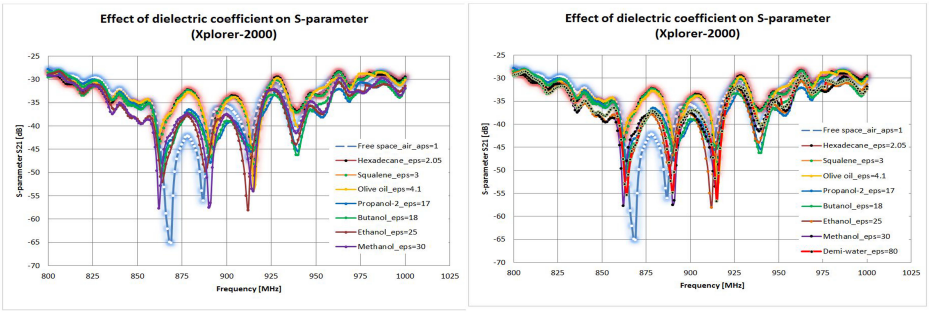

A. XplorerS21 No Water (Cover)

B. XplorerS21 with Water (Cover)

Figure 26: Xplorer S-parameters with cover: S11 and S21 in decibel (dB)

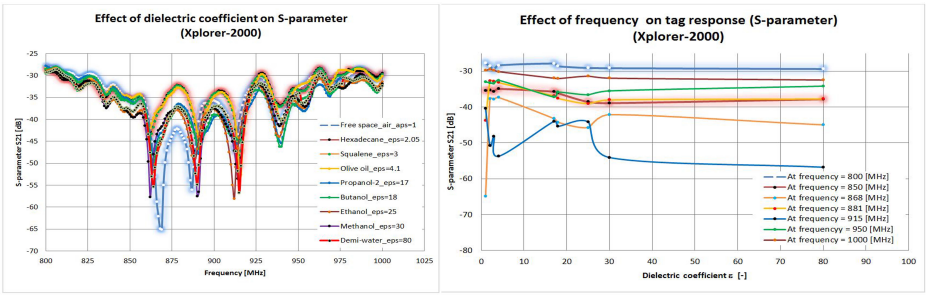

A. XplorerS21 with Water (Cover)

B. XplorerS21 vs Dielectric coefficient

Figure 27: Xplorer S-parameters (S21) with cover

ignore the effect of the conductivity.

(Fig.28) shows experimentally the minimum power to activate the tag, P_{min}, versus the frequency. For all media except air, away from the lower frequency (825MHz) the P_{min} starts to decrease until a minimum is obtained after which P_{min} again increases. For the medium air we can see two minima. For all plots of P_{min} except for demi-water, the power increases with an increasing dielectric coefficient. However, in the case of demi-water, contrary to expectation the power decreases. (Fig.29) shows the radar cross-section as a function of frequency and the same trend as for P_{min} is observed. (Fig.30) shows the backscattered power as a function of frequency. Now the trends are reversed, i.e., the backscattered power starts at low values and for higher frequencies it reaches a maximum, after which the back scattered power again decreases.

After plotting the S-parameters, P_{min}, $P_{backscattered}$ and ΔRCS versus frequency, the next step was to use the resulting data to obtain a relation between the RFID response at varying frequencies and the dielectric coefficient values. Thus, four graphs were created respectively showing the S-parameters, P_{min}, $P_{backscattered}$ and ΔRCS at different frequencies versus dielectric coef-

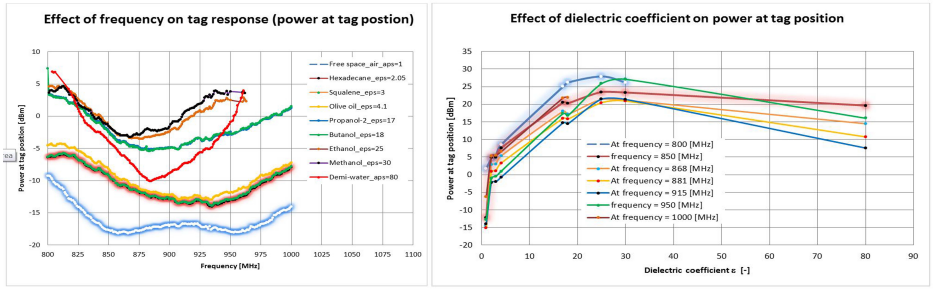

A. Xplorer Pmin vs Frequency (Cover)

B. Xplorer Pmin Dielectric Coefficient

Figure 28: Xplorer power at tag position (Pmin)

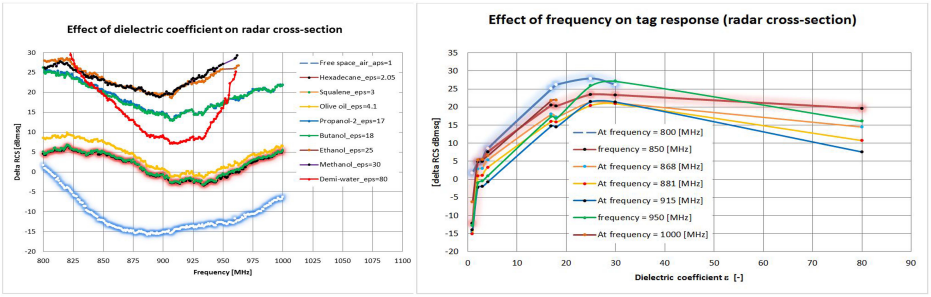

A. XplorerRCS vs frequency (Cover)

B. XplorerRCS vs Dielectric Coefficient

Figure 29: Xplorer radar cross-section (RCS)

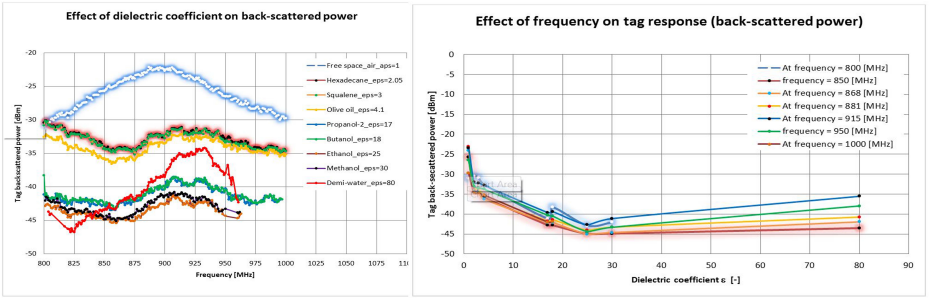

A. Xplorer back-scatterd power (Cover)

B. Xplorer back-scattered power vs Dielectric Coefficient

Figure 30: Xplorer backscattered power (Pbackscattered)

ficients ranging from 1 to 80. (Fig.27) plots S_{21} versus dielectric coefficient for selected frequencies (800-1000MHz, with finite increments). We chose the plot that shows the strongest dependence on the dielectric coefficient in the domain of interest, i.e., the plots at 915MHz for the diethyl ether-oleic mixtures and at 881MHz for the diethyl ether-water mixtures. (Fig.28) plots $\mathrm{P_{min}}$ versus the dielectric coefficient for selected frequencies (800-1000MHz, with finite increments). Again we chose the plot that shows the strongest dependence on the dielectric coefficient in the domain of interest, so the plots at 881MHz and 950MHz for the diethyl ether-oil and diethyl ether-water mixtures respectively. In (Fig.30 and 29), the same selecting procedure was applied for the $\mathrm{P}_{backscattered}$ and ΔRCS parameters. Here (Fig.30) indicates that frequencies 915MHz and 950MHz best show the dependence for the diethyl ether-oil and diethyl ether-water mixtures respectively, while for ΔRCS the frequencies 915MHz (oleic) and 850MHz (aqueous) are the best choice frequencies (Fig.29). The final goal however of the experiment is to determine the relation between the RFID response and the volume fraction of diethyl ether in the oleic and aqueous phase. We obtained this relation as follows. First we determined the volume fraction of diethyl ether using the data from the phase behavior measurements (3) obtained with the density meter (3.1). From the data from the density meter calibration curve, where the weight fraction of diethyl ether versus density was plotted, we estimated the partial molar volume of diethyl ether in the aqueous and oleic phase. From the estimation of the partial molar volume we calculated the volume fraction of diethyl ether. Next we calculated the effective dielectric coefficient for the diethyl ether-oil (hexadecane) and diethyl ether-water mixture using the Böttcher mixing rule (3.3.1). Subsequently we used an Excel-solver to solve the non-linear Böttcher equation and the dielectric coefficient of the mixtures. The effective dielectric coefficients were plotted versus the volume fraction of diethyl ether and from this plot the regression equation was obtained. We used the coefficients of the regression equation to obtain the volume fraction of diethyl ether. Likewise, an equation was derived from the graph plotting the RFID response versus the dielectric coefficients at various frequencies. We used the coefficients of this equation to obtain S_{21}. We plot S_{21} versus the volume fraction of diethyl ether to establish the relation between the RFID response ($\mathrm{S_{21}}$ and $\mathrm{P_{min}}$) and the volume fraction of diethyl ether in oleic and aqueous phase. (Fig.31) shows that at a frequency of 915MHz the relation is parabolic, so at both volume fraction 0.4 and 0.8 the S_{21} response is -51dB. In order to attain uniqueness in the S_{21} response, we therefore combine the curve of 915MHz with that of 850MHz in the area of volume fraction 0.4 and 0.8. At a frequency of 850MHz we observe a monotonous curve, which gives a dB-value of -17 at volume fraction 0.4 and a dB-value of -22 at volume fraction 0.8. By combining the data from the two frequencies (850MHz and 915MHz) we achieve a uniqueness in the measurement of solvent concentrations in the oleic phase. Note that since solvent is soluble in oil at all proportions, we must look at the entire volume fraction area to see if each response is unique.

(Fig.31) plots S_{21} versus volume fraction of diethyl ether in the aqueous phase. First we take a look at frequency 868MHz, as we previously established

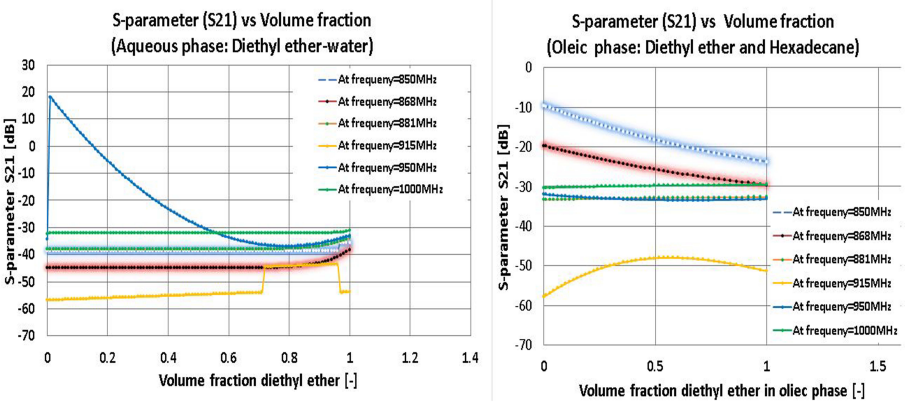

A. XplorerS21 Volume Fraction Aqueous

B. XplorerS21 Volume Fraction Oleic

Figure 31: Xplorer S-parameter (S21)versus volume fraction

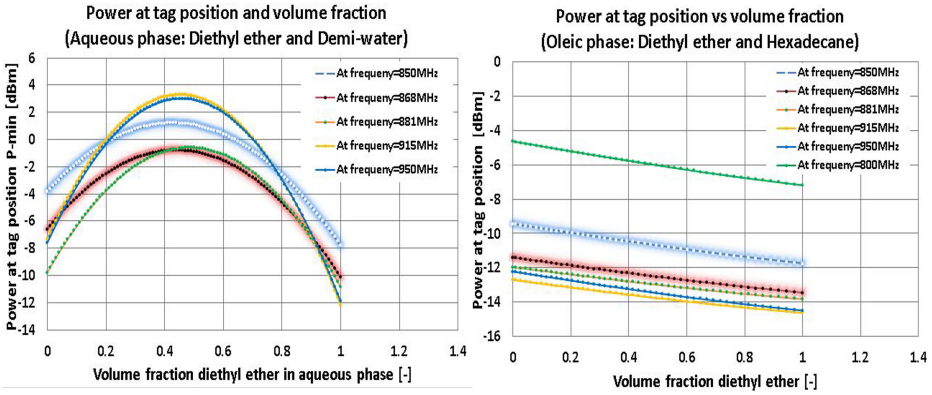

A. Xplorer Pmin Volume Fraction Aqueous

B. Xplorer Pmin Volume Fraction Oleic

Figure 32: Xplorer power at tag position (Pmin) versus volume fraction

that at this frequency the difference between diethyl ether and demi-water is most visible. Since diethyl ether is soluble in water up to a volume fraction of 0.08, we only focus on the volume fraction of diethyl ether in the aqueous phase ranging from 0 to 0.08 in the graph. Again we see that at frequency 868MHz the relation between response and volume fraction is parabolic. Therefore we combined frequency 868MHz with 950MHz in order to achieve uniqueness of dB-values for each solvent volume fraction (concentration) in the aqueous phase. (Fig.32) plots P_{min} versus volume fraction of diethyl ether in oleic phase. We observe that at the frequency 888MHz the relation takes the form of a monotonous curve as well, thus indicating a uniqueness of values. (Fig.32) plots P_{min} versus the volume fraction of diethyl ether in the aqueous phase. Here we focus on frequency 950MHz, as we previously established that at this frequency the difference between diethyl ether and water is most visible. Again taking into account the solubility of diethyl ether in water, we only focus on the volume fraction of diethyl ether in aqueous phase ranging from 0 to 0.08 in the graph. We observe that at frequency 950MHz, the relation between response and volume fraction takes the form of a parabolic curve in the entire domain (0-1) while in the area from 0 to 0.08 volume fractions of diethyl ether the curve seems to be monotonous so we achieve uniqueness of dB-values in the area from 0 to 0.08 volume fractions of diethyl ether.

6 Conclusions

The main aim of this research was to study the feasibility of using RFID technology to measure solvent concentrations in a spontaneous imbibition experiment. The output data of the measurements with the CISC RFID Xplorer-2000 indicate a strong dependence between the RFID response in terms of the response parameters (S-parameter S_{21}, the minimum power to activate the tag - P_{min}, the backscattered radiation $P_{backscattered}$ and the tag radar cross-section ΔRCS) as a function of the dielectric coefficients of the media surrounding the tag at various frequencies. Simulations with COMSOL^{TM} aided to improve the understanding of this relation and showed the effect of the tag's encasement and the dependency on the volumes of the media blocks covering the tag on both sides.

From the graphs where we plotted the RFID response versus the dielectric coefficient we can conclude that some frequencies indicate a larger dependence on the concentration (volume fraction) of diethyl ether in oil and diethyl ether in water than other frequencies. For instance, in a graph where we plotted the S_{21} response versus the dielectric coefficients, we observe that the frequencies 915MHz and 868MHz show a distinguishable difference in response for the dielectric coefficients between diethyl ether-oil and diethyl ether-water respectively.

Plotting the RFID response versus the volume fraction of diethyl ether in the oleic and the aqueous phase, we observe that in a situation where the dependence of the optimal frequency of the reponse versus volume fraction resulted

in a curve containg one or several maxima, more frequencies must be used to obtain a unique result. For example, the plot of S_{21} ($f = 915$MHz) versus diethyl ether volume fractions in hexadecane (fig.31) produced a parabolic curve, where at 915MHz we obtain the same s-parameter value at a volume fraction of 0.4 and 0.8. The S-parameter values obtained at 868MHz, shows a monotonic, however, more shallow behavior. By combining the response function at these frequencies we are able to achieve both accuracy and uniqueness. From the response functions versus the diethyl ether volume fraction plots we could furthermore conclude that the advisable response parameter for measurements in an oil-solvent-water system is the 'minimum power at the tag position' or P_{min} (Fig.32).

Due to the strong dependency of the RFID response on the dielectric coefficient, the system can therefore be used for identification of dielectric coefficients. Nonetheless, we need more measurements of media with dielectric coefficients ranging from 30 to 80 for the aqueous phase compositions and dielectric coefficients ranging from 2.1-4.0 for the oleic phase compositions to obtain accurate results. The measurements until now, however, show feasibility of using RFID technology to determine the diethyl ether-water and diethyl ether-oil composistions.

7 Appendix-A: Permittivity measurement

This section provides an explanation on the permittivity (dielectric coefficient) measurements performed in the section phase behavior. Permittivity is one of the key parameters that affect the propagation of electric fields. In general, a medium is made up of a composition (or lattice) of molecules or atoms, which have some sort of dipole moment. Without the presence of an external electric field, the molecules will align randomly. However, when we place the material between two charged metal plates, the molecules are aligned by their dipole moment and the external electric field [A*]. Due to the dipole moment of the materials, molecules oppose the external electric field **E**, resulting in a reduction of the net electric field within the material. Permittivity changes with frequency, temperature, and humidity. The permittivity is a measure of how much the molecules oppose the external **E**-field. If we consider the E-field due to a single point charge of value q [C] at a distance R:

$$|\mathbf{E}| = \left[\frac{q}{4\pi\varepsilon_0 R^2}\right] \text{ where } \varepsilon_0 = \text{permitivity of free space} \tag{16}$$

$$= 8.854 * 10^{-12}[\ \frac{\text{farad}}{\text{meter}}], \text{ where q=point charge [C],R=distance[m]} \tag{17}$$

The permittivity of a medium ε is expressed as the product of the dielectric coefficient ε_r and the free space permittivity ε_0:

$$\varepsilon = \ \varepsilon_r \ * \varepsilon_0 \Longrightarrow |\mathbf{E}| = \left[\frac{q}{4\pi\epsilon R^2}\right] \tag{18}$$

The permittivity is the multiplier that relates the Electric Flux **D** Density and the Electric Field **E**:

$$\mathbf{D} = \varepsilon \mathbf{E} \tag{19}$$

[A*].

The objective of this section is to measure the dielectric coeffcient as function of frequencies (and temperature $\pm 23^o$C) in different media (water, saltwater, oil, diethyl ether and alcohol) by using the insulation diagnostic system (IDAX-300) and impedance network analyzer (Wayne Kerr precision-6640A).

7.1 Insulation diagonstic system (IDAX-300)

With the insulation diagnostic system we measured the impedance of the media diethyl ether, hexadecane, squalene, oilve oil, propanol, butanol, ethanol and methanol, from which we can calculate the corresponding permittivities.

7.1.1 Setup and measurement process

The IDAX-300 setup consists of a cylindrical core attached to two cables (low and high voltage), which are connected to the IDAX-300 system box. The cylindrical core consists of a solid inner cylinder (male) connected to the low voltage cable (low voltage winding) and a hollow female cylinder surrounding the male part connected to a high voltage cable (high voltage winding). The solid male cylinder consists of two parts: the lower part has a wide lower bottom section (height $h = 0.09$m, radius ɾ $= 0.01$m) and a narrow upper section ($h = 0.02$m, ɾ $= 0.005$m; the volume is $v = 1.6x10 - 6\text{m}^3$); the upper part consists of a plastic cover and consists of a narrow lower part ($h = 0.015$m, ɾ $= 0.015$m) and a wider upper part ($h = 0,025$m, ɾ $= 0,02$m). The plastic part of the male cylinder is sealed with a guarding ring in order to prevent influence of electric current leakage during the measurements. The hollow female cylinder consists of two parts: a lower part ($h = 0.09$m, inner radius $= 0.015$m), and an upper part ($h = 0.035$m, inner radius $= 0.035$m). The upper section of the lower part of the female cylinder has a small dead-end exit line (Fig.8).

The male part fits effortlessly into the female part, leaving only a small space between the two cylinders, namely in the area where the male cylinder has its narrow section; this is the chamber where the measurements take place. To start the measurements, first the male cylinder is inserted into the female cylinder in order to measure the output capacitance of air. Note that all the measurements take place at a temperature of $\pm 23°$C. With the capacitance for air known, now a quantity of the fluid medium (hexadecane, diethyl ether and various types of alcohol) was injected into the female cylinder. This time as the male part is inserted, the volume of the male cylinder causes the medium to migrate upwards in the space between the two cylinders, where the medium enters the chamber. The surplus medium exits the cylinder through the exit-line. The capacitance of the medium in the chamber was then measured. The ratio between the output

capacitance measured in air and the output capacitance of the medium gives the real dielectric coefficient of this medium.

7.2 Impedance analyzer (Wayne Kerr precision-6640A)

With the impedance network analyzer we measured the impedance of the media demi-water and water with varying salt concentrations (1mM, 2mM, 5mM, 0.5M) from which we can calculate the corresponding permittivities.

7.2.1 Setup and measurement process

For these measurements two cylindrical electrodes are used. The cylindrical electrodes are attached to the network analyzer through a coaxial cable (transmission line) (Fig.9). The two cylindrical electrodes have the same central axis and height ($h = 0.1$m). We assume that the height of the two cylindrical electrodes is long enough to allow neglecting the edge effect of the cylinder. The outer cylindrical electrode has a diameter D (D= 0.03m) and the inner cylindrical electrode has a diameter d (d= 0.009m), hence the spacing between two electrodes is D-d (0.021m). The spacing between the electrodes is alternately filled with the liquid pure components. The dielectric permittivity response of these media and the conductivity (resistance) to an alternating voltage difference is calculated. These calculations of the electric permittivity and the conductivity are performed using classical boundary conditions, namely that the cylindrical electrodes are uncharged in the absence of an applied electric field (voltage difference). This means that it is assumed that neither charge transfer nor absorption takes place [B*].

The first step in the measurement process is to prepare the different media (water and saltwater). In case of the medium saltwater, four solutions with varying levels of salinity (1mM, 2mM, 5mM and 0.5M) were prepared. Subsequently, the space between the cylindrical electrodes was filled with the solution. The volume between the electrodes is approximately 0.065 to 0.07 liter. Then a measurement was conducted with the full amount of medium in the electrodes, after which 0.01 liter was taken out and the measurement was repeated. This procedure continued, each time lowering the liquid quantity with 0.01 liter up until the extraction of 0.06 liter in total. The aim of this method is to examine the effect of volume distribution of the medium on the electric permittivity and conductivity measurements.

7.2.2 Theoretical background

Impedance is an important parameter in the characterization of an electronic circuit. Impedance Z can be defined as the total opposition of a device or circuit to the flow of an alternating current AC at a given frequency. It is represented as a complex quantity: Z=R+jX, where R is the real part of the resistance and jX is the imaginary part of the resistance [C*]. In this experiment we used an impedance analyzer (Wayne Kerr precision-6640A) with an equivalent circuit

model in which the resistance R and the capacitor C are parallel to each other. The system operates in a frequency range of 200Hz to 3MHz. The equivalent circuit model can be calculated with:

$$V = ZI \tag{20}$$

$$Z = R + jX \text{ where, } j = \sqrt{-1} \text{ complex number} \tag{21}$$

$$\frac{1}{Z} = \frac{1}{R} + \frac{1}{X} \Rightarrow X = \frac{-j}{\omega C} \Rightarrow \frac{1}{X} = j\omega C \tag{22}$$

$$\frac{1}{Z} = \frac{1}{R} + jC\omega = \frac{1 + jRC\omega}{R} \Longrightarrow \mathrm{Re}(\frac{1}{Z}) = \frac{1}{R} \;\&\; \mathrm{Im}(\frac{1}{Z}) = C\omega \Longrightarrow \tag{23}$$

$$Z = \frac{R}{1 + jRC\omega} = \frac{R}{1 + jRC\omega}\frac{(1 - jRC\omega)}{(1 - jRC\omega)} = \frac{R - jR^2C\omega}{1 + (RC\omega)^2} \tag{24}$$

where ω is the angular frequency in radius per second [rad/s] [D*].
In polar form we can write the impedance Z as:

$$Z = R + jX = |Z|\, e^{j\phi} = |Z|\,(\cos\phi + j\sin\phi) \tag{25}$$

where ϕ is the phase angle in degrees and e is the exponential function.
Combining equation (Eq.23) and (Eq.25) we get:

$$|Z|\cos\phi = \frac{R}{1 + (RC\omega)^2} \Longrightarrow \text{Real part} \tag{26}$$

$$|Z|\sin\phi = \frac{-R^2C\omega}{1 + (RC\omega)^2} \Longrightarrow \text{Imaginary part} \tag{27}$$

If we use the advantage of $(\cos\phi)^2 + (\cos\phi)^2 = 1$ and rewrite equations (Eq.26) and (Eq.27), we get:

$$|Z| = \frac{R\sqrt{1 + (RC\omega)^2}}{1 + (RC\omega)^2} = \frac{\sqrt{R^2 + (R^2C\omega)^2}}{1 + (RC\omega)^2} \tag{28}$$

then we devide equation (Eq.27) over equation (Eq.26) and we get:

$$\frac{|Z|\sin\phi}{|Z|\cos\phi} = \tan\phi = -\frac{R^2C\omega}{R} = -RC\omega \tag{29}$$

If we rewrite equation (Eq.28), we get:

$$R = |Z|\sqrt{1 + \underbrace{(RC\omega)^2}} \text{ where } (RC\omega)^2 = \tan\phi^2 \tag{30}$$

Then we rewrite equation (Eq.29) and combine it with equation (Eq.28)

$$C = -\frac{\tan\phi}{R\omega} = -\frac{\tan\phi}{|Z|\underbrace{\omega}} = \frac{\tan\phi}{|Z|\underbrace{2\pi f}} \tag{31}$$

where ϕ in degrees is an argument of Z $= \frac{\pi}{180} = rad$ and f is frequency.
In polar form we can rewrite equation (Eq.**??**) as

$$Z = |Z|(\cos\phi + j\sin\phi) \Longrightarrow \frac{1}{Z} = \frac{1}{|Z|(\cos\phi + j\sin\phi)} \tag{32}$$

Next we rewrite equation (Eq.32), then we get

$$\frac{1}{Z} = \frac{1}{|Z|(\cos\phi + j\sin\phi)} = \frac{|Z|\cos\phi - |Z| j\sin\phi}{|Z|^2\cos^2\phi - |Z|^2 j\sin^2\phi} \tag{33}$$

$$= \frac{|Z|\cos\phi - |Z| j\sin\phi}{|Z|^2} = \frac{1}{|Z|}\cos\phi - j\frac{1}{|Z|}\sin\phi \tag{34}$$

Since we know from equation (Eq.**??**) that real part $\mathrm{Re}(Z) = \frac{1}{R}$ and the imaginary part $\mathrm{Im}(Z) = C\omega$, we can combine equation (Eq.**??**) and (Eq.33) to get

$$k = \frac{1}{2\pi h}\cos\phi\frac{1}{|Z|} = \frac{1}{2\pi h}\mathrm{Re}(\frac{1}{Z}) \Longrightarrow \text{Conductivity =Real part of (Z)} \tag{35}$$

where h is height.

$$\varepsilon = -\sin\phi\frac{1}{|Z|}\frac{1}{2\pi h}\frac{1}{\underbrace{\omega}\varepsilon_0} = -\sin\phi\frac{1}{|Z|}\frac{1}{2\pi h}\frac{1}{\underbrace{2\pi f}\varepsilon_0} \tag{36}$$

$$= \frac{1}{2\pi h}\frac{1}{\underbrace{2\pi f}\varepsilon_0}\mathrm{Im}(\frac{1}{Z}) \Longrightarrow \text{Permittivity} \tag{37}$$

Note that we can write the complex permittivity and conductivity as:

$$\overset{*}{k} = k + j\omega\varepsilon_0\varepsilon \Longrightarrow \text{ complex conductivity} \tag{38}$$
$$\overset{*}{\varepsilon} = \varepsilon + \frac{k}{j\omega\varepsilon_0} \Longrightarrow \text{ complex permittivity}$$

Now if we rewrite equations (Eq.38), we get relation between complex conductivity and permittivity

$$\overset{*}{k} = j\omega\varepsilon_0\overset{*}{\varepsilon} \tag{39}$$

If we combine equation (Eq.38) and equation (Eq.21), we get:

$$Z = \frac{1}{\overset{*}{k}}\frac{1}{2\pi h} = \frac{1}{k + j\omega\varepsilon_0\varepsilon}\frac{1}{2\pi h} = \frac{1}{j\omega\varepsilon_0\overset{*}{\varepsilon}}\frac{1}{2\pi h} \tag{40}$$

$$\frac{1}{Z} = 2\pi h(k + j\omega\varepsilon_0\varepsilon) \tag{41}$$

$$\mathrm{Re}(\frac{1}{Z})\frac{1}{2\pi h} = k \;\&\; \mathrm{Im}(\frac{1}{Z})\frac{1}{2\pi h\varepsilon_0} = \omega\varepsilon \tag{42}$$

7.2.3 Model equations

The network analyzer measures the impedance of media. From the impedance the resistance and the capacitance values can be derived, according to the equations:

$$R = |Z|\sqrt{1 + \underbrace{(Rc\omega)^2}} \Longrightarrow (Rc\omega)^2 = \tan\theta \tag{43}$$
$$C = -\frac{\tan\theta}{|Z|\omega} = -\frac{\tan\phi}{R\omega}$$

From the calculated resistance and capacitance we can determine the medium's dielectric coefficient and conductivity values, using the following expressions:

$$\varepsilon = C\ln(\frac{D}{d})\frac{1}{2\pi\varepsilon_0 h} \Rightarrow \ln(\frac{D}{d}) = K = \text{constant} \Rightarrow \varepsilon = \frac{C}{2\pi h\varepsilon_0}K \tag{44}$$
$$\sigma = \frac{1}{R}\frac{1}{2\pi h}\ln(\frac{D}{d}) \Rightarrow \ln(\frac{D}{d}) = K = \text{constant} \Rightarrow \sigma = \frac{1}{2\pi hR}K$$

where D is the diameter of the outer electrode ($D = 0.03$m) and d is the diameter of the inner electrode ($d = 0.009$m).

The calculated values ε and σ are temperature and frequency dependent. In case of a low frequency range, the measurement will be affected due to electrode polarization. By using the analytical model (Analytical Solution) [13][14], we reduce the effect of the electrode polarization. More information on electrode polarization and the analytical model can be found in the following part of this appendix.

7.2.4 Analytical model for electrode polarization correction

The electromagnetic behavior of the material has been studied and investigated from a long time ago. The physical and electrochemical models for electrode polarization EP in dielectric measurements started with the study of electrostatic screening (damping of electric fields caused by the presence of mobile charge carriers). The first to offer a description of the phenomenon was Von Helmholtz.

He considered the formation of a layer of absorbed ions along the electrode surface, due to migration of free ions in the solution (e.g., the electrolyte) under the influence of an external field, described as the inner Helmholtz layer. Due to the difference in adsorption and solubility between different types of ions, the Helmholtz layer is often called the electrical double layer EDL. More of physical models have followed taking into consideration the diffusive nature of ion transport under such conditions, for example the Gouy–Chapman model. In this model the potential drop over the diffuse layer is modelled as an exponentially decreasing function of distance. The characteristic length of this exponential decay is given by the Debye-Huckel expression:

$$\lambda_D = \sqrt{\frac{\varepsilon_r \varepsilon_0 K_B T}{2e^2 \sum n_j}} \tag{45}$$

where ε_r is the relative permittivity of the medium, ε_0 is the absolute permittivity of free space, K_B is Boltzmann's constant $(1.38\ (\pm 0.0000013) \cdot 10^{-23} JK^{-1})$, T is the temperature, e is the fundamental unit of charge and n_j is the concentration of free ions. With the two-electrode cell technique, electrode polarization EP can strongly affect impedance spectroscopy measurements on measured samples (NaCl solutions with diffrent salinity or concentrations $1, 2, 5$mM (mole per liter). It is caused by the formation of an electric double layer at the boundary between electrodes and the sample under test. As a consequence, the electric response of the medium is contaminated by EP, especially at lower frequencies (and at high concentration of NaCl solution). This research used the model of Chassagne, Bedeaux, Ploeg and Koper to correct the polarization between concentric cylindrical electrodes. Electrode polarization refers to the phenomenon whereby charge builds up in the salt-water solution (electrolyte) near the two opposing electrodes. This process is particularly visible in the case of low frequency transmission during which most information regarding dielectric enhancement and frequency relaxation becomes apparent. [13][14]. The model equations that we used are the following:

$$\varepsilon^* = \frac{\varepsilon_1}{\kappa \frac{1}{\frac{2}{D}+\frac{2}{d}} (\frac{\omega}{\kappa^2 D_0}) \ln(\frac{D}{d})} \tag{46}$$

$$\sigma^* = \varepsilon_0 \varepsilon_1 \kappa^2 D_0$$

$$K^2 = \frac{2q^2 c\xi}{\varepsilon_0 \varepsilon_1 KT} \tag{47}$$

$$D_0 = \frac{D_1 + D_2}{2} \tag{48}$$

Where:
ω = angular frequency in radius per second [rad/s] $(2\pi f)$
ε_0 = dielectric coefficient of free space $(\varepsilon = 1)$
ε_1 = dielectic coefficient of water $(\varepsilon = 79.08)$

c = salt concentration (e.g. 1mM, 2mM, 5mm and 0.5M)
D_1 = ionic diffusion coefficient for ion-1 ($Na \approx 2.032 \times 10^{-9}$)
D_2 = ionic diffusion coefficient for ion-2 ($Cl \approx 1.957 \times 10^{-9}$)
K = Debye Length ($K = 1.37 \times 10^{-23}$)
T = temperature in Kelvin (298.15)
D = outer diameter of the cylindrical electrode is 0.03m
d = inner diameter of the cylindrical electrode 0.009m
ξ = Avogadro constant $6.022140857 \times 10^{23}$ [mol^{-1}]
q = electron charge in Coulomb (C) $\approx 1.6 \times 10^{-19}$

8 Appendix-B: Maxwell's equations

This section will provide some history and background information in terms of key concepts and terminology which are reoccurring throughout this research, from the field of electromagnetics. The section will start by explaining some themes that help understanding the Maxwell equations, constitutive properties of the medium, generalized 3D wave equations, harmonic (sinusoidal) Maxwell forms and wave propagation.

8.1 Introduction and historical background

At the beginning of the nineteenth century, the concept of the force field in relation to electrostatics and magnetism was established. That is to say, around every magnet there is a magnetic field and around every charged object there is an electrostatic field. The difference between a magnetic and an electrostatic field is that an electrostatic field will transfer its energy on to insulators that can hold the electric charge, whereas a magnetic field will apply its force directly on to magnetic materials. Back in those days it was a commonly accepted theory that electrostatic and magnetic fields do not affect each other. This notion changed when scientist Hans C. Orsted (1777-1851) observed that when electrically charged objects were placed in a conductor, generating an electric current, this would create a force field which was able to affect a free moving magnet. As the only force that can have an impact on a free moving magnet is a magnetic field, from this experiment it could be concluded that electrically charged objects moving through a conductor produce a (temporary) magnetic force field. Note that a changing electric field produces a magnetic field [E*]. Halfway through the19^{th} century James Clerk Maxwell analyzed and formulated Orsted's findings on electromagnetism, along with the findings of other scientists in the field. From these analyses he formulated the Maxwell equations, which include Gauss' law, Faraday's law and Ampere's law. Within his relatively short lifetime Maxwell laid with his formulations the fundamental basis of electromagnetism, making him one of the greatest scientists along with Isaac Newton and Albert Einstein [F*].

8.2 Maxwell's equations

Maxwell's Equations are a complete set of four equations that describe and characterize the electromagnetic phenomena. These equations describe how electric and magnetic fields propagate, interact, and how they are influenced by objects or media [A*]. The Maxwell equations (the known laws of electricity and magnetism) are a result of many years of research of the factors associated with electricity and magnetism. Controversially, the equations have not derived from a completely analytical methodology. Nevertheless, they produce reasonable results and so far no experiments have proved them to be wrong. Therefore, they are accepted by the scientific community as valid laws to characterize electromagnetic phenomena. However, it must be noted that the Maxwell equations are only applicable in a situation where the dimensions are large compared to the atomic dimensions [65]. The first of Maxwell's equations (law of Gauss for electric fields) expresses that the divergence of the electric flux $\mathbf{D}$ is the charge density ρ over ε_0. This means that the total electric flux depends on the amount of electric charge inside a closed surface. Thus, in the case of a vacuum where there is no charge density, consequently the electric flux is equal to zero. Gauss law for electric fields is valid in both dynamic as well as in static fields [65]. In the second Maxwell equation (law of Gauss for magnetic fields) the divergence of magnetic flux $\mathbf{B}$ is equal to zero. Therefore the total magnetic flux through a closed surface is zero. This statement is true due to the fact that magnetic monopoles do not exist [A*]. The third Maxwell equation is Faraday's law of induction; this equation states that the changing magnetic field $\mathbf{H}$ with time produces an electric field $\mathbf{E}$, and vice versa. The curl of the electric field is equal to the derivative of the magnetic field in time [65]. The last equation of Maxwell's equations is the Ampere-Maxwell law. This equation shows that an electric current and a changing magnetic field produce a magnetic field. Mathematically speaking, this equation is noted as follows $\nabla \times \mathbf{H} = \mathbf{J} + \frac{\partial \mathbf{D}}{\partial t}$. The last term of the Ampere-Maxwell law is called the displacement current, which was added by Maxwell himself to the existing Ampere's law in order to guarantee charge conservation [A*].

$$\oint_s \mathbf{D} \cdot ds = \int_v \rho \cdot dv \text{ (Integral form)} \implies \nabla \cdot \mathbf{D}(\overrightarrow{r}, t) = \rho_v(\overrightarrow{r}, t) \text{ (Point form)} \tag{49}$$

$$\implies \text{Gauss' Law for Electric field } \overrightarrow{\mathbf{E}} \tag{50}$$

where s is surface, v is volume, r is position and t is time [A*].

$$\oint_s \mathbf{B} \cdot ds = 0 \text{ (Integral form)} \implies \nabla \cdot \mathbf{B}(\overrightarrow{r}, t) = \mathbf{0} \text{ (Point form)} \tag{51}$$

$$\implies \text{Gauss' Law for Magnetic fields } \overrightarrow{\mathbf{H}} \tag{52}$$

$$\oint_c \mathbf{E} \cdot d\mathbf{I} = -\frac{d}{dt}\int_s \mathbf{B} \cdot ds \text{ (Integral form)} \Longrightarrow \nabla \times \mathbf{E}(\overrightarrow{r}, t) \tag{53}$$

$$= -\frac{\partial \mathbf{B}(\overrightarrow{r}, t)}{\partial t} \text{ (Point form) } \Longrightarrow \text{ Faraday's law} \tag{54}$$

$$\oint_c \mathbf{H} \cdot d\mathbf{I} = \int_s \mathbf{J} \cdot ds + \frac{d}{dt}\int_s \mathbf{D} \cdot ds \text{ (Integral form)} \Longrightarrow \nabla \times \mathbf{H}(\overrightarrow{r}, t) \tag{55}$$

$$= \mathbf{J}(\overrightarrow{r}, t) + \frac{\partial \mathbf{D}(\overrightarrow{r}, t)}{\partial t} \text{ (Point form)} \Longrightarrow \text{ Ampere-Maxwell's law} \tag{56}$$

where $\mathbf{I}$ is the current in Ampere and $\mathbf{J}$ is the current density in Ampere per m^2 [65].

8.3 Constitutive Properties of the Medium (constitutive relations)

The constitutive properties of a medium (or constitutive relations) are the physical and chemical characteristics which depend on the molecular structure of the medium [65]. The constitutive relation (constitutive equation) is the relation between two physical properties that is specific to a medium and estimates the response of the medium to external fields and forces. Constitutive equations are combined with physical laws (e.g. Maxwell's equations), in order to solve physical problems. In the case of the Maxwell's equations they are combined with constitutive relations in order to characterize the electromagnetic wave propagation through specific media [H*]. The electric and magnetic flux densities $\mathbf{D}$, $\mathbf{B}$ and current density $\mathbf{J}$ are related to the field intensities $\mathbf{E}$, $\mathbf{H}$ via the constitutive relations, whose exact form depends on the material in which the fields exist. We consider only media that are linear, isotropic and homogeneous such that:

$$\mathbf{D} = \varepsilon \mathbf{E} \tag{57}$$

$$\mathbf{B} = \mu \mathbf{H} \tag{58}$$

$$\mathbf{J} = \sigma \mathbf{E} \tag{59}$$

In vacuum, constitutive relations take their simplest form:

$$\mathbf{D} = \varepsilon_0 \mathbf{E} \tag{60}$$

$$\mathbf{B} = \mu_0 \mathbf{H} \tag{61}$$

where the scalar permeability $\mu = \mu_0 = \mathbf{4}\pi \cdot \mathbf{10}^{-7}$[henry/m] and permitivity $\varepsilon = \varepsilon_0 = \mathbf{8.854} \cdot \mathbf{10}^{-12}$[farad/m].

For sinusoidal variation of field in linear, isotropic and homogeneous media, the scalars permittivity, permeability and conductivity often depend on frequency. Moreover, these scalars are typically valid at low frequencies ranges. We can also rewrite Maxwell's Equations with only **E** and **H** present. This means we are going to get rid of **D**, **B** and the electric current density **J**. We can do this by substituting equations (Eq.57, 58 and 59) in equations (Eq.49, 51, 53 and 55)

$$\nabla \cdot \mathbf{E} = \frac{\rho_v}{\epsilon} \tag{62}$$

$$\nabla \cdot \mathbf{H} = \mathbf{0} \tag{63}$$

$$\nabla \times \mathbf{E} = -\mu \frac{\partial \mathbf{H}}{\partial t} \tag{64}$$

$$\nabla \times \mathbf{H} = \sigma \mathbf{E} + \epsilon \frac{\partial \mathbf{E}}{\partial t} \tag{65}$$

[65].

8.4 The wave equation

The wave equation is one of the most fundamental equations in the world of electromagnetics, which shows that all waves travel at a single speed (the speed of light). The aim in this subsection is to derive generalized 3D equations from the Maxwell's equations. This can be achieved as follows: we assume we are in a source free area so no charges or currents are flowing ($\rho_v = 0; \mathbf{J} = \mathbf{0}$), where ρ_v and **J** are the electric charge and current density respectively. The wave equation will be derived from Faraday's and Ampere's law [A*]. The aim of this wave equation derivation is to determine how electric and magnetic fields propagate through the area. Firstly, we look at Faraday's law and take the curl of both sides, then we get:

$$\nabla \times \bigtriangledown \times \mathbf{E} = -\frac{\partial(\nabla \times \mathbf{B})}{\partial \mathbf{t}} \tag{66}$$

Since we consider only media that are linear, isotropic and homogeneous, we can rewrite the magnetic flux density as ($\mathbf{B} = \mu\mathbf{H}$) then equation (Eq.67) becomes:

$$\nabla \times \bigtriangledown \times \mathbf{E} = -\mu * \frac{\partial(\nabla \times \mathbf{H})}{\partial \mathbf{t}} \tag{67}$$

We can write the curl of the curl of the electric field intensity **E** as:

$$\nabla \times \bigtriangledown \times \mathbf{E} = \bigtriangledown(\bigtriangledown \cdot \mathbf{E}) - \bigtriangledown^2 \mathbf{E} \tag{68}$$

[65]

Since we operate under the assumption that we are in a source free region, the first term on the right side of equation (Eq.66) known as the gradient of the divergence is zero, then we can rewrite equation (Eq.68) as

$$\nabla \times \bigtriangledown \times \mathbf{E} = -\bigtriangledown^2 \mathbf{E} \tag{69}$$

[A*].

The term which remains on the right side of equation (Eq.69) is called the Laplacian. This is basically the sum of second-order partial derivatives, as seen in equation (Eq.70)

$$\bigtriangledown^2 \mathbf{E} = \bigtriangledown^2 \begin{matrix} \mathbf{E}_x \\ \mathbf{E}_y \\ \mathbf{E}_z \end{matrix} = \begin{matrix} \frac{\partial^2 \mathbf{E}_x}{\partial x^2} & \frac{\partial^2 \mathbf{E}_x}{\partial y^2} & \frac{\partial^2 \mathbf{E}_x}{\partial z^2} \\ \frac{\partial^2 \mathbf{E}_y}{\partial x^2} & \frac{\partial^2 \mathbf{E}_y}{\partial y^2} & \frac{\partial^2 \mathbf{E}_y}{\partial z^2} \\ \frac{\partial^2 \mathbf{E}_z}{\partial x^2} & \frac{\partial^2 \mathbf{E}_z}{\partial y^2} & \frac{\partial^2 \mathbf{E}_z}{\partial z^2} \end{matrix} \tag{70}$$

[A*].

Now, we can rewrite the left side of equation (Eq.67) (the curl of the curl of $\mathbf{E}$) with the help of equation (Eq.69), and we can rewrite the right side of equation (Eq.67) by substituting in Ampere's law:

$$\nabla \times \bigtriangledown \times \mathbf{E} = -\bigtriangledown^{\mathbf{2}} \mathbf{E} = -\mu \frac{\partial(\nabla \times \mathbf{H})}{\partial \mathbf{t}} = -\mu \frac{\partial}{\partial t} \left[\frac{(\partial \mathbf{D})}{\partial \mathbf{t}} + \mathbf{J} \right] \tag{71}$$

Since we assume we are in a source free region ($\mathbf{J}= \mathbf{0}$), then we can rewrite equation [6] as:

$$\nabla \times \bigtriangledown \times \mathbf{E} = -\bigtriangledown^{\mathbf{2}} \mathbf{E} = -\mu \frac{\partial(\nabla \times \mathbf{H})}{\partial \mathbf{t}} = -\mu \frac{\partial}{\partial t} \left[\frac{(\partial \mathbf{D})}{\partial \mathbf{t}} + \mathbf{0} \right] \tag{72}$$

Since we consider only media that are linear, isotropic and homogeneous, we can rewrite the electric flux density as: ($\mathbf{D}= \varepsilon \mathbf{E}$) then equation (Eq.72) become

$$-\bigtriangledown^{\mathbf{2}} \mathbf{E} = -\mu \frac{\partial(\partial \mathbf{D})}{\partial \mathbf{t}} = -\mu\epsilon \frac{\partial}{\partial t} \left[\frac{(\partial \mathbf{E})}{\partial \mathbf{t}} \right] \tag{73}$$

As last, when we rewrite equation (Eq.73), the vector wave equation becomes

$$\bigtriangledown^{\mathbf{2}} \mathbf{E} = \mu\varepsilon \frac{\partial^2 \mathbf{E}}{\partial t^2} \tag{74}$$

[A*].

The vector wave equation or the wave equation is actually three equations, since we have three components (x, y and z) in the electric static field $\mathbf{E}$(x,y,z)

and **E**(x,y,z,t) in time-varying field that exists in source-free region. Further, we consider that we have only an electric field that is polarized in the x-direction. In addition, we assume that the E-field is travelling in the z-direction and there is no variation in the x- and y-direction (partial derivatives with respect to x- and y-direction are zero). Then equation (74) is simplified and becomes:

$$\bigtriangledown^{\mathbf{2}}\mathbf{E}_x = \mu\varepsilon\frac{\partial^2\mathbf{E}_x}{\partial t^2} \Longrightarrow \frac{\partial^2\mathbf{E}_x}{\partial z^2} = \mu\varepsilon\frac{\partial^2\mathbf{E}_x}{\partial t^2} \tag{75}$$

The solution of the differential equation in Equation (Eq.75) can be written as $(f(z-ct))$ or $(f(z+ct))$; these two terms will satisfy the differential equation in equation (Eq.75)

$$\mathbf{E}^- = f(z-ct) \Longrightarrow \mathbf{E}^+ = f(z+ct) \Longrightarrow \tag{76}$$

$$\mathbf{E} = f(z-ct) + f(z+ct) \Longrightarrow \mathbf{E}_x = f(z-ct) \tag{77}$$

$$\frac{\partial\mathbf{E}_x}{\partial z} = \frac{\partial f(z-ct)}{\partial z} = f'(z-ct)\frac{\partial(z-ct)}{\partial z} = f'(z-ct) \tag{78}$$

$$\frac{\partial^2\mathbf{E}_x}{\partial z^2} = \frac{\partial}{\partial z}\left[\frac{\partial\mathbf{E}_x}{\partial z}\right] = f''(z-ct)\frac{\partial(z-ct)}{\partial z} = f''(z-ct) \tag{79}$$

$$\frac{\partial\mathbf{E}_x}{\partial t} = \frac{\partial f(z-ct)}{\partial t} = f'(z-ct)\frac{\partial(z-ct)}{\partial t} = f'(z-ct) \tag{80}$$

$$\frac{\partial^2\mathbf{E}_x}{\partial t^2} = \frac{\partial}{\partial t}\left[\frac{\partial\mathbf{E}_x}{\partial t}\right] = f''(z-ct)\frac{\partial(z-ct)}{\partial t} = f''(z-ct) \tag{81}$$

$$\bigtriangledown^{\mathbf{2}}\mathbf{E}_x = \frac{\partial^2\mathbf{E}_x}{\partial z^2} = \mu\epsilon\frac{\partial^2\mathbf{E}_x}{\partial t^2} \implies \text{if} \implies \mathbf{E}_x = f(z-ct) \text{ and } c = \frac{1}{\sqrt{\mu\epsilon}} \tag{82}$$

[A*].

Equation (Eq.82) says that any function of the form f(z-ct) satisfies the vector wave equation or the wave equation. This means that Maxwell's equations allow waves of any shape, or in other words, we can send any type of signal through radio waves to propagate through the universe. The term f(z-ct) represents a wave travelling in positive z-direction at speed of c (speed of light).

$$c = \frac{1}{\sqrt{\mu\varepsilon}} \Longrightarrow \text{ Speed of light} \tag{83}$$

In free space (vacuum), where the scalar permeability $\mu = \mu_0 = 4\pi{\cdot}10^{-7}[H/m]$ and permitivity $\varepsilon = \varepsilon_0 = 8.854\cdot10^{-12}$(F/m). Note that, (H = henry; F = farad units)

$$c_0 = \frac{1}{\sqrt{\mu_0 \varepsilon_0}} \Longrightarrow \ 299,795,638(\text{m/s}) \tag{84}$$

$$\approx 3 \cdot 10^8(\text{m/s}) \Longrightarrow \text{Speed of light in vacuum} \tag{85}$$

[A*].

In case of the characteristic impedance in vacuum η_0:

$$\eta_0 = \sqrt{\frac{\mu_0}{\varepsilon_0}} \Longrightarrow \sqrt{\frac{\mathbf{4\pi \cdot 10^{-7}}}{\mathbf{8.854 \cdot 10^{-12}}}} = 377 \text{ (ohm)} \tag{86}$$

[65].

8.5 Time-Harmonic Form of Maxwell's Equations (phasor form)

In order to have a clear understanding of the propagation of an electromagnetic field, we first need to comprehend the nature of the a wave. Wave motion occurs when a disturbance at point A at time t_0 is related to what happens at point B at time $t > t_0$. Thus, a wave is function of both space and time. In equation (75), we described a scalar wave equation in the x-direction assuming that the **E**-field is travelling in the z-direction and there is no variation in the x- and y-direction. If we rewrite equation (Eq.75) by substituting equation (Eq.83) into equation (Eq.75) we get:

$$\frac{\partial^2 \mathbf{E}_x}{\partial t^2} - c^2 \frac{\partial^2 \mathbf{E}_x}{\partial z^2} = 0 \tag{87}$$

where c is the wave velocity in which the medium is source free (no charges or currents are flowing $\rho_v = 0; \mathbf{J} = \mathbf{0}$) [65].

From the theory of Fourier Transforms, every signal in time can be rewritten as the sum of sinusoids (sign or cosine) [A*]. So, if we assume sinusoidal or harmonic time dependence $e^{j\omega t}$, equation (87) becomes

$$\frac{\partial^2 \mathbf{E}_x}{\partial z^2} + \beta^2 \mathbf{E}_s = 0 \tag{88}$$

where, $\mathbf{E}_s$ is the phasor form of electric field intensity **E** and β is ω/c, in which ω is the angular frequency ($\omega = 2\pi f$)[65].

With the time factor inserted in the wave equation (Eq.87), then the possible solution of the wave equation (Eq.88) can be rewritten as follows

$$\mathbf{E}^- = Ae^{j(\omega t + \beta z)} \Longrightarrow \mathbf{E}^+ = Be^{j(\omega t + \beta z)} \Longrightarrow \tag{89}$$

$$\mathbf{E} = Ae^{j(\omega t + \beta z)} + Be^{j(\omega t - \beta z)} \Longrightarrow \mathbf{E}_x = Ae^{j(\omega t + \beta z)} \tag{90}$$

In a situation where there is a harmonic (sinusoidal) time dependence, the Maxwell equations are significantly simplified. In general the solution of Maxwell's

equations can be assembled as linear combinations of single-frequency solutions through the inverse Fourier transform. Here the field factors can be noted in the form of phasors. This notation results in a considerable simplification of a large number of the mathematical details. Maxwell's Equations in time-harmonic form (or phasor form) are

$$\nabla \cdot \mathbf{D} = \rho_v \tag{91}$$

$$\nabla \cdot \mathbf{B} = \mathbf{0} \tag{92}$$

$$\nabla \times \mathbf{E} = -\mathbf{i}\omega \cdot \mathbf{B} = -\mathbf{j2}\pi\mathbf{f} \cdot \mathbf{B} \tag{93}$$

$$\nabla \times \mathbf{H} = \mathbf{J} + \mathbf{j}\omega \cdot \mathbf{D} \tag{94}$$

[65].

Maxwell's equations in time-harmonic Form (**E**,**B**) maintained by (ρ, $\overrightarrow{J}$) in simple electromagnetic EM media are: where $\frac{\partial}{\partial t} = j\omega$, **D**= ε**E** and **B**= μ**H**

$$\nabla \cdot \mathbf{E}(\overrightarrow{r}) = \frac{\rho_v}{\varepsilon} \tag{95}$$

$$\nabla \cdot \mathbf{B}(\overrightarrow{r}) = \mathbf{0} \tag{96}$$

$$\nabla \times \mathbf{E}(\overrightarrow{r}) = -j\omega \cdot \mathbf{B}(\overrightarrow{r}) = -j\mathbf{2}\pi\mathbf{f} \cdot \mathbf{B}(\overrightarrow{r}) = \tag{97}$$

$$\nabla \times \mathbf{B}(\overrightarrow{r}) = \mu \overrightarrow{\mathbf{J}}(\overrightarrow{r}) + \mu(\sigma + j\omega\varepsilon) \cdot \mathbf{E}(\overrightarrow{r}) \tag{98}$$

[65]

8.6 Derivation of Maxwell's equation used in the COMSOL simulation

We start with Ampere-Maxwell's law (Eq.55)

$$\oint_c \mathbf{H} \cdot d\mathbf{I} = \int_s \mathbf{J} \cdot ds + \frac{d}{dt}\int_s \mathbf{D} \cdot ds \text{ (Integral form)} \tag{99}$$

$$\implies \nabla \times \mathbf{H}(\overrightarrow{r}, t) = \mathbf{J}(\overrightarrow{r}, t) + \frac{\partial \mathbf{D}(\overrightarrow{r}, t)}{\partial t} \text{ (Point form)} \tag{100}$$

$$\implies \text{Ampere-Maxwell's law} \tag{101}$$

As mentioned before, the electric and magnetic flux densities **D** and **B** are related to the field intensities **E**, **H** via the constitutive relations. We substitute equations (Eq.57 and 58) in equation (Eq.99) then we get

$$\nabla \times \frac{\mathbf{B}(\overrightarrow{r},t)}{\mu} = \mathbf{J}(\overrightarrow{r},t)+\frac{\partial \varepsilon \mathbf{E}(\overrightarrow{r},t)}{\partial t} \text{ Note, } \mathbf{D}=\varepsilon\mathbf{E} \text{ and } \mathbf{B}=\mu\mathbf{H} \tag{102}$$

We take the integeral in time for both sides so we get:

$$\nabla \times \frac{1}{\mu}\frac{\partial \mathbf{B}(\overrightarrow{r},t)}{\partial t} = \frac{\partial}{\partial t}\mathbf{J}(\overrightarrow{r},t)+\frac{\partial}{\partial t}\frac{\partial \varepsilon \mathbf{E}(\overrightarrow{r},t)}{\partial t} \tag{103}$$

Then we substitute Faraday's law (Eq.53) in equation (Eq.103) and rewrite equation (Eq.103), then we get

$$\nabla \times \frac{1}{\mu}\ \nabla \times \mathbf{E} = \frac{\partial}{\partial t}\mathbf{J}(\overrightarrow{r},t)+\varepsilon\frac{\partial^2 \mathbf{E}(\overrightarrow{r},t)}{\partial t^2} \tag{104}$$

We rewrite the right side of equation (Eq.104) in time harmonic (phasor) form, in order to get

$$\nabla \times \frac{1}{\mu}\ \nabla \times \mathbf{E} = \mathbf{J}_0 e^{j\omega t}+\varepsilon\omega^2\mathbf{E} \tag{105}$$

Then if we rewrite futher equation (Eq.105), we get

$$\nabla \times \ \frac{1}{\mu}\ (\nabla \times \mathbf{E}) = (j\omega\frac{\mathbf{J}_0}{\mathbf{E}}+\varepsilon\omega^2)\mathbf{E} \tag{106}$$

We can rewrite the current density $\mathbf{J}$ as following

$$\mathbf{J}_0=\sigma\mathbf{E} \tag{107}$$

If we substitute equation (Eq.107) into equation (Eq.106), we get

$$\nabla \times \ \frac{1}{\mu}\ (\nabla \times \mathbf{E}) = (j\omega\sigma+\varepsilon\omega^2)\mathbf{E} \tag{108}$$

If we substitute the term of the relative permitivity $\varepsilon_r = \varepsilon/\varepsilon_0$ into equation (Eq.108), we get

$$\nabla \times \ \frac{1}{\mu}\ (\nabla \times \mathbf{E}) = \varepsilon_0(\frac{j\omega\sigma}{\varepsilon_0}+\varepsilon_r\omega^2)\mathbf{E} \tag{109}$$

We rewrite futher equation (Eq.109), so we get

$$\nabla \times \ \frac{1}{\mu}\ (\nabla \times \mathbf{E}) = \omega^2\varepsilon_0(\frac{j\sigma}{\omega\varepsilon_0}+\varepsilon_r)\mathbf{E} \tag{110}$$

Now we substitute the term of relative permeability $\mu_r = \mu/\mu_0$ into equation (Eq.110),

$$\nabla \times \ \frac{1}{\mu_r\mu_0}\ (\nabla \times \mathbf{E}) = \omega^2\varepsilon_0(\frac{j\sigma}{\omega\varepsilon_0}+\varepsilon_r)\mathbf{E} \tag{111}$$

Next we rewrite equation (Eq.111), so we get

$$\nabla \times \frac{1}{\mu_r}(\nabla \times \mathbf{E}) = \omega^2 \varepsilon_0 \mu_0 (\frac{j\sigma}{\omega \varepsilon_0} + \varepsilon_r)\mathbf{E} \tag{112}$$

If we put $k_0^2 = \omega^2 \varepsilon_0 \mu_0$ and replace k_0^2 in equation (Eq.112), we get

$$\nabla \times \frac{1}{\mu_r}(\nabla \times \mathbf{E}) = k_0^2 (\frac{j\sigma}{\omega \varepsilon_0} + \varepsilon_r)\mathbf{E} \tag{113}$$

Now we rewrite equation (Eq.114) and we get

$$\nabla \times \frac{1}{\mu_r}(\nabla \times \mathbf{E}) - k_0^2 (\varepsilon_r - j\frac{\sigma}{\omega \varepsilon_0})\mathbf{E} = \mathbf{0} \tag{114}$$

Note that $k_0^2 = \omega^2 \varepsilon_0 \mu_0$ defines the wavenumber k_0 for a lossless medium where $\sigma = 0$, while in general for an unbounded simple medium (linear, isotropic and homogeneous) k is written as follows

$$k_0^2 = \omega^2 \varepsilon_0 \mu_0 (1 - \frac{j\sigma}{\omega \varepsilon}) \text{ where, } \sigma \neq 0 \tag{115}$$

9 Appendix-C: Electromagnetic wave modulation and propagation

This section provides a basic theoretical background on electromagnetic EM wave modulation and wave propagation; indispensable concepts in the communication processes in an RFID system. Firstly, three different types of modulation, i.e. amplitude, frequency and phase modulation, are addressed. Subsequently, various factors that influence wave propagation are highlighted, i.e. reflection, refraction and signal interference.

9.1 Wave modulation

Communication processes revolve around sending information from one location to another [I*]. EM energy, which is a mixture of electricity and magnetism, is transmitted through EM waves. Waves have a certain speed, length, and frequency. The speed indicates how fast the wave travels between transmitter and receiver. The wavelength is the distance between one wave peak (crest or trough) and the next, while the frequency is the number of waves that arrive each second, measured in Hertz (Hz) [J*]. Waves must be modulated in order to transmit information. Modulation is the process of shifting some characteristics (such as amplitude, phase and frequency) of the carrier signal, and can involve both analogue or digital methods. A carrier wave is a wave that 'carries' the EM wave containing the information. In the modulation process, the carrier wave and the electromagnetic wave are combined, forming a modulating signal (message signal). The modulating signal is modulated due to variations in the amplitude, frequency or phase of the carrier wave, which is created in the transmitter. At the receiver end the carrier wave is separated from the signal to retrieve the information signal; this is called demodulation [H*; J*].

9.1.1 Amplitude modulation

In amplitude modulation (AM), the distance between the wave crests and troughs of the carrier signal, and therefore also the modulating signal, are made bigger or smaller. In the amplitude modulation transmitter, adjusted amplitude variations of the carrier waves are combined with the radio frequency signal. In other words, the transmitter uses the information signal, $\mathrm{V}_m(\mathrm{t})$ to vary the amplitude of the carrier, $\mathrm{V}_c(\mathrm{t})$ to produce a modulated signal, $\mathrm{V}_{AM}(\mathrm{t})$. The information, carrier and amplitude modulation signals are shown in mathematical form as:

$$\begin{aligned} V_m(t) &\Longrightarrow \text{ Information signal} \\ V_c(t) = V_{c0}\sin(2\phi f_c t + \phi) &\Longrightarrow \text{ Carrier signal} \\ V_{AM}(t) = [V_{c0} + V_m(t)]\sin(2\phi f_c t + \phi) &\Longrightarrow \text{ Amplitude modulation signal} \end{aligned} \tag{116}$$

[K*]

The combined signals that are send from the transmitter antenna to the receiver antenna can be affected by all kinds of random noise, such as lightning or other electrical devices. Random noises might add new variations in the wave length of the composed signals. The antenna receiver of the AM system cannot distinguish between composed RF signal and random noise and will pick up both of them from transmitting antenna. The signal and the noise will combine through the detector of the receiver antenna and interrupt the amplitude frequency signals that come out of the receiver antenna. Noise generally only affects the amplitude of the signal, not the frequency of the wave. That is why frequency modulation (FM) was in fact a logical development in the field of radio wave transmission [L*].

9.1.2 Frequency modulation & Phase modulation

Frequency modulation and phase modulation are very similar to amplitude modulation. In frequency modulation fluctuations are made in the frequency of the carrier signal. These fluctuations take place within the frequency range of the signal (system). In phase modulation, the phase of the carrier wave is adjusted according to the bandwidth (baseband) of the modulating signal [H*]. Frequency modulation uses the information signal, $\mathrm{V}_m(\mathrm{t})$ to vary the carrier frequency within some small range about its original value. Here are the three signals in mathematical form:

$$\begin{aligned} V_m(t) &\Longrightarrow \text{ Information signal} \\ V_c(t) = V_{c0}\sin(2\phi f_c t + \phi) &\Longrightarrow \text{ Carrier signal} \\ V_{FM}(t) = V_{c0}\sin(2\pi[f_c + (\frac{\triangle f}{V_{m0}})V_m(t)]t + \phi) &\Longrightarrow \text{ Frequency modulation signal} \end{aligned} \tag{117}$$

[L*].

9.2 Wave propagation

EM waves originate from disturbances in electric and magnetic fields. From the start a wave actually propagates outwards in all directions. In a medium with no variation in characteristics such as air, the wave spreads out consistently. At a large distance from its departure location, the wave will appear to have the same amplitude in all directions. As the wave propagates similar in all directions, in an analysis it is more practical to think of the entire wave as if it was travelling in a single direction. This idealized concept of the wave is called a plane wave. In a vacuum, EM waves travel at the speed of light c_0. When a wave propagates through different media however, the velocity c_m of the wave will decrease. Mathematically speaking the refraction index n can thus be noted as follows: $n = c_0/c_m$ and is equal to 1.0003 and 1.33 in case of air and water respectively [J*].

9.2.1 Reflection

In a situation where a plane wave propagates through a different medium, part of the wave energy might enter the medium (transmitted portion) and part might be reflected away from the medium (reflected portion). The reflected portion of the wave behaves rather straightforward. Namely, the plane wave hits the surface of the medium at certain angle. The angle between the direction of the wave and the line perpendicular to the surface on the same side of that surface is called the angle of incidence. The angle between the direction of the reflected wave and the line perpendicular to the surface on the same side is called the angle of reflection. Thus the rule for reflection is that the angle of reflection is equal to the angle of incidence. When a medium has a lower index refraction index, the wave undergoes a 180^o phase shift upon reflection. However, in case a medium has a larger index of refraction, the reflected wave has no phase shift [J*].

9.2.2 Refraction

As stated previously, when an EM wave propagates through a medium, the velocity of the wave will reduce. The higher the index of refraction a medium has, the more the velocity and wavelength of the wave will decrease. Note that the frequency of the wave must stay the same due to the boundary conditions. In order for the incident wave and transmitted wave to match at the interface of the medium, the transmitted wave will change its direction one that is closer to the perpendicular line. In other words, when the indices of refraction increase, the speed of propagation of the transmitted wave through the media decreases which results in a closer approximation of the transmitted wave in the media to the perpendicular line. The relationship between the angles and indices of refraction can be calculated according to Snell's Law: $n_i \sin\theta_I = n_t \sin\theta_t$ where θ_I and θ_t are the angles of incident and refract wave respectively. When the direction of propagation changes, the wave is said to refract. It is most useful

to know in which direction the wave will refract, not necessarily by how much [J*].

9.2.3 Interference

EM waves can overlap each other; the electric and magnetic fields simply add at each point. In a situation where two waves with the same frequency overlap, this results in a constant interference pattern. Interference can have both a strengthening or destructive effect on the wave. The quantity of interference depends on the difference in phase $\triangle\phi$ at a certain point. The phase is a constant that tells at what value the sine function has when $t = 0$ and $x = 0$. Furthermore, the phase is an angle measured either in degrees or radians. In general, interferences from phase differences of $0^o - 120^o$ and $240^o - 360^o$ have a strengthening effect on the wave. However, destructive interference takes place from $120^o - 360^o$. For two identical waves, no phase shift $\triangle\phi$ results in total constructive interference, where the strength is maximum and 180^o phase shift will create total destructive interference (no signal at all). The phase shift that causes the interference can occur either due to a difference in path length, $\triangle x$, or a difference in the arrival time $\triangle t$

$$\triangle\phi = 2\pi \triangle x\frac{1}{\lambda} \;\&\; \triangle\phi = 2\pi \triangle t\frac{1}{T} \tag{118}$$

Where λ is the wavelenght and $\frac{1}{T}$ is the time from one wave peak to the next [J*].

10 Appendix-D: RFID communication systems

The following three sections are centered around the main aim of this research, namely exploring the feasibility of measuring solvent concentrations in an spontaneously imbibition experiment by using ultra high frequency UHF radio frequency identification RFID technology. The approach and results of this experiment can be found in the sections COMSOL^{TM} simulation and CISC RFID Xplorer-2000. This section first provides a relevant contextual framework regarding various aspects of RFID. The first part of this section provides a general overview of the history and practice of RFID. In the second part a brief introduction is given as to where and how RFID is currently used in the oil and gas industry. The third part of this section will continue with a general overview of an RFID communication system and its main components.

10.1 History and practice of RFID

The early beginnings of RFID date back to World War II, when passive RFID systems were put into action in order to distinguish enemy planes from friendly aircrafts in the airspace above Europe. Despite its military origins, the first

related patent was in the hands of actress Hedy Lamarr and music composer George Anthiel, who got the idea for Spread Spectrum Radio transmission from the synchronization of player pianos [M*]. Spread Spectrum Radio is a system whereby the transmitter and the receiver use frequency-hopping to create a stronger and hard to detect transmission, a technology that is now incorporated in almost every new RFID communication system [N*]. RFID readers are for the most part frequency-hopping devices. The first patent associated with acronym RFID was awarded to Charles Walton in the year 1983 [O*].

Since the 40s RFID technology has seen tremendous innovations, moving from sizable transistors to microchip technology. This evolutionary trend can be explained by a phenomenon called Moore's Law, named after Gordon E. Moore. Moore's Law was an empirical observation which predicts the future of the evolution of integrated circuits (or wireless sensors networking - WSN). In 1965, Moore looked at the circuits being produced and predicted that the number of transistors in integrated circuits could be doubled every two years [12]. Moore's Law has been of great influence in the development of RFID technology and Smart Dust Technology.

RFID technology is part of the broader field of Automatic Identification and Data Capture AIDC technology. One of the first, most well-known and widespread AIDC applications is the barcode. RFID was initially developed as a replacement technology for the barcode identification system. The difference between the barcode technology and RFID technology is that with the latter no physical contact between the tag and the reader is required. That is to say, "the tag does not need to be within the line of sight of the reader and can be embedded in the tracked object" [42][48][11][45].

At the present time, RFID has been used as a cost effective and efficient tool in several branches of industry. One of the most common uses of RFID is asset tracking, whereby companies place RFID tags on products that might get stolen or misplaced [O*]. Still, the usefulness of RFID technology within the oil and gas industry has up until recently not received a lot of interest due to skepticism. However, nowadays this negative stance towards the technology is rapidly changing, and oil and gas firms around the world are beginning to explore the possibilities of RFID communication systems.

10.2 General applications of RFID technology in the oil and gas industry

Nowadays the use of RFID technology forms an increasing development in the oil and gas industry. Here follow some cases where RFID is already implemented or could be implemented in the sector. First of all, RFID can be used to optimize track and trace throughout the supply chain. Namely, RFID technology enables real-time monitoring of the inventory while reducing manpower in the logging process. The decrease in manpower substantially reduces asset loss and theft. Secondly, the use of RFID could facilitate efficient inspection and maintenance. Pipeline maintenance, especially in dangerous and hostile conditions, is an extremely time-consuming undertaking. RFID tags can be embedded in

all pipeline components, thus enabling a continuous registration of events in the part's lifespan, while taking into account variables such as prior maintenance history and any faults associated with the product line. As a consequence less time and workforce are required during maintenance inspections, whereas the interactive service history can prevent unforeseen costs, downtime and environmental damage due to technical breakdowns. Additionally, workforce performance can be improved by equipping the staff with RFID tags and the placement of readers throughout the facilities. This way the work performance can be optimized by analyzing routine work patterns. Moreover, when the staff is equipped with tags, the RFID technology enables the fast organization of an escape plan with all personnel accounted for in an emergency situation. Lastly, an RFID system could provide a good alternative on-site work on hazardous and isolated installations. Currently such a system is developed for the area of floating production, storage and offloading FPSO units. The effective computerization of FPSOs will save a huge amount of hours of manpower which was previously spend on the manning inaccessible outposts and can instead be spend on more profitable labor-intensive tasks elsewhere [42][23][8][48] .

10.3 The RFID System

Radio Frequency Identification RFID is a wireless data-collection technology. In general, an RFID communication system consists of at least one reader (interrogator), at least one tag (transponder), and antennas to enable energy transmission in voltages on wires and waves in the air. The communication (radio link) between the reader and the tag is referred to as downlink or forward link; communication from tag to reader is called uplink or reverse link [23][56].

RFID communication systems can be used for a very wide range of situations and purposes; hence there are many specifications within RFID systems. Generally RFID systems are divided according to the frequency of the system, whether the system uses active or passive tags, and the protocols used to communicate between the tag and the reader. Here, first some aspects regarding frequency and protocol will be highlighted; RFID tags will be discussed in more detail later on in this chapter. In terms of frequencies there are different frequency ranges distinguishable: low frequency LF which spans from125 kHz, high frequency HF which spans from 13.56 MHz, and lastly ultra-high frequency UHF which spans the 700-1200 MHz range. LF readers have a short read range, which means the tag must be within a few centimeters distance from the reader in order to achieve a response. However, an advantage of LF transmission is that the signal can transmit through thin layers of metal as well as liquid media. HF systems have a longer read range than LF devices, reaching distances from a few centimeters up to approximately a meter. These RFID systems are currently often used in, for example, public transport and electronic payments. HF tags still work relatively well around metals and liquids [Q*]. UHF frequencies offer a better read range and faster data transfer than LF or HF frequency transmissions. Passive UHF tags can operate from a few centimeters up to a few meters and semi-passive tags (with a battery integrated into the tag) and active

tags (with an active transmitter) can respond at distances up to approximately a hundred meters. As such, UHF devices are very suitable for real-time, long distance purposes. Disadvantages of UHF are however that due to the short wavelengths of the signal, the signal is more sensitive to attenuation than LF or HF transmissions. Signal transmission through metal or water is also very difficult. The frequency is also related to the mode of coupling (inductive or capacitive) used in the system [23][22].

When using an RFID communication system it is important to make sure the system operates conform the countries' frequency regulations. Initially the standards for frequency ranges were determined by a group of organizations, namely the International Organization for Standardization ISO e.g. ISO-18000-6-*C*, the International Electro-technical Commission IEC, ASTM International, and EPC Global [R*]. Frequency regulations form part of the protocol by which a system operates. A communication protocol specifies how the reader sends and receives data from the tag. More specifically, it determines how the signal is transmitted and modulated, the manner in which the devices interact (e.g. interrogator-talks-first) and which data characteristics and data transmission modes are used. The protocol which is nowadays commonly used for UHF RFID systems is the ISO/IEC-18000-6 (Type-C) / Gen-2 standard. This particular protocol consists of two parts. The first part is the ISO/IEC-18000, which specifies the physical and logical requirements for a passive-backscatter, Interrogator-Talks-First ITF system. Part-6 refers to the parameters for air interface communications at 860MHz to 960MHz [S*].

10.3.1 The RFID Reader

In an RFID system, the reader (interrogator) is the device that performs the actual identification. It can either be located in a fixed position or integrated into a mobile device, depending on its features and purpose. The system's reader may contain a user interface of its own but can also be connected to a network or a computer, which interacts with the user to control the reader and stores and displays the resulting data. The reader receives data through wireless electromagnetic wave transmission from the RFID tags [8][22]. Each tag has a unique number, the Electronic Product Code EPC, by which the tag can be identified by the reader. Where the identification process starts depends partly on whether active or passive tags are used (these will be explained in more detail in the following part). Active tags are not dependent on activation through external energy supply from the reader. However, many UHF-RFID systems use passive tags, which operate on the principle of backscatter radiation and are activated by the modulated electromagnetic signal from the reader.

In an RFID system similar to the one used in this research, which uses an UHF interrogator-talks-first communication protocol and passive tags, the reader sends a signal to the transmitting reader antenna Tx via a coaxial cable. The reader antenna converts the voltage signal into electromagnetic waves, which are transmitted wirelessly to the tag. The passive tag absorbs the energy and uses it to charge itself and scatters a (modulated) signal back to the

receiving reader antenna Rx [T*]. Some RFID systems have one reader antenna (monostatic configuration) while others have separate transmitting and receiving antennas (bistatic configuration) [U*]. The reader antenna or antennas may be integrated with the reader or physically separate and connected with a (coaxial) cable (Fig.22).

10.3.2 The RFID Tag

The type of RFID tag which is used in the RFID communication system greatly affects the form, read range, attachment methods and price range of the system. First and foremost, a general distinction can be made between active and passive tags. Whether an RFID tag is active or passive is related to the power source of the tags. Active tags have a battery attached to them and can actively transmit a signal to the reader. This type is therefore relatively expensive however achieves the longest read range. Passive tags carry no battery but instead receive all their power from the transmitted waves from the RFID reader. Part of this electromagnetic (modulated) wave is scattered back to the receiving reader antenna. In other words, passive tags cannot transmit signals without activation from the reader. As a consequence, the read range of passive tags is restricted by the power density of the transmitted signal. On the plus side, passive tags are relatively cheap to manufacture as no battery or transmitters are required and lasts longer due to the fact that the battery does not die [91][26]. There is also a third type of tag, which is the semi-active tag (battery assisted passive, BAP tag). The semi-active tag does have an integrated battery, hence the read range is improved over that of a passive tag however it does not have an active transmitter.

Besides the tags energy source, there are three other general factors which are key characteristics in the design of an RFID tag, namely the integrated circuit IC [56][73], the encasement of the tag and the tag antenna. These are discussed in the paragraphs below, starting with the description of the IC. In case of a passive tag, the EM wave which is send from the transmitting reader antenna will accumulate alongside the tag antenna which is connected to the IC of the tag. The tag converts the EM energy into voltage which subsequently powers the IC. The tag's IC or chip determines the performance, memory and extended features of the tag, and contains the Electronic Product Code EPC by which the tag can be identified. An RFID tag may contain one or more integrated circuits and storage capacity can differ from one type of IC to another. Most UHF-RFID tags follow the Class-1 Generation-2 standard protocol (ISO-18000-6-C) and use 96 bits of memory. This is enough space to store 24 hexadecimal characters. It is possible to expand the memory of the RFID tag, though this makes the tags more expensive to manufacture [V*].

The second component is the encasement of the tag. The encasement of the tag describes the tag's physical form. Namely, tags can have numerous shapes and sizes. The most simple form of layout is the RFID inlay, which can come in a waterproof (wet) and non-waterproof (dry) version. The inlay contains the IC and the antenna of the tag. A more advanced design-form is the RFID

label. An RFID label contains an RFID inlay, however it could also function without RFID. In case the RFID inlay was missing, the label could still provide information, whether in the form of a barcode or another form. The RFID inlay could also be provided with a special encasement to protect the tag from external influences such as impact, temperature, water or metal, depending on its intended purpose [V*].

The final important feature of an RFID tag is the antenna. Generally, the tag antenna is physically integrated with the tag. The size of the tag antenna indicates the read range of the tag and the media through which the signal is transmitted. In general, a small antenna indicates a shorter read range then larger tags with larger antennas. Moreover, as briefly mentioned in the previous chapter, the UHF RFID tag performance can be strongly influenced by signal absorption (permittivity) or reflection surrounding environment. Another important aspect in the antenna design is the number of dipoles present in the tag. For example, a dual dipole tag is readable from several different direction, whereas a single dipole tag might need to be placed more fixed in the orientation of the RFID reader [V*].

10.3.3 The RFID antennae (reader & tag antennae)

In general, an antenna in a wireless communication system can be defined as the device that radiates an RF signal (which is generated in a transmitter) to a receiver. More precisely, the transmitting antenna emits a signal in the form of an electromagnetic field through space to a receiving antenna. When the electromagnetic field reaches the receiving antenna, the radio waves are converted to voltage. Antennas are therefore types of transducers; they convert a signal in one form of energy into a signal in a different form of energy [2]. Antennas are generally characterized according to the following parameters: the pointing vector, the power intensity, radiation pattern, radiated power, fields regions, directivity, gain, polarization, axial ratio, input impedance, return loss, reflection coefficient, the voltage standing wave ratio VSWR, impedance bandwidth and the effective aperture.

There are several different types of antennas, such as wire antennas (e.g. dipole), aperture antennas (e.g. horn antennas), reflector antennas (e.g. parabolic or corner reflectors), lens antennas (convex plane) and micro-strip antennas (rectangular or circular) [W*]. The RFID Xplorer-2000 system uses circular micro-strip antennae as Tx and Rx antennae; the tag contains dipole wire antenna.

Dipole antenna The most common type of antenna is the dipole antenna (Fig.23). A dipole antenna is in fact a straight piece wire. When electrical energy is applied to the wire, the flow causes electrical charges to pile up at both ends of the wire. A dipole is a balance in positive and negative charges that are separated by a certain distance. The charge times the separation distance is equal to the dipole moment. The dipole moment oscillates alongside the antenna when a changing voltage current is applied to the antenna. As a result of the

oscillating current, concurring electric **E** and magnetic **H** fields are created. These fields create more fields which results in the formation of an outward propagating EM wave. When the electromagnetic wave reaches a medium with a high conductivity it creates a corresponding current in the medium. For this reason, a dipole antenna can also be used as a receiving antenna which modulates the signal back to voltage [X*].

Micro-strip antenna Micro-strip antennas, also known as patch antennas, are generally relatively low cost and easy to manufacture. Due to the fact that patch antennae are usually flat (although 3D structures do exist) they are sometimes referred to as planar antennae [64]. A patch antenna consists of a micro-strip transmission line, ground plane and a micro-strip antenna attached to a substrate. A substrate in this context is a dielectric circuit board. The ground plane is a conducting surface connected to the transmitter's ground wire which reflects the radio waves. The micro-strip transmission line and the ground plane are made of highly conductive material (such as copper).

The circular patch antennae in the RFID Xplorer-2000 are connected to the reader box via a coaxial cable, however note that other types of feeds are possible.

The length of the micro-strip antenna should be half a wavelength within the dielectric (substrate) medium. The width W of the micro-strip antenna influences the input impedance and the bandwidth. A larger width can increase bandwidth and reduce impedance; however the reduction of input impedance to 50 Ohms requires a very wide antenna which takes up a lot of space. The width of the antenna furthermore influences the radiation pattern, which can be determined according to the following equations:

$$E_e = \frac{\sin(\frac{kW\sin\theta\sin\phi}{2})}{\frac{kW\sin\theta\sin\phi}{2}}\cos(\frac{kl}{2}\sin\theta\cos\phi)\cos\phi \tag{119}$$

$$E_\varphi = -\frac{\sin(\frac{kW\sin\theta\sin\phi}{2})}{\frac{kW\sin\theta\sin\phi}{2}}\cos(\frac{kl}{2}\sin\theta\cos\phi)\cos\theta\sin\phi \tag{120}$$

where k is the wavenumber in free space, given by $2\pi/\lambda$, λ is the wavelength, θ is the angle measured off the x-axis of the radiation pattern and ϕ is the angle measured counterclockwise from the x-axis. The magnitude of the fields is given by:

$$f(\theta,\phi) = \sqrt{E_\theta^2 + E_\phi^2} \tag{121}$$

The distance between the patch and the ground plane determines the bandwidth. The directivity of patch antennas is around 5 to 7dB [Y*]. A half wave long patch operates in the so-called fundamental mode: the electric field is zero at the center of the patch, maximum (positive) on one side, and minimum (negative) on the opposite side. The negative and positive constantly change sides like the phase of the RF signal. However, the electric field does not stop near the edges of the patch but spreads out beyond the edges. These field extensions are called fringing fields and cause the patch to radiate [64].

Polarization The orientation of the electric and magnetic fields is also known as polarization. The orientation of the electric field corresponds with the alignment of the transmitting antenna. The magnetic field is orientated in the direction of the perpendicular line to the electric field and propagation direction. As stated earlier, electric fields that originate from a dipole antenna orientate in the direction of the axis of the antenna. This is also referred to as linearly polarized field. A distinction can be made between a vertical and a horizontal linearly polarized EM wave, which is determined by the alignment of the transmitting antenna. When both the transmitting and receiving antenna are aligned equally (so both horizontal or both vertical) and have the same type of polarization, this will result in the most optimal signal response. In addition to linear polarization there is also a different type of polarization, namely circular polarization. In circular polarization the electric field rotates as it propagates, similar to the form of a corkscrew. Here a distinction can be made between clockwise or right-hand circular polarization RHCP and counter-clockwise or left-hand circular polarization LHCP [Y*]. The electric field varies in two ortogonal planes (x and y direction) with the same magitude and a 90 degree phase difference. The result is the simultaneous radiation of two modes, where one of the modes has a 90 degree phase delay (I and Q modes) [64].

References

[1] Hans Adel, Jan Bauer, and Christoph Grabowski. 3d passive rfid tag over-the-air measurement. In *Antennas and Propagation (EUCAP), 2012 6th European Conference on*, pages 1557–1560. IEEE, 2012.

[2] Anant Agarwal and Jeffrey Lang. *Foundations of analog and digital electronic circuits*. Morgan Kaufmann, 2005.

[3] Greg M Anderson and David A Crerar. Phase equilibria.(book reviews: Thermodynamics in geochemistry. the equilibrium model.). *Science*, 262:1911–1912, 1993.

[4] Tsutomu Arakawa and Serge N Timasheff. Mechanism of protein salting in and salting out by divalent cation salts: balance between hydration and salt binding. *Biochemistry*, 23(25):5912–5923, 1984.

[5] Subhash C Ayirala, Chandra S Vijapurapu, and Dandina N Rao. Beneficial effects of wettability altering surfactants in oil-wet fractured reservoirs. *Journal of petroleum science and engineering*, 52(1):261–274, 2006.

[6] T Babadagli et al. Scaling of co-current and counter-current capillary imbibition for surfactant and polymer injection in naturally fractured reservoirs. In *SPE/AAPG Western Regional Meeting*. Society of Petroleum Engineers, 2000.

[7] S Serkan Basat, Kyutae Lim, Joy Laskar, and Manos M Tentzeris. Design and modeling of embedded 13.56 mhz rfid antennas. In *Antennas and*

Propagation Society International Symposium, 2005 IEEE, volume 4, pages 64–67. IEEE, 2005.

[8] Duccio Bertoni, Giovanni Sarti, Giuliano Benelli, Alessandro Pozzebon, and Gianluca Raguseo. Radio frequency identification (rfid) technology applied to the definition of underwater and subaerial coarse sediment movement. *Sedimentary Geology*, 228(3):140–150, 2010.

[9] Toni Björninen, Mikko Lauri, Leena Ukkonen, Risto Ritala, Atef Z Elsherbeni, and Lauri Sydänheimo. Wireless measurement of rfid ic impedance. *Instrumentation and Measurement, IEEE Transactions on*, 60(9):3194–3206, 2011.

[10] CJF Böttcher, OC Van Belle, P Bordewijk, A Rip, and David D Yue. Theory of electric polarization. *Journal of The Electrochemical Society*, 121(6):211C–211C, 1974.

[11] William C Brown. The history of wireless power transmission. *Solar energy*, 56(1):3–21, 1996.

[12] Paul E Ceruzzi. Moore's law and technological determinism: Reflections on the history of technology. *Technology and Culture*, 46(3):584–593, 2005.

[13] C Chassagne, D Bedeaux, JPM Van Der Ploeg, and GJM Koper. Theory of electrode polarization: application to parallel plate cell dielectric spectroscopy experiments. *Colloids and Surfaces A: Physicochemical and Engineering Aspects*, 210(2):137–145, 2002.

[14] C Chassagne, D Bedeaux, JPM vd Ploeg, and GJM Koper. Polarization between concentric cylindrical electrodes. *Physica A: Statistical Mechanics and its Applications*, 326(1):129–140, 2003.

[15] Vipul Chawla and Dong Sam Ha. An overview of passive rfid. *Communications Magazine, IEEE*, 45(9):11–17, 2007.

[16] Cary T Chiou. Partition coefficient and water solubility in environmental chemistry. *Hazard Assessment of Chemicals: Current Departments*, 1:117, 2012.

[17] Robert H Clarke, Diana Twede, Jeffrey R Tazelaar, and Kenneth K Boyer. Radio frequency identification (rfid) performance: the effect of tag orientation and package contents. *Packaging Technology and Science*, 19(1):45–54, 2006.

[18] Michel Clénet and RD Defence. *Design of a UHF Circularly Polarized Patch Antenna as a feed for a 9.1 metre Parabolic Reflector*. Defence R & D Canada-Ottawa, 2004.

[19] Lucian Copolovici and Ülo Niinemets. Salting-in and salting-out effects of ionic and neutral osmotica on limonene and linalool henry's law constants and octanol/water partition coefficients. *Chemosphere*, 69(4):621–629, 2007.

[20] Daniel D Deavours. A circularly polarized planar antenna modified for passive uhf rfid. In *RFID, 2009 IEEE International Conference on*, pages 265–269. IEEE, 2009.

[21] Vojtech Derbek, Christian Steger, Reinhold Weiss, Josef Preishuber-Pflügl, and Markus Pistauer. A uhf rfid measurement and evaluation test system. *e & i Elektrotechnik und Informationstechnik*, 124(11):384–390, 2007.

[22] Daniel M Dobkin. *The RF in RFID: UHF RFID in Practice*. Newnes, 2012.

[23] Daniel M Dobkin and Titus Wandinger. A radio oriented introduction to radio frequency identification. *RFID Tutorial, High Frequency Electronics*, 2005.

[24] Daniel M Dobkin and Steven M Weigand. Uhf rfid and tag antenna scattering. part ii: Theory. *Microwave journal*, 49(6), 2006.

[25] Varadarajan Dwarakanath, Tanmay Chaturvedi, Adam Jackson, Taimur Malik, Arsyad Andreansyah Siregar, Ping Zhao, et al. Using co-solvents to provide gradients and improve oil recovery during chemical flooding in a light oil reservoir. In *SPE Symposium on Improved Oil Recovery*. Society of Petroleum Engineers, 2008.

[26] Klaus Finkenzeller. *RFID Handbook: Radio-frequency identification fundamentals and applications*. Wiley, 1999.

[27] Abbas Firoozabadi et al. Recovery mechanisms in fractured reservoirs and field performance. *Journal of Canadian Petroleum Technology*, 39(11), 2000.

[28] Wely Brasil Floriano and Marco Antonio Chaer Nascimento. Dielectric constant and density of water as a function of pressure at constant temperature. *Brazilian Journal of Physics*, 34(1):38–41, 2004.

[29] S Folea and M Ghercioiu. Radio frequency identification fundamentals and applications. *Design Methods and Solutions, ch. Tag4M, a Wi-Fi RFID Active Tag Optimized for Sensor Measurements*, pages 287–310, 2010.

[30] Pradeep Ananth Govind, Swapan Kumar Das, Sanjay Srinivasan, Thomas James Wheeler, et al. Expanding solvent sagd in heavy oil reservoirs. In *International Thermal Operations and Heavy Oil Symposium*. Society of Petroleum Engineers, 2008.

[31] Joshua D Griffin, Gregory D Durgin, Andreas Haldi, and Bernard Kippelen. Rf tag antenna performance on various materials using radio link budgets. *Antennas and Wireless Propagation Letters, IEEE*, 5(1):247–250, 2006.

[32] S Gupta, S Gittins, P Picherack, et al. Field implementation of solvent aided process. In *Canadian international petroleum conference*. Petroleum Society of Canada, 2002.

[33] SC Gupta, SD Gittins, et al. Effect of solvent sequencing and other enhancements on solvent aided process. *Journal of Canadian Petroleum Technology*, 46(09), 2007.

[34] Michael Heiss and Wolf-Joachim Fischer. Wireless uhf rfid chip impedance measurement by only using an rfid reader. In *Antennas and Propagation (EUCAP), 2012 6th European Conference on*, pages 3014–3016. IEEE, 2012.

[35] George Hirasaki, Danhua Leslie Zhang, et al. Surface chemistry of oil recovery from fractured, oil-wet, carbonate formations. *Spe Journal*, 9(02):151–162, 2004.

[36] Tsung-Yen Ho, Shih-Yuan Chen, and Hsueh-Jyh Li. A method to determine the structure mode and antenna mode of a rfid tag antenna scattering. In *2009 IEEE Antennas and Propagation Society International Symposium*, 2009.

[37] LW Holm, AK Csaszar, et al. Oil recovery by solvents mutually soluble in oil and water. *Society of Petroleum Engineers Journal*, 2(02):129–144, 1962.

[38] Siavash Kahrobaei, Rouhollah Farajzadeh, Vural Sander Suicmez, and Johannes Bruining. Gravity-enhanced transfer between fracture and matrix in solvent-based enhanced oil recovery. *Industrial & Engineering Chemistry Research*, 51(44):14555–14565, 2012.

[39] B Kalpakci, TG Arf, JW Barker, AS Krupa, JC Morgan, RD Neira, et al. The low-tension polymer flood approach to cost-effective chemical eor. In *SPE/DOE Enhanced Oil Recovery Symposium*. Society of Petroleum Engineers, 1990.

[40] Jon Kleppe, Richard A Morse, et al. Oil production from fractured reservoirs by water displacement. In *Fall Meeting of the Society of Petroleum Engineers of AIME*. Society of Petroleum Engineers, 1974.

[41] Kaneyuki Kurokawa. Power waves and the scattering matrix. *Microwave Theory and Techniques, IEEE Transactions on*, 13(2):194–202, 1965.

[42] Jean-Marc Laheurte, Christian Ripoll, Dominique Paret, and Christophe Loussert. *UHF RFID technologies for identification and traceability*. John Wiley & Sons, 2014.

[43] Larry W Lake. *A generalized approach to primary hydrocarbon recovery*, volume 4. Elsevier Science Limited, 2003.

[44] William J Lambert. Modeling oil-water partitioning and membrane permeation using reversed-phase chromatography. *Journal of Chromatography A*, 656(1):469–484, 1993.

[45] Jeremy Landt. The history of rfid. *Potentials, IEEE*, 24(4):8–11, 2005.

[46] Marcel Latil. *Enhanced oil recovery*. Editions OPHRYS, 1980.

[47] Albert Leo, Corwin Hansch, and David Elkins. Partition coefficients and their uses. *Chemical reviews*, 71(6):525–616, 1971.

[48] YE Li-sha. Application of rfid technology. *Communications Technology*, 12:102, 2007.

[49] Alfred N Martin, Patrick J Sinko, and Yashveer Singh. *Martin's physical pharmacy and pharmaceutical sciences: physical chemical and biopharmaceutical principles in the pharmaceutical sciences*. Lippincott Williams & Wilkins, 2012.

[50] Leonid Mats, Peter J Hawrylak, and Marlin H Mickle. In-situ characterization of passive rfid tag performance at absolute minimum power levels. In *2007 IEEE Antennas and Propagation Society International Symposium*, 2007.

[51] Calvin C Mattax, JR Kyte, et al. Imbibition oil recovery from fractured, water-drive reservoir. *Society of Petroleum Engineers Journal*, 2(02):177–184, 1962.

[52] Lukas W Mayer and Arpad L Scholtz. Efficiency measurement method for uhf transponder antennas. In *The first international EURASIP Workshop on RFID Technology*, pages 17–20. Citeseer, 2007.

[53] Petra Meyer and Gerd Maurer. Correlation and prediction of partition coefficients of organic solutes between water and an organic solvent with a generalized form of the linear solvation energy relationship. *Industrial & engineering chemistry research*, 34(1):373–381, 1995.

[54] Walter John Moore. *Basic physical chemistry*. Prentice Hall, 1983.

[55] Norman R Morrow et al. Wettability and its effect on oil recovery. *Journal of Petroleum Technology*, 42(12):1–476, 1990.

[56] David Murfett. The challenge of testing rfid integrated circuits. In *Field-Programmable Technology, 2004. Proceedings. 2004 IEEE International Conference on*, pages 410–412. IEEE, 2004.

[57] Pavel V Nikitin and KV Seshagiri Rao. Theory and measurement of backscattering from rfid tags. *Antennas and Propagation Magazine, IEEE*, 48(6):212–218, 2006.

[58] Pavel V Nikitin and KV Seshagiri Rao. Labview-based uhf rfid tag test and measurement system. *Industrial Electronics, IEEE Transactions on*, 56(7):2374–2381, 2009.

[59] Pavel V Nikitin, KV Seshagiri Rao, Rene Martinez, and Sander F Lam. Sensitivity and impedance measurements of uhf rfid chips. *Microwave Theory and Techniques, IEEE Transactions on*, 57(5):1297–1302, 2009.

[60] Pavel V Nikitin and KVS Rao. Measurement of backscattering from rfid tags. In *Proceedings of AMTA Symposium*, 2005.

[61] Pavel V Nikitin and KVS Rao. Antennas and propagation in uhf rfid systems. *challenge*, 22:23, 2008.

[62] Pavel V Nikitin, KVS Rao, and RD Martinez. Differential rcs of rfid tag. *Electronics Letters*, 43(8):431–432, 2007.

[63] Keat Ghee Ong, CA Grimes, CL Robbins, and RS Singh. Design and application of a wireless, passive, resonant-circuit environmental monitoring sensor. *Sensors and Actuators A: Physical*, 93(1):33–43, 2001.

[64] D Orban and GJK Moernaut. The basics of patch antennas, updated, 2009.

[65] Clayton R Paul and Syed A Nasar. *Introduction to electromagnetic fields*. McGraw-Hill Companies, 1982.

[66] Andrew F Peterson, Scott L Ray, Raj Mittra, Institute of Electrical, and Electronics Engineers. *Computational methods for electromagnetics*, volume 2. IEEE press New York, 1998.

[67] Matthai Philipose, Joshua R Smith, Bing Jiang, Alexander Mamishev, Sumit Roy, and Kishore Sundara-Rajan. Battery-free wireless identification and sensing. *Pervasive Computing, IEEE*, 4(1):37–45, 2005.

[68] B Predel. Landolt-bornstein, group iv: Physical chemistry, 2006.

[69] Pekka Pursula, Mervi Hirvonen, Kaarle Jaakkola, and Timo Varpula. Antenna effective aperture measurement with backscattering modulation. *Antennas and Propagation, IEEE Transactions on*, 55(10):2836–2843, 2007.

[70] Pekka Pursula, Dan Sandström, and Kaarle Jaakkola. Backscattering-based measurement of reactive antenna input impedance. *Antennas and Propagation, IEEE Transactions on*, 56(2):469–474, 2008.

[71] Xianming Qing, Chean Khan Goh, and Zhi Ning Chen. Impedance characterization of rfid tag antennas and application in tag co-design. *Microwave Theory and Techniques, IEEE Transactions on*, 57(5):1268–1274, 2009.

[72] Merle Randall and Crawford Fairbanks Failey. The activity coefficient of non-electrolytes in aqueous salt solutions from solubility measurements. the salting-out order of the ions. *Chemical Reviews*, 4(3):285–290, 1927.

[73] Kanury Venkata Subba Rao. An overview of backscattered radio frequency identification system (rfid). In *Microwave Conference, 1999 Asia Pacific*, volume 3, pages 746–749, 2002.

[74] KV Seshagiri Rao, Pavel V Nikitin, and Sander F Lam. Antenna design for uhf rfid tags: a review and a practical application. *Antennas and Propagation, IEEE Transactions on*, 53(12):3870–3876, 2005.

[75] KV Seshagiri Rao, Pavel V Nikitin, and Sander F Lam. Impedance matching concepts in rfid transponder design. In *Automatic Identification Advanced Technologies, 2005. Fourth IEEE Workshop on*, pages 39–42. IEEE, 2005.

[76] F Ravera, M Ferrari, L Liggieri, R Miller, and A Passerone. Measurement of the partition coefficient of surfactants in water/oil systems. *Langmuir*, 13(18):4817–4820, 1997.

[77] AM Saidi et al. Simulation of naturally fractured reservoirs. In *SPE Reservoir Simulation Symposium*. Society of Petroleum Engineers, 1983.

[78] Jean-Louis Salager, Nelson Marquez, Alain Graciaa, and Jean Lachaise. Partitioning of ethoxylated octylphenol surfactants in microemulsion-oil-water systems: influence of temperature and relation between partitioning coefficient and physicochemical formulation. *Langmuir*, 16(13):5534–5539, 2000.

[79] Hamidreza Salimi, Johannes Bruining, et al. The influence of wettability on oil recovery from naturally fractured oil reservoirs including non-equilibrium effects. In *SPE Latin American and Caribbean Petroleum Engineering Conference*. Society of Petroleum Engineers, 2010.

[80] BB Sandiford et al. Laboratory and field studies of water floods using polymer solutions to increase oil recoveries. *Journal of Petroleum Technology*, 16(08):917–922, 1964.

[81] Jose E Schutt-Aine and Raj Mittra. Scattering parameter transient analysis of transmission lines loaded with nonlinear terminations. *Microwave Theory and Techniques, IEEE Transactions on*, 36(3):529–536, 1988.

[82] Ari Sihvola. Mixing rules with complex dielectric coefficients. *Subsurface Sensing Technologies and Applications*, 1(4):393–415, 2000.

[83] JM Smith, HC Van Ness, and MM Abbott. Introduction to chemical engineering thermodynamics, ; macgraw hill. *Inc.: New York*, 1987.

[84] Shalom Srebrenik and Sasson Cohen. Theoretical derivation of partition coefficient from solubility parameters. *The Journal of Physical Chemistry*, 80(9):996–999, 1976.

[85] S Standal, J Haavik, AM Blokhus, and A Skauge. Effect of polar organic components on wettability as studied by adsorption and contact angles. *Journal of Petroleum Science and Engineering*, 24(2):131–144, 1999.

[86] S Stevens, V Kuuskraa, and J ODonnell. Enhanced oil recovery scoping study. *EPRI, Editor*, 1999.

[87] S Thomas. Enhanced oil recovery-an overview. *Oil & Gas Science and Technology-Revue de l'IFP*, 63(1):9–19, 2008.

[88] Percy Cyril Lesley Thorne. Xxxii.-the solubility of ethyl ether in solutions of sodium chloride. *Journal of the Chemical Society, Transactions*, 119:262–268, 1921.

[89] Stanley M Walas. *Phase equilibria in chemical engineering*. Butterworth-Heinemann, 2013.

[90] Harry Walter. *Partitioning In Aqueous Two–Phase System: Theory, Methods, Uses, And Applications To Biotechnology*. Elsevier, 2012.

[91] Roy Want. An introduction to rfid technology. *Pervasive Computing, IEEE*, 5(1):25–33, 2006.

[92] JE Warren, P Jj Root, et al. The behavior of naturally fractured reservoirs. *Society of Petroleum Engineers Journal*, 3(03):245–255, 1963.

[93] S Wille, M Buggert, L Mokrushina, W Arlt, and I Smirnova. Effect of electrolytes on octanol-water partition coefficients: Calculations with cosmo-rs. *Chemical Engineering & Technology*, 33(7):1075–1082, 2010.

[94] Christian Wohlfarth. *Static dielectric constants of pure liquids and binary liquid mixtures: Supplement to IV/6*, volume 17. Springer Science & Business Media, 2008.

[95] Jeffries Wyman Jr. Dielectric constants: ethanol-diethyl ether and urea-water solutions between 0 and 50. *Journal of the American Chemical Society*, 55(10):4116–4121, 1933.

[96] Hyun Tae Yang, Christopher Britton, Pathma Jith Liyanage, Sriram Solairaj, Do Hoon Kim, Quoc Phuc Nguyen, Upali Weerasooriya, Gary Arnold Pope, et al. Low-cost, high-performance chemicals for enhanced oil recovery. In *SPE Improved Oil Recovery Symposium*. Society of Petroleum Engineers, 2010.

[97] MS Yeoman, BD Reddy, HC Bowles, P Zilla, D Bezuidenhout, and T Franz. The use of finite element methods and genetic algorithms in search of an optimal fabric reinforced porous graft system. *Annals of biomedical engineering*, 37(11):2266–2287, 2009.

[98] Lei Zhang and Zhi Wang. Integration of rfid into wireless sensor networks: architectures, opportunities and challenging problems. In *Grid and Cooperative Computing Workshops, 2006. GCCW'06. Fifth International Conference on*, pages 463–469. IEEE, 2006.

[99] Xianmin Zhou, Norman R Morrow, Shouxiang Ma, et al. Interrelationship of wettability, initial water saturation, aging time, and oil recovery by spontaneous imbibition and waterflooding. *SPE Journal*, 5(02):199–207, 2000.

11 Extended summary

Characterization of fluid properties is significant in the petroleum engineering practice, especially in solvent-based enhanced oil recovery, SEOR, where the use of injected chemicals should ideally be reduced to a bare minimum in order to minimize the costs and environmental impact of SEOR. However, current techniques for measurement inside cores, pipes and other enclosed spaces are inconvenient as the measurement devices must be connected from the inside to the outside, inevitably causing leakage problems. A possible solution to this problem is the usage of a Radio Frequency Identification RFID communication system. RFID concerns the use of wireless electromagnetic fields to transfer data. This research examines the feasibility of using RFID technology for wireless laboratory measurement of the dielectric coefficients of diethyl ether-oil-brine mixtures in enhanced imbibition experiments. A typical enhanced imbibition experimental setup consists of an oil saturated core placed in brine containing a solvent (Amott-cell); the solvent used in this experiment is diethyl ether. By means of measurements with the RFID system we aim to determine the concentration of diethyl ether in the oleic and aqueous phase of the mixture according to the corresponding dielectric coefficients. Therefore we first measure, with a Anton Paar density meter, the ratio of solvent concentration in the oleic and aqueous phase respectively, which is also known as the partition coefficient. We then determine the dielectric coefficients of the pure components (hexadecane, diethyl ether and water), as well as the effective dielectric coefficient of the mixture of these components, using the Böttcher mixing rule. The data from the density-meter experiment and mixing rule calculation is combined with the response output from measurements with a state of the art RFID communication system (Xplorer-2000).

As said above, to verify the feasibility of using RFID to characterize fluid media in an imbibition experiment, we first determine the phase behavior of the diethyl ether-oil-brine system, i.e. the partition coefficient, by means of density

measurements. The density measurements are preceded by tests to determine the maximum full solubility of diethyl ether in the oleic and aqueous phase. In particular, as we seek to determine the partition coefficient between the oleic and aqueous phase, the diethyl ether itself may not form a third phase. In the solubility test increasing levels of diethyl ether were added to water with varying levels of salinity (0M, 0.05M and 0.5M), leading to measured maximum full solubility levels of diethyl ether at 6.5, 6.1 and 5.6 percent respectively. These values are in agreement with the relevant literature data. Diethyl ether is fully soluble in oil in all proportions. With the maximum full solubility of diethyl ether in the oleic and aqueous phases identified, next the density of the binary mixtures (diethyl ether-hexadecane, diethyl ether-water 0M, 0.05M, 0.5M) is measured with the Anton Paar density meter DMA-4100M. For the aqueous phases, the solvent concentration was kept equal or below the solubility limit. As a result we establish four graphs where the density of the binary mixtures is plotted versus the weight fractions of diethyl ether in that mixture. Subsequently, the density values of these four curves are converted to partial molar volumes and the diethyl ether weight fractions are converted to mole fractions in the oleic or aqueous phase. The resulting curves are considered to be the calibrations curves. In order to determine the partition coefficient in the diethyl ether-oil-brine system, we now mix the oleic phase and the binary aqueous mixture in equal proportions for 24 hours, after which a sample is extracted from the upper layer (oleic phase) and the lower layer (aqueous phase) of the mixture. The density of these samples is measured and converted to partial molar volume. Using the calibration curves we can determine the corresponding diethyl ether mole fraction in the samples. The ratio of the diethyl ether mole fraction in the oleic phase and the diethyl ether mole fraction in the aqueous phase is the partition coefficient. The density-meter measurements are followed by experiments to determine the real part of the dielectric coefficients of the pure components as a function of frequency, at a temperature of ± 23 degrees Celsius. The dielectric coefficients of the pure components can be calculated from their complex impedance properties. For the pure components diethyl ether and hexadecane, these properties are measured with the insulation diagnostic system (Megger IDAX-300); the complex impedance of the water and salt solutions is measured with the impedance network analyzer (Wayne Kerr precision-6640A). The values of the calculated permittivity in the case of water and salt solutions are compared with an analytical model for validation and correction of the effect of electrode polarization on the measured data. With the dielectric coefficients of the pure components known (hexadecane=2.049, diethyl ether= 4.43 and water=79.084), we use the Böttcher equation to calculate the effective dielectric coefficient of mixtures with a known composition. The concept of effective dielectric coefficients is based on the assumption that "a mixture responds to electromagnetic energy as if it were a homogeneous substance".

Subsequently, the research continues with the determination of the relation between RFID response and diethyl ether volume fractions in the oleic and aqueous phase. The section on RFID measurements starts with simulations of three RFID models using COMSOL^{TM} Multiphysics software. The aim of

the simulation is to measure the scattering parameters (S-parameters) as a function of the dielectric coefficient (1-80) and frequency (500-2000MHz); the additional aim is to provide an understanding of the S-parameter (S_{21}) response dependence on the presence of the tag's encasement and the thickness of the blocks (media) surrounding the tag. Model-1 consists of a transmitting antenna (port-1) and a receiving antenna (port-2). In the second model the Rx antenna is replaced by an RFID tag (port-2). In model-3 the receiving antenna (port-3) returns the EM signal and the RFID tag (port-2) is placed between the two antennae. From the COMSOL output data we observe a dielectric coefficient dependency on the S-parameter (S_{21}) response and resonance frequencies. The S-parameter (S_{21}) refers to the voltage ratios between the input power at port-2 and the output power at port-1. Moreover, in model-1 we distinguish that the tag's cover influences S_{21} and changes the resonance frequency. In addition we discern an effect of the media volume surrounding the receiving antenna on the S-parameter (S_{21}), however only up to a medium thickness of 0.03m. In model-2 and 3 we observe that the thickness of the transmitting antenna also influences the S-parameter response.

In the RFID Xplorer-2000 setup we use the understanding obtained with the COMSOL^{TM} simulations to measure the dependence of the Xplorer-2000 response as a function of the frequency and the dielectric coefficient. In terms of response we focus on the following response parameters: the S-parameter (S_{21}), the minimum power at tag position (P_{min}), the scalar difference between the radar cross-sections of the tag (ΔRCS) and the backscattered power ($P_{backscattered}$). Firstly, the response parameters are separately plotted as a function of frequency. Subsequently the response parameters are plotted as a function of the dielectric coefficients for selected frequencies between 800-1000MHz, with finite increments. Finally, we determine the relation between the response parameters and the volume fractions of diethyl ether in the oleic and aqueous phase, using the data from the density-meter measurements and the Böttcher equation calculations. From the output data of these graphs we can conclude the following:

- From the graphs where we plotted RFID response versus the dielectric coefficient we observe that some frequencies show a larger dependence in the domain of interest than others.
- However, when applying this most optimal frequency in a graph where we plot the RFID response as a function of diethyl ether volume fractions in the oleic or aqueous phase, in some cases the relation results in a curve containing one or several maxima; in this situation more frequencies must be used to attain unique and accurate response values.
- From the RFID response parameters, the power at tag position (P_{min}) is the advisable response parameter when determining ether fractions in a diethyl ether-oil-water system.
- In order to investigate the full potential of the RFID Xplorer-2000 system for the determination of dielectric coefficients in an imbibition experiment, more measurements are required of media with dielectric coefficients ranging from 4.43 to 79.08 for the aqueous phase mixtures and dielectric coefficients

ranging from 2.05 to 4.43 for the oleic phase mixtures.

- Nevertheless based on this research we can conclude that it is possible to use RFID technology to determine the diethyl ether concentration in the oleic and the aqueous phase with a few percent (0.02).
- We can apply the approach (combination of density-meter, Böttcher mixing rule and RFID technology) of this thesis in any other system mixtures with range of dielectric coefficient between 1 and 80.

12 Definitions

- **Antenna aperture**

The antenna aperture is a measure of how effective an antenna is at receiving the power of radio waves (also known as effective area). This area is oriented perpendicular to the direction of the incoming radio wave.

$$A_{eff} = \frac{P_0}{PFD} \text{ [m}^2\text{]}$$

where, P_0 is the power in watts that is received by the antenna and available to the receiver and PFD is Power Flux Density. The amount of radio power passing through one square meter. The antenna aperture is proportional to the antenna gain. The formula for effective aperture is

$$A_{eff} = \frac{\lambda^2}{4\pi G}$$

[H*]

- **Antenna efficiency**

The antenna efficiency is the ratio of the power delivered to the antenna to the power radiated by the antenna. Antenna efficiency can be low due to impedance mismatch

$$\varepsilon R = \frac{P_{\text{radiated}}}{P_{\text{delivered}}}$$

where, ε is dielectric coefficient and R is resistance [Y*].

- **Antenna gain**

Antenna gain is the amount of power send in the direction of peak radiation to that which would be send by an isotropic antenna. For example, an antenna with a gain of 3dB indicates that this antenna transmits 3dB more power in that direction at far field distance then a lossless isotropic antenna with the same input power would. Gain G can be related to directivity D according to the following equation.

$$G = \varepsilon RD$$

where, ε is dielectric coefficient and R is resistance [Y*].

- **Antenna Polarization**

The antenna polarization indicates how the electric and magnetic fields of a plane wave oscillate along the direction of propagation of the wave. There are different types of polarization, of which linear and circular polarization are most common. A linearly polarized wave travels in the direction of the axis of the antenna, while the electric and magnetic fields oscillate in a straight line perpendicular to each other and the direction of the wave. In circular polarization the electric field rotates as it propagates, similar to the form of a corkscrew. The x and y components of the electric field are 90 degrees out of phase. A distinction can be made between clockwise or right-hand circular polarization RHCP and counter-clockwise or left-hand circular polarization LHCP [J*].

- **ASK**

Amplitude-shift keying ASK is a form of modulation whereby the variations in the amplitude of a carrier wave are used to represent digital data. The frequency and the phase of the carrier wave remain constant. In ASK, a finite number of amplitudes are assigned a unique pattern of binary digits. Each amplitude encodes an equal number of bits and each pattern of bits forms a symbol that is represented by the particular amplitude [H*].

- **Axial Ratio**

The polarization of an electromagnetic wave can be characterized according to the axial ratio AR. The axial ratio is the ratio of the orthogonal components of an electric field. Ideally, the axial ratio of a circularly polarized field is 1, or 0dB. The axial ratio degrades away from the main beam, hence it is often referred to in combination with a specified angular range [Y*].

- **Backscatter**

The way by which a tag communicates with a reader. The tag modulates the reverse link waveform by changing its impedance, thereby modifying the amplitude or phase of the reflected signal [Z*].

- **Band pass filter**

Component that enables a band of frequencies to be passed through a filter, while others are rejected by the stop band of the band pass filter. Typically it is used where a small band of frequencies need to be passed through the filter and all others must be rejected [a*].

- **Baseband**

Baseband (also known as lowpass) refers to the original frequency range of a transmission signal before it is converted, or modulated, to a different frequency range. Most protocols require the original baseband signal to be modulated to a higher frequency before transmission. On reception the signal is demodulated back to the original baseband signal [b*].

- **Beamwidth**

The beamwidth is the diameter along a line that is perpendicular to the beam axis and intersects it. The beamwidth can be measured in units of length but can also refer to the angular width (beam divergence), which is the angle between the intersection of the half power points $10^{10} \log 0.5 \approx -3$dB of the main lobe and the -3dB circle. There are several measures of beamwidths which can be distinguished within antenna theory, of which the Half Power Beamwidth HPBW and the Beamwidth between the First Nulls BWFN are most notable [H*; Y*].

- **Beamwidth between First Nulls**

The beamwidth between the first nulls BWFN is the angle between the Null Directions. The null directions are the directions at which the radiation is 0dB, in the direction away from the peak power of the main beam [H*; Y*].

- **Bistatic configuration**

Bistatic configuration refers to an RFID system in which the transmit and receive antenna are separate entities, as opposed to a system where one antenna is used for both transmission and reception (monostatic configuration) [U*].

- **BLF**

Backscatter Link Frequency. The subcarrier frequency of the Tag backscatter. A Miller subcarrier s used for performance testing to minimize the impact of the transmitted carrier at the receiver [T*].

- **Boresight**

The boresight is the axis of maximum gain (maximum radiated power) of a directional antenna. For most antennas the boresight is the axis of symmetry of the antenna [H*].

- **Capacitance**

Capacitance is the ability of a medium to store electric charge [H*].

- **C/N**

Carrier-to-noise ratio of a modulated signal. Digitally modulated signals are made up of two components (I and Q), which carry information in the form of encoded bits or symbols. Therefore, digitally modulated signals are usually referred to as carriers. A high C/N ratio indicates a good quality of reception [H*].

- **Complex impedance**

Complex capacitive impedance Z is the opposition of a circuit to a current when a voltage is applied and is measured in Ohm (Ω). It consists of a real part (resistance R) and an imaginary part (reactance X): Z = R + X. Impedance in an alternating circuit AC possesses both phase and magnitude. Reactance is the opposition to the current caused by the inductance and capacitance. In a sinusoidal current or voltage input, the magnitude of the complex impedance is the ratio of the voltage amplitude to the current amplitude, whereas the phase of the complex impedance is the phase shift by which the current delays the voltage [H*].

- **Control logic**

The control logic controls the operations of a program. It responds to commands from the user but can also acts on its own to perform automated tasks that have been structured into the program [H*].

- **CPU**

Central Processing Unit. This part is considered the 'brains' of a computer where most of the calculations take place.In the CPU the source information is created which is later send to the transmitter. Other tasks of the CPU include performing configurations in the hardware, controlling test flow, and processing and storage of the data [http://www.webopedia.com/TERM/C/CPU.html].

- **dB**

Decibel is a logarithmic unit that expresses the ratio of two values of a physical quantity, often power or intensity [H*].

- **dBd**

Decibel (dipole) is the forward gain of an antenna compared with a half-wave dipole antenna. Note that 0dBd = 2.15dBi [H*].

- **dBiC**

Decibel (isotropic circular) is the forward gain of an antenna compared to a circularly polarized isotropic antenna. There is no fixed conversion rule between dBiC and dBi, as it depends on the Rx antenna and the field polarization [H*].

- **dBi**

Decibel (isotropic) is the forward gain of an antenna compared with the hypothetical isotropic antenna, which uniformly distributes energy in all directions. Linear polarization of the EM field is presumed unless noted otherwise [H*].

- **dBil**

dBil represents the decibel units for antenna gain as measured by a linearly polarized measuring antenna. The more standard unit for antenna gain, dBi, does not convey the polarity of the measuring antenna. For example, the gain of a circularly polarized antenna may be 9 dBi when measured by a matched circularly polarized measuring antenna and 6 dBil as measured by a linearly polarized measurement antenna [H*].

- **dBm**

Decibel (mW) is the power relative to one milli-Watt. In the radio field, dBm is referenced to a 50 Ohm load, with the resultant voltage being 0.224 volts [H*].

- **dBsm**

Decibel (m2) is the decibel relative to one square meter. This unit is the measure of the Radar Cross Section RCS of a target. The power reflected by a target is relative to its RCS [H*].

- **Default**

A preset setting or value that will be used if no choice is made [c*].

- **Dense reader PR-ASK**

Dense reader PR-ASK is the term used for a particular set of forward link signaling parameters specific for the dense reader operation in the field [T*].

- **Direct current**

Direct current is the flow of electric charge in a constant single direction [H*].

- **Directivity**

Directivity is the ratio of the radiation intensity in a specific direction to the average radiation in all directions. The directivity of an isotropic antenna is 1, thus the directivity for any other antenna is a number above 1 [H*; Y*].

- **EIRP**

The Effective Isotropic Radiated Power represents the amount of power that would have to be emitted by an isotropic antenna to produce the power density observed in the direction of maximum antenna gain. EIRP is a measure of the signal strength in a particular direction leaving a transmitter [T*].

- **Electrical impedance**

The resistance a circuit presents to a current when a voltage is applied. The unity of impedance is Ohm. Impedance Z can express a real number or a complex value. The complex value consists of the real resistance component R and the imaginary reactance component X [H*].

- **EM-field (electromagnetic)**

  The electromagmetic field consists of electrical and magnetic fields. Magnetic fields and electrical fields are orthogonal to each other and to the direction of the plane-wave [H*].

- **Encoding**

Encoding is the process of converting a message into symbols [H*].

- **EPC**

The electronic production code EPC is the unique code by which a tag can be identified [H*].

- **Equivalent baseband signal**

The equivalent baseband signal is the complex valued representation of a modulated signal (RF signal). The equivalent baseband signal can be noted as Z(t)=I(t)+jQ(t), where I(t) is the in-phase signal, Q(t) is the quadrature phase signal and j is the imaginary unit [H*].

- **EUREQA**

Eureqa is a mathematical software tool which uses symbolic regression to determine mathematical equations that describe sets of data in their simplest form. The program can discover equations, provide answers to equations and is able to identify data gaps [H*].

- **Far-field region**

The space surrounding an antenna can be devided into three regions, namely the reactive near field region, the radiating near field region and the far field region. The far field region is the region far from the antenna where the radiation pattern takes place. In this region, the radiation pattern does not change shape with distance however, the fields still die off as 1/R, the power density dies off as $1/R^2$ [Y*].

- **Forward link**

Signaling from the reader to the tag [T*].

- **Friis Transmission equation**

The Friis Transmission Equation is used to calculate the power received P_R from Rx antenna (with gain G_R), when transmitted P_T from Tx antenna (with gain G_T), separated by a distance R, and operating at frequency f or wavelength λ

$$P_R = \frac{P_T G_T G_R \lambda^2}{(4\pi R f)^2}$$

[Y*].

- **Full-duplex radio**

Full-duplex radio indicates that an RFID system can simultaneously transmit and receive signals [22].

- **Half Power Beamwidth**

The half power beamwidth HPBW is the angle between the half power points of the main beam. The half power points are localized at 50% of the power on both sides of the peak power of the main beam, so at -3dB [Y*].

- **Hexadecimal characters**

  In mathematics and computing, hexadecimal (also base 16) is a positional numeral system with a base, of 16. It uses sixteen distinct symbols, most often the symbols 0–9 to represent values zero to nine, and A, B, C, D, E, F (or alternatively a, b, c, d, e, f) to represent values ten to fifteen. Hexadecimal numerals are widely used by computer systems designers and programmers [H*].

- **I, Q**

  In-phase and Quadrature-phase digital samples collected at the output of the receiver [T*].

- **IC**

Integrated Circuit. IC typically refers to the chip used in the tag. The IC determines all of the operational capabilities of the tag [T*].

- **Impedance bandwidth**

The impedance bandwidth of a patch antenna is influenced by the space between the patch and the ground plane. That is to say, the closer the patch is located to the ground plane, the less energy is radiated and more energy is stored in the patch; hence factor Q increases. Factor Q is the effect of electrical resistance. Other effects which might influence impedance bandwidth in a system which uses patch antennas are: the size of the ground plane in relation to the patch, and the feed structure [H*, Y*].

- **Impedance bridging**

Impedance bridging is commonly used in signal processing. Here a low impedance source is attached to a high impedance load in order to achieve maximum voltage to minimize signal degradation during transmission. In this case the signal strength is more important than achieving the maximum possible power transfer [H*].

- **Impedance matching**

The output impedance from a source (transmitter) must match the input impedance of the load (antenna) in order to facilitate an optimal power transfer. Therefore, the resistance R of the impedances must be equal, while the magnitude of the reactance must be equal but of opposite signs [H*].

- **Inductance**

Inductance is the property of a conductor to be able to produce electrical energy in itself and nearby conductors, instigated by a current flowing through it, according to the concept of mutual inductance. Therefore, inductance is usually defined as the electrical potential for a source in a circuit [H*].

- **Input impedance**

The ratio of voltage to current at the terminals of the transmitting antenna [Y*].

- **Internal impedance**

The ratio of voltage to current at the terminals of the receiving antenna [H*].

- **Isotropic antenna**

An isotropic antenna is an antenna which radiates equally in all directions. In reality no such antenna exists, however in antenna theory the isotropic antenna is often used as a reference to calculate parameters such as directivity and gain [d*].

- **ITF**

Interrogator Talks First is a protocol used in Generation 2, whereby the Interrogator (Reader) wakes up the tag [T*].

- **LHCP**

Left-Hand Circular Polarization LHCP is a type of circular polarization whereby the electric field circulates counter-clockwise in the direction in which the wave propagates. The wave does not change in strength, but only changes direction in rotary manner. A complete 360^o rotation is accomplished every wave length [H*, Y*].

- **LPF**

Low pass filter. Component that filters out the high frequency carrier from an AM wave [e*].

- **Main beam**

The main beam or main lobe is the area around the direction of maximum radiation, normally within 3dB of the peak effective radiated power [Y*].

- **Msps**

Mega-sample per second. The rate at which the receiver samples the base-band backscatter signal. For example, 1 Msps means that the signal is converted to one million I digital words and one million Q digital words per second [T*].

- **Mutual inductance**

The process whereby a change in current in an inductor induces electrical energy in a nearby inductor [H*].

- **N-connector**

The Type N connector is a threaded, weatherproof, medium-size RF connector used to join coaxial cables. It was one of the first connectors capable of carrying microwave-frequency signals, and was invented in the 1940s by Paul Neill; hence the name N connector [H*].

- **Path loss**

The difference between the power received and the power transmitted [T*].

- **PIE**

Pulse Interval Encoding. A method of sending data to an RFID tag by emitting pulses of energy with varying intervals, in order to indicate the ones and zeroes of binary code stored on the tag [f*].

- **PFD**

Power Flux Density. The amount of radio power passing through one square meter [H*].

- **Plane wave**

A plane wave is a constant-frequency wave whose wavefronts have points of constant phase form a plane surface parallel to the face of the source. A plane wave is emitted by a planar source and it travels in one direction (ideally). It is not possible in practice to have a true plane wave however, many waves are approximately plane waves in a localized region of space. For example, a localized source such as an antenna produces a field that is approximately a plane wave far from the antenna in its far-field region[H*; g*].

- **Polarizability**

The polarizability of a particle is the relation between the dipole moment induced by the polarization and the external electric field [82].

- **Power intensity**

Power intensity is the power in Watts which is radiated in a specific direction per unit solid angle (steradian) [H*].

- **Poynting Vector**

The Poynting vector describes the rate of energy transport per unit area, and is related to the density of the electric **E** and magnetic **B** fields. The magnitude of the Poynting vector gives the average power of the EM wave [h*].

- **Preamble**

A preamble is a signal used in network communications to synchronize transmission timing between two or more systems. In general, preamble is a synonym for "introduction." The role of the preamble is to define a specific series of transmission criteria that is understood to mean that data is about to be transmitted [i*].

- **PR-ASK**

Phase-reversal amplitude shift keying PR-ASK is a type of modulation suitable for narrowband, long-range transmissions due to its low C/N and narrow bandwidth requirements. In addition it maximizes power transport to the tag. PR-ASK uses a combination of 180° phase transitions every symbol and a 100% modulation depth [j*].

- **PSK**

Type of digital modulation. Conveys data by modulating the phase of the reference signal (carrier wave) [H*].

- **Quadrature demodulation**

A sinusoid with angle modulation can be decomposed into two amplitude-modulated sinusoids that are offset in phase by one-quarter cycle. The amplitude modulated sinusoids are known as in-phase and quadrature components. A conventional in-phase and quadrature demodulator uses analog components to translate an RF signal to baseband analog I and Q signals before converting it to digital data samples [H*].

- **Quadrature Demodulator Receiver**

A Quadrature Demodulator Receiver is a type of receiver and is part of the RFID reader. The device functions as follows. First, the backscattered RF signal is filtered by the RF Bandpass Filter to obtain the required frequency band. The filtered angle modulated signal is then amplified and split up by the RF in-phase splitter into two amplitude modulated AM sinusoids that are offset in phase by one-quarter cycle. These sinusoids are known as the in-phase I and quadrature-phase Q components. The final down-conversion to baseband occurs by means of splitting a local oscillator LO signal through a 90 degree hybrid. I and Q are then amplified and passed through a low pass filter LPF, which filters out the high frequency carrier wave. Lastly, the I and Q signals are passed through an analog-to-digital converter ADC where the signals are converted into digital data samples [T*].

- **Radiation pattern**

The radiation pattern of an antenna is a graphical representation of far field radiation properties in space. It defines the variation of the radiated power as a function of the direction away from the antenna. Radiation patterns are among others defined by directivity, beamwidths and sidelobes. In effect, the radiation pattern only shows relative values. Therefore, the values are usually normalized by the maximum value. The power pattern is a graphical representation of the radiated power density of the far field in a certain direction at a fixed distance from the antenna [H*; Y*].

- **RCS**

The radar cross section RCS indicates how detectable an object is on a radar. It is a property of the target's reflectivity; the more electromagnetic energy is reflected back to the source the more easily the target is detected. RCS consists of the a structural and antenna mode. The portion of EM energy that bounces off the antenna into space without absorption is called the structural mode; the absorbed energy which is scattered back into space due to impedance mismatches is called antenna mode scattering [H*].

- **Reactance**

Reactance is the resistance of a circuit element to a variation in current or voltage as a result of the elements' inductance or capacitance. Inductive reactance is the opposition to the change of current and is proportional to the signal frequency and inductance. Capacitive reactance is the opposition to the change of voltage and is inversely proportional to the signal frequency and capacitance. Hence, as frequency increases, the inductive reactance goes up and the capacitive reactance goes down [H*].

- **Read Range**

The distance at which a tag can still be read by the reader. In order to maximize the read range the antenna impedance is matched to the chip impedance at

the minimum power required for the chip to work. Usually the tag keeps functioning properly when brought closer to the RFID reader antenna. However, it is possible that a higher input power due to close vicinity to the source results in tag impedance mismatches and causes dead spots within the operational range of the tag. In addition to impedance, the tag's read range is determined by frequency, antenna gain, effective area and the substrate on which the tag is mounted [57].

- **Reflection coefficient**

Reflection coefficient is the electric field ratio between the reflected beam and the incident beam:

$$|\Gamma| = \frac{VSWR - 1}{VSWR + 1}$$

The reflection coefficient is the ratio of the amplitude of the reflected wave (Vr) to the amplitude of the incident wave (Vi). In case the source and load impedances are identified, the reflection coefficient can be calculated according to the following equation: Γ= (Zl-Zs)/(Zl-Zs), where Zs is the impedance toward the source and Zl is the impedance toward the load. The reflection coefficient is also referred to as S11 or return loss [antenna-theory]. In case the reflection coefficient is expressed in dB it is always a negative number. The magnitude of the reflection coefficient is always a number between 0 and 1[H*; Y*; k*].

- **Return loss (RL)**

Return loss is the loss of power in a reflected signal (negative of the magnitude of the reflection coefficient) in decibels dB. Since power is proportional to the square of the voltage, return loss is given by

$$RL(dB) = 10 \log 10(P_i/P_r)$$

where Pi is the incident power and Pr is the reflected power. The return loss is related to the voltage standing wave ratio VSWR and the reflection coefficient [H*].

- **Reverse link**

Reverse link is the signaling from the tag to the reader [T*].

- **RHCP**

Right-Hand Circular Polarization RHCP is a type of circular polarization whereby the electric field circulates clockwise in the direction in which the wave propagates. The wave does not change in strength, but only changes direction in rotary manner. A complete 360^o rotation is accomplished every wave length [H*, Y*]..

- **RIP**

The Received Isotropic Power is the power measured at the output of a 0dBi gain Rx antenna. RIP is a measure of the signal strength at a point in space, typically the input to a Rx antenna [T*].

- **Sidelobe**

Sidelobes are undesired smaller beams radiating away from the main beam. The maximum value of the sidelobes is called the Sidelobe Level [Y*].

- **S-parameters**

Scattering parameters describe the voltage input and output ratio. Quantities of S-parameters are usually measured in terms of voltage volts (V) or power watts (W) or decibels (dB) [H*; l*].

- **State machine**

A state machine is a device that stores the status of something at a given time and can operate on input to change the status and cause an action or output to take place for any given change [m*].

- **Tari**

TypeA Reference Interval. A value which indicates the time interval required to transmit a zero in the case of pulse interval encoding PIE. According to the ISO 18000-6-C standard, tags should respond to commands whenever the Tari value is between 6.25 and 25μs [T*].

- **Transmission coefficient**

The transmission coefficient is the ratio of the amplitude of the complex transmitted wave to that of the incident wave at a discontinuity in the transmission line. It is moreover used as a quality indication of the transmission line [H*].

- **Transmission line**

The transmission line is the line that connects the transmitter or receiver to the antenna (Coaxial cable). In a low frequency LF circuit the transmission lines have zero resistance, however in a high frequency HF short-circuit, transmission lines can have an infinite impedance. Since antennas are high-frequency devices, the length of the transmission line can significantly alter the input impedance causing only a small current to be able to enter the antenna from the source (or vice versa in case of a receiving antenna) [Y*].

- **Transistor**

A transistor is a device that can amplify and switch electronic signals and electrical power [H*].

- **User interface**

A point of interaction between a computer and humans [H*].

- **Voltage rectifier**

A voltage rectifier is a device that converts an alternating current AC into a direct current DC [H*].

- **VSWR**

VSWR stands for voltage standing wave ratio, a measure that indicates how well the antenna impedance is matched to the radio or transmission line it is connected to. VSWR is a function of the reflection coefficient Γ as can be seen in the following formula:

$$VSWR = \frac{1 + |\Gamma|}{1 - |\Gamma|}$$

It describes how well the antenna impedance Z_a is matched with the transmission line (coaxial cable) impedance $Z_c = 50\Omega$.

$$\Gamma = \frac{Z_a - Z_c}{Z_a + Z_c}$$

VSWR is always a positive number from 1 or above, where 1 indicates a perfect match [H*; Y*].

- **Word**

A 16-bit row in EPC memory conform the system's protocol [T*].

Website references
A* www.maxwells-equations.com
B* Albano et al, 1979-1980
C* http://cp.literature.agilent.com
D* www.pewa.de
E* onlinelibrary.wiley.com
F* www.maxwellyear2006.org
H* www.wikipedia.com
I* fas.org/man/dod-101/navy/docs/es310/propagat/Propagat.htm
J* www.explainthatstuff.com
K* http://fas.org/man/dod-101/navy/docs/es310/AM.htm
L* http://fas.org/man/dod-101/navy/docs/es310/FM.htm
M* www.aetherczar.com
N* http://timkastelle.org

O* www.engineersgarage.com
Q* http://blog.atlasrfidstore.com
R* http://blog.atlasrfidstore.com
S* www.iso.org
T* Tag Performance Parameters and Test Methods Version 1.1.3.
U* www.rfidjournal.com/blogs/experts/entry?7623
V* http://blog.atlasrfidstore.com
W* http://nptel.ac.in/courses/117107035/
X* http://nptel.ac.in/courses/117107035/8
Y* www.antenna-theory.com
Z* www.gs1.org
a* www.radio-electronics.com
b* www.techterms.com
c* www.encyclo.nl/begrip/default
d* www.telecomabc.com/i/isotropic
e* http://electronics.stackexchange.com
f* www.rfid.com/blogs/experts/entry?7623
g* www.cis.rit.edu
h* http://hyperphysics.phy-astr.gsu.edu.
i* http://whatis.techtarget.com/definition/preamble
j* www.ni.com/tutorial/6645/en/
k* http://home.sandiego.edu
l* www.microwaves101.com
m* http://whatis.techtarget.com/definition/state-machine

13 Abbreviations

ADC	Analog-to-Digital Converter
AIDC	Automatic Identification and Data Capture technology
AM	Amplitude Modulation
AUT	Antenna Under Test
BAP	Battery Assisted Passive tag
BWFN	Beamwidth between the First Nulls
CEOR	Chemically Enhanced Oil Recovery
CW	Continuous Wave
DC	Direct Current
EDL	Electrical Double Layer
EIRP	Effective Isotropic Radiated Power
EOR	Enhanced Oil Recovery
EP	Electrode Polarization
EPC	Electronic Product Code
FM	Frequency modulation
FPSO	Floating Production, Storage and Offloading
GUI	Graphic User Interface
HF	High Frequency

HPBW	Half Power Beamwidth
IC	Integrated Circuit
INA	Impedance Network Analyzer
ITF	Interrogator Talks First (reader talks first)
LF	Low Frequency
LHCP	Left-Hand Circular Polarization
NRLT	Nonrandom to Liquid Theory
PIE	Pulse-Interval Encoding
PL	Path Loss
PM	Phase Modulation
PML	Perfectly Matched Layer
PSK	Phase shift keying or phase shift keyed
PR-ASK	Phase-reversal amplitude shift
PW	Pulse width
RCS	Tag radar cross section (RCS1 & RCS2)
RF	Recovery Factor
RFID	Radio Frequency Identification
RIP	Received isotropic power
RF	Radio frequency
RFID	Radio-frequency identification
RHCP	Right-Hand Circular Polarization
SEOR	Solvent-based Enhanced Oil Recovery
TUT	Tag under test
UHF	Ultra High Frequency
VSWR	Voltage Standing Wave Ratio
WSN	Wireless Sensor Networking

14 Symbols

a_0	constant with value 14.1113
a_1	constant with value 341.5902
atm	atmosphere
$\mathbf{B}$	magnetic flux density [Wb/m^2 or T]
BLF	Backscatter link frequency [kHz]
dB	Decibel
dBm	Decibel (milli)
dBi	Decibel (isotropic)
dBd	Decibel (dipole)
dBsm	Decibel [m^2]
c	speed of light ($2.99792458E^8$ [m/s])[3×10^8m/s]
c_0	wave velocity in air
c_m	wave velocity in a medium
C_v	contour (closed volume)
°C	Celcius, measure of temperature
C	capacitance

C the average of the diethyl ether concentrations

$\triangle$C square root of the variance in diethyl ether concentrations

$\triangle$C/C square root of the variance in diethyl ether concentrations (standard deviation) devided by the average of the diethyl ether concentrations

d inner diameter of the cylindrical electrode is 0.009m

D outer diameter of the cylindrical electrode is 0.03m

D electric flux density [C/m^2]

D_0 $D_0 = \frac{D_1 + D_2}{2}$

D_1 the diffusion coefficient of Cl, which equals 1.957×10^{-9}

D_2 the diffusion coefficient of Na, which equals 2.032×10^{-9}

DR Divide ratio

e fundamental unit of electrical charge [6×10^{23}]

E electric field intensity [V/m]

E_s the phasor form of electric field intensity **E**

E_T transverse electric field

$EIRP_{Tx}$ Effective isotropic radiated power from transmitter [dBm]

$EIRP_{TUT}$ Effective isotropic radiated power from tag [dBm]

f frequency

f_c frequency of the carrier signal

G gain

G_{Rx} Receiver electronics gain [dBV]

G_{RxA} Receive antenna gain – linear [dBil]

G_{TxA} Transmit antenna gain – linear [dBil]

h height [m]

H magnetic field intensity [A/m]

Hz Hertz

I current through a circuit in Ampere [A]

Im imaginary part

j complex number

J current density [A/m2]

jX imaginary part of resistance

k conductivity

°k Kelvin, measure of temperature

K factor K indicates the influence of the load impedance mismatch on the amount of re-radiated power

k_s wavenumber

K partition coefficient

K_s Debye's Length; $K = \frac{2e^2 C \xi_a}{\varepsilon_0 \varepsilon_1 kT}$, where $e = 1.6 \times 10^{-19}$

k_0 $k_0 = 2\pi/\lambda_0$ is the wave number of the propagation in air

K_0 wavenumber for a lossless medium with zero conductivity

K_B Boltzmann's constant:k= 1.38 ($\pm$ 0.0000013)$\cdot 10^{-23}$ JK^{-1}

l length

L inductance

m meter

M	Molar, measured in mole per liter [Mol/L]
M_{av}	average molecular weight [g/Mol]
M_i	the molecular weight of species i
M_r	magnetic relative permeability
mM	milli-mole per liter [10^{-3} mole/l]
MHz	mega Hertz
n	refraction index [c_0/c_m]
n_j	concentration of free ions
NaCl	sodium chloride
nH	nano Henry
P	pressure in bars
P_e	pure mass density of diethyl ether
$P_{\min}$	minimum power required to activate the tag
P_{mix}	mass density of the mixture
P_{Rx}	received power at output of receive antenna [dBm]
P_{Tx}	transmit power at input to transmit antenna [dBm]
P_w	pure mass density of diethyl ether
q	single point charge in Coulomb [C]
Q	Slot-count parameter used in Query command
r	distance [m]
r̨	radius
ŕ	position
R	resistance
R̨	real axis
rand()	rand() represents a uniformly distributed random number
Re	real part
RIP_{Rx}	Received isotropic radiated power at receiver (dBm)
RIP_{TUT}	Received isotropic radiated power at tag (dBm)
Rx	receiving antenna
s	surface
S	solubility
S_{11}	the voltage ratio of input (port-1) and output (port-1)
S_{21}	the voltage ratio of input (port-2) and output (port-1)
S_{31}	the voltage ratio of input (port-3) and output (port-1)
sd	standard deviation
Sij	the voltage ratio between i is input and j is output voltage
t	time [s]
T	temperature
$\frac{1}{T}$	time between two peaks of a wave
Tx	transmitting antenna
v	volume
v_e	volume fraction of diethyl ether
v_w	volume fraction of water
V	Voltage ratio in Volt [v]
V_e	voltage applied to the Tx antenna (emitting voltage)

V_r	voltage received by Rx antennae (receiving voltage)
$V_c(t)$	carrier signal
$V_m(t)$	information signal (voltage)
$V_{AM}(t)$	amplitude modulated signal (voltage)
$V_{FM}(t)$	frequency modulated signal (voltage)
W	width
w_e	weight fraction of diethyl ether
w_w	weight fraction of water
X	reactance
X	coordinate
X_i	mole fraction
z	space
Z	impedance
$\check{\mathrm{Z}}$	complex impedance
$\lvert Z \rvert$	magnitude
$\nabla\cdot$	divergence
$\nabla\times$	curl

15 Greek

β	is the angular frequency divided by the wave velocity ω/c
ε	permittivity
ε_0	absolute permittivity of free space (air =1)
ε_1	dielectric constant of water (= 79.08)
ε_2	dielectric constant of diethyl ether (= 4.43)
ε_m	effective permittivity of the mixture
ε_e	dielectric coefficient of the environment (background medium)
ε_i	dielectric coefficient of the inclusion of the guest component
ε_r	relative permittivity
ε^*	theoretical value of the dielectric coefficient (analytical model)
η_0	impedance in a vacuum
θ	phase, the argument of Z
θ	angle between transmit and receive antennas (degrees)
λ	wavelength
λ_D	thickness of the double-layer (Debye-Hückel expression)
μ	magnetic permeability
μ_0	magnetic permeability in free space ($4\pi \times 10^{-7}$henry/m)
μ_r	relative magnetic permeability
ρ	volume charge density [C/m^3]
ρ_v	volume charge density [C/m^3]
σ	conductivity
σ_{RCS}	tag's radar cross-section [RCS]
ϕ	phase angle in degrees
ω	angular frequency in radius per second [rad/s]
Ω	Ohm

ξ	Avogadro constant $6.022140857 \times 10^{23}$ [mol^{-1}]